PROJECT PERIODIC REPORT

Grant Agreement number: 244067

Project acronym: EUCLIPSE

Project title: EU Cloud Intercomparison, Process Study & Evaluation Project

Funding Scheme: FP7

Date of latest version of Annex I against which the assessment will be made:

Periodic report: 1st ☐ 2nd **X** 3rd ☐ 4th ☐

Period covered: from 1 August 2011 to 1 February 2013

Name, title and organisation of the scientific representative of the project's coordinator[1]:

Prof.dr. A.P. Siebemsa, KNMI

Tel: +31 30 2206760

Fax: +31 30 2210407

E-mail: siebesma@knmi.nl

Project website[2] address: http://www.euclipse.eu

[1] Usually the contact person of the coordinator as specified in Art. 8.1. of the Grant Agreement .
[2] The home page of the website should contain the generic European flag and the FP7 logo which are available in electronic format at the Europa website (logo of the European flag: http://europa.eu/abc/symbols/emblem/index_en.htm logo of the 7th FP: http://ec.europa.eu/research/fp7/index_en.cfm?pg=logos). The area of activity of the project should also be mentioned.

Declaration by the scientific representative of the project coordinator

I, as scientific representative of the coordinator of this project and in line with the obligations as stated in Article II.2.3 of the Grant Agreement declare that:

- The attached periodic report represents an accurate description of the work carried out in this project for this reporting period;
- The project (tick as appropriate) [3]:

  X has fully achieved its objectives and technical goals for the period;

  ☐ has achieved most of its objectives and technical goals for the period with relatively minor deviations.

  ☐ has failed to achieve critical objectives and/or is not at all on schedule.

- The public website, if applicable

  x is up to date

  ☐ is not up to date

- To my best knowledge, the financial statements which are being submitted as part of this report are in line with the actual work carried out and are consistent with the report on the resources used for the project (section 3.4) and if applicable with the certificate on financial statement.
- All beneficiaries, in particular non-profit public bodies, secondary and higher education establishments, research organisations and SMEs, have declared to have verified their legal status. Any changes have been reported under section 3.2.3 (Project Management) in accordance with Article II.3.f of the Grant Agreement.

Name of scientific representative of the Coordinator: ..Prof.dr. A.P. Siebesma..................................

Date: 12./ 04./ 2013

For most of the projects, the signature of this declaration could be done directly via the IT reporting tool through an adapted IT mechanism.

[3] If either of these boxes below is ticked, the report should reflect these and any remedial actions taken.

3.1 Publishable summary

Objectives:
Cloud Feedbacks in Earth System Models (ESMs) remain the largest source of uncertainty in projections of future climate. Consequently, the central challenge of EUCLIPSE is:

to determine, understand and reduce the uncertainty due to cloud-climate feedback.

In order to respond to this challenge, EUCLIPSE represents a focused multi-disciplinary by fostering coordinated research in the area of cloud processes in relation to climate change. The specific objectives of EUCLIPSE to achieve this challenge are:

- Evaluation of cloud processes in Earth System Models.
- Development of physical understanding of how cloud processes respond and feedback to climate change.
- Development of a metric to measure the relative credibility of the cloud feedbacks by different Earth System Models.
- Improvement of the parameterization of cloud related processes in current Earth System Models.

Context:
Earth system models (ESMs) are our major modelling tools used to address how our climate will respond to increasing greenhouse gases such as atmospheric carbon dioxide. Nevertheless, the global warming of the various ESM's that participated in the World Climate Research Programme's (WCRP) third phase of the Coupled Model Intercomparison Project (CMIP3) in support of the Intergovernmental Panel on Climate Change (IPCC) Fourth Assessment Report (AR4) exhibit a large spread of global equilibrium temperature ranging from 2.3 to 4.2 K as a response of carbon dioxide doubling (see Figure 1).

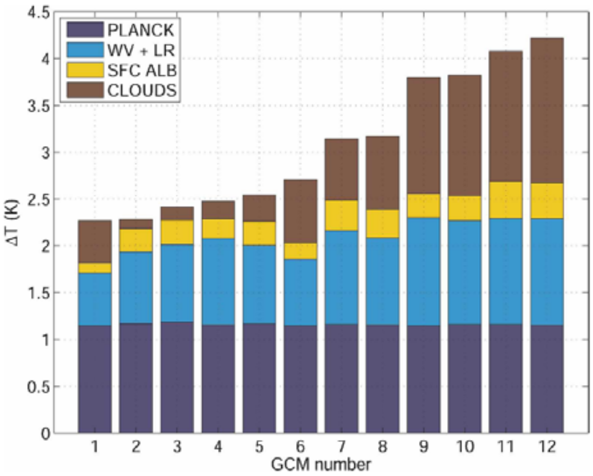

Figure 1. *(source Dufresne and Bony, J. of Climate 2008)*

The global warming of each ESM can be broken down into different contributions: i) direct warming due to doubling of carbon dioxide (dark blue) only, ii) enhanced warming due to an increase of water vapour in the atmosphere, the so called water vapour feedback (light blue), iii) enhanced warming due to an decrease of the Earth's surface albedo as an result of decreasing ice coverage (yellow) and iv) an enhanced warming due changes in cloud amount and cloud properties, also known as the cloud feedback (brown). This analysis illustrates one of the main conclusions of the latest IPCC report (IPCC AR4 SPM 2007):

"*Cloud effects remain the largest source of uncertainty in model based estimates of climate sensitivity.*"

Clouds are also a major contributor to uncertainty in other feedbacks (e.g., surface albedo, carbon cycle) in the Earth System. Through interactions with the large-scale circulation, cloud processes also contribute to synoptic circulations and regional climate. They are therefore critical to the prediction of future changes in precipitation patterns, climate variability and extreme events.

In EUCLIPSE, four distinct communities will work together across a set of integrated work packages over a four-year period: the observational community will provide state-of-the-art measurements from ground- and space-based active and passive remote sensing; the numerical weather prediction community will provide analyses of short timescale model biases induced by cloud processes; the cloud modeling community will provide fine-scale models as an additional tool for understanding cloud behavior in a changing climate; finally, the climate modeling community will synthesize the physical understanding and observational constraints identified by the other communities to improve the representation and assessment of cloud processes in ESMs and so improve the predictive skill of ESMs.

Main Results Achieved So far

EUCLIPSE is now in its second phase (month 18–month 36) during which most of the core objectives of WP2 (evaluation and analysis of the cloud related processes in climate models) and WP3 (Process_Level Evaluation) has been achieved. WP1 (Climate Simulations and Diagnostic Tools) has been finalized and WP4 (Sensitivity Experiments and Hypothesis Testing) is now in good progress. At the moment of writing this report 34 papers have been published or submitted to peer reviewed journals as a result of the EUCLIPSE project. All the submitted papers that acknowledge EUCLIPSE can be found on the EUCLIPSE website at http://www.euclipse.eu/Publications_new.html/ . Many of these reported results will also be used in the upcoming IPCC's fifth assessment report. It is impossible to describe all the result but the a summary of these 34 papers can be found in the progress report where the results are described along the lines of the deliverables such as described in the Description of Work (DOW) of the EUCLIPSE project (http://www.euclipse.eu/downloads/DOW_EUCLIPSE_final.pdf).

Here we will briefly summarize the main results of WP2 and WP3 that have been achieved in the second phase of the project.

WP2 has analyzed and evaluated the climate runs such as prescribed by the CMIP5 protocol. Most of the analyses are centered around the historical runs, the AMIP run and several perturbed runs such as a 4XCO2 run and SST perturbed runs, but also coupled Atmosphere-Ocean perturbed runs have been used.

WP2 Main Results:

- For the present day climate runs the CMIP5 results show similar overall cloud biases as the CMIP3 runs. Climate models still underpredict the global cloud fraction when compared with the ISCCP data set. However the distribution of the clouds in terms of their optical depth has improved, thereby reducing the longstanding "too few too bright" bias. (Deliverable 2.1)

- Various cloud regimes cloud regimes (arctic clouds, marine subtropical clouds and midlatitude marine clouds over the Southern Ocean) have been evaluated in more detail by using satellite simulators (COSP), novel satellite products (e.g. CALIPSO) and novel clustering techniques. These analyses allow to determine which cloud types contribute mostly to the major cloud and radiative biases for these cloud regimes. For instance, it has been found that for the midlatitude clouds over the Southern Ocean the midlevel clouds are the cause of the outgoing shortwave radiation (OSR) bias in most of the CMIP5 runs. For the marine tropical clouds, for the first time a comprehensive evaluation on the representation of vertical cloud structure by using CALIPSO data. All these analayses have been proven to be extremely useful to further pinpoint at which specific points parameterizations of these cloud types fail. (Deliverable 2.1)

- A Detailed analysis of indirect aerosol effects have been reported in Deliverable 2.2 by a comprehensive comparison between preindustrial and present-day climate runs. An evaluation of the period 2001-2005 for the historical runs with MODIS data show that the CMIP5 models do reproduce a reasonable geographical distribution of Aerosol Optical Depth (AOD) and Top of the Atmosphere (TOA) radiation. However, the modeled Cloud Droplet Number Concentration (CDNC) is generally substantially lower in the models compared to the MODIS retrieval, except for CSIRO which shows larger values. This hints at compensating errors in most of the models that other processes compensate for this underestimation of CDNC as to get the correct TOA radiation. (Deliverable 2.2)

- All participating EUCLIPSE climate models have reduced their precipitation double ITCZ bias compard to the previous CMIP3 versions. (Deliverable 2.4)

- Present day warm temperature extremes are in general overestimated by the CMIP5 climate models in Central Europe and underestimated in Scandinavia and Western Europe. Cold extremes in the present climate are in general underestimated in Scandinavia and South-Western Europe and overestimated in North-Eastern Europe. Summertime warm extremes are expected to rise in frequency of 10% (by definition) in present day climate (1979-2008) to 50% for future climate (2070-2099) while cold extremes are projected to decrease from 10% to 1%. It should be remarked that these changes are subjected to large uncertainties due to a large inter-model spread. A breakdown of the uncertainties (intermodal spread) into a large-scale dynamical contribution and non-dynamical (local) contributions show that the dynamical contributions are minor in Summer but substantial in Winter. (Deliverable 2.4)

- Equilibrium climate sensitivity (ECS) has been determined for 14 CMIP5 climate models. The ECS for CMIP5 spans up a range of 2.1-4.7K similar to the 2.1-4.4K range obtained with the previous CMIP3 generation of models. Cloud feedbacks are responsible for about 70% of the spread of climate sensitivity estimates amongst models, with a large contribution from the tropics. The combined water vapor + lapse rate feedback is found to also provide a non negligible contribution to the spread of climate sensitivity. (Deliverable 2.4)

- A physical formulation has been formulated that explains the positive cloud feedback through an increase of the vertical gradient of the moist static energy that supports the import of low moist static energy and dry air into the boundary layer and promotes a decrease of cloud amount. This hypothesis will be further explored to find out whether this mechanism can explain the spread of tropical cloud feedback exhibited by CMIP5 models under climate change. (Deliverable 2.4)

- Tropical Precipitation change patterns have been analysed and strong regional resemblances have been found..Decomposition into a thermodynamical and a dynamical component allows to to distinghuish between precipitation responses to the fast dynamical component and due to the slower (feedback driven) thermodynamic component. (Deliverable 2.4)

WP3 Main Results

- Large Eddy Simulation (LES) runs have run toward equilibrium for present and future climate conditions for three cloud types (Stratocumulus, Cumulus under Stratocumulus, Cumulus). These are the cloud types that contribute most to the uncertainty in cloud climate feedback. LES results show a negative feedback (in terms of change in cloud radiative forcing) for Stratocumulus and a neutral to positive feedback for the other two cloud types. (Deliverable 3.3 and 3.9)

- Further analysis for the Stratocumulus case show that the weakening subsidence and the increased Sea Surface Temperatures (SST) have opposite responses: weakening the subsidence leads to thicker clouds and hence to a negative feedback, while higher SST's lead to thinner clouds and hence to a positive feedback. The net effect is subtle and leads to a negative feedback. (Deliverable 3.3 and 3.9)

- Mixed Layer Model studies has brought further understanding physical understanding on how Stratocumulus fields are changing under a wider range of perturbations of SST, surface wind, free tropospheric temperature and humidity and subsidence. The results are in further support of the LES results. (Deliverable 3.5)

- 15 Single Column versions of climate models run have been run toward equilibrium present and future climate conditions for three cloud types (Stratocumulus, Cumulus under Stratocumulus, Cumulus). Analyses of these models in terms of changes in cloud radiative forcing and comparisons with the LES results show that SCM's vary strongly in both sign and magnitude in a way that is not supported by the LES results. The reasons for the mismatches of the SCM's with the LES results vary from model to model and individual analyses of the SCM's are needed to understand this. At least the LES results do provide a strong constraint that should be obeyed by the SCM's. (Deliverable 3.3 and 3.9)

- An ensemble of 6 LES codes have run a transition case of stratocumulus to cumulus such as observed during the ASTEX field experiment. A remarkable good agreement between the LES resultsand the observations have been found, that allow to use these LES results as a benchmark for Single Column Model (SCM) versions of climate models. A systematic comparison of 30 SCM codes with the LES codes do show that parameterization packages that perform the best are those that are either i) entirely newly conceived concepts or are ii) existing schemes have seen significant renovation of their internal structure in recent years. (Deliverable 3.3)

- High frequency output from six CFMIP climate models at selected gridpoints allowed to examine the diurnal cycle of clouds and cloud feedbacks. Models do capture the observed phase of the diurnal cycle in low cloud properties over the oceans. The models tend to show larger changes in low cloud properties in the warmer climate in the morning when more low cloud is present in the control. This results in shortwave cloud feedbacks being strongest and having the largest inter-model spread at this time of day.

Project Consortium:
EUCLIPSE is a collaborative effort of 12 European partners. The Management Board of the EUCLIPSE project is made up of the following persons: A. Pier Siebesma (Royal Netherlands Meteorological Institute, coordinator), Sandrine Bony (Institute Pierre Simon Laplace), Bjorn Stevens (Max Planck Institute for Meteorology), George Tselioudis (Academy of Athens), Stephan de Roode (Delft University of Technology),. The EU project officer is Dr. Claus Brüning (European Commission, DG Research).
The principle investigators of the other project partners are: Mark Webb, Mark Ringer Alejandro Bodas (Met Office), Frank Selten, Roel Neggers (KNMI), Johannes Quaas (MPI-Hamburg), Helene Chepfer, Frederique Cheruy, Jean-Louis Dufresne, Eric Guilyardi, Frederic Hourdin (CNRS-IPSL), Anastasia Romanou (Academy of Athens), Tim Palmer, Mark Rodwell (ECMWF), Harm Jonker (TU Delft), Hervé Douville, Isabelle Beau, Gilles Bellon, Dominique Bouniol, Francois Bouyssel, Michel Déqué, Françoise Guichard (Météo France), Gunilla Svensson, Michael Tjernstrom (Stockholm University), Ulrike Lohmann (ETHZ), Hanna Pawlowska (University of Warsaw), Michael Lautenschlager (DKRZ).The Advisory Board of EUCLIPSE is made up of the following persons: Christian Jakob (Monash University, Australia), Graeme Stephens (JPL NASA, USA), Ghassem Asrar (WCRP, Switzerland), Susanne Crewell (Cologne University). The Project Office at KNMI (The Netherlands) which is responsible for the routine administration of the project and the scientific direction, is staffed by Karin van der Schaft and A. Pier Siebesma.

Project Website:
http://www.euclipse.eu

3.2 Core of the report for the period: Project objectives, work progress and achievements, project management

3.2.1 Project objectives for the period August 2011 – February 2013

The EUCLIPSE Objectives are

Project Management:

- Manage efficiently the project.
- Communication between the European Commission and EUCLIPSE, including all forms of reporting specified in the consortium contract agreement.
- Provide the communication tools for the project: public and internal web sites.
- Organise annual general assemblies and project meetings.
- Ensure promotion of clustering and cooperation with related projects (both in FP7 and other international and national projects).
- Organization EUCLIPSE Summer School
- Preparation Comprehensive Textbook on “Clouds and Climate”

WP1

- Execute a suite of ESM simulations that include current-climate conditions, perturbed climate warming conditions, and idealised aqua-planet simulations. Implement model diagnostics packages that facilitate the application of process-based model evaluation techniques. Ensure cooperation with related projects, both in FP7 and in other international and national projects.\

WP2

- To evaluate the simulation of clouds, precipitation and radiation by climate and weather prediction models, point out systematic and compensating errors, and develop cloud metrics.
- To investigate whether and how the simulation of cloud and moist processes influences the simulation of the current climate, in particular the mean tropical precipitation and large-scale circulation, the tropical variability at intra-seasonal and inter-annual timescales, and the simulation of temperature extremes over Europe
- To quantify and to interpret the inter-model spread of climate sensitivity estimates and of the cloud and precipitation responses to climate change predicted by ESMs, to identify the regions, the cloud regimes and the meteorological conditions primarily responsible for this spread, and to explore the mechanisms that control this response in the different models.

WP3

- To conduct dedicated high resolution simulations with Large Eddy Simulation (LES) models and SCMs that will provide further insight in the cloud dynamical processes
- To evaluate ESMs experiments with observations for key cloud regimes on selected locations for present climate
- To analyse the response of boundary layer clouds in idealised and future climate conditions through the use of LES models and SCMs

WP4

- Develop and test hypotheses proposed to explain inter-model spread in cloud feedback and climate sensitivity in ESMs.

3.2.2 Work progress and achievements during the period

WP1: Evaluation Techniques and Climate Model Experiments

Most of the work for WP1 was already completed during the first 18 month period (see first progress report: http://www.euclipse.eu/index.html/) and will only be summarized here:

- All Climate Models participating in EUCLIPSE have implemented CFMIP Observation Simulator Package (http://cfmip.metoffice.com/COSP.html),
- All Climate Models participating in EUCLIPSE have finished a hierarchy of model experiments as proposed by CFMIP-2 as part of the CMIP-5 coordinated experiments.
- All Climate Models participating in EUCLIPSE have produced the output such as required by CFMIP2.

The model output diagnostics is available on the Earth System Grid (ESG) and has formed the basis for many of the analyses in WP2 and WP3 of EUCLIPSE. As such WP1 has formed the basis of much of the work that has been carried out in WP2 and partly in WP3.

The only left deliverable of this WP1 will be to archive the reprocessed version of EUCLIPSE model data products for long-term archiving beyond the runtime of the project. This will be done by the end of the project, when it has become clear which additional model runs EUCLIPSE wants to archive beyond the runtime beyond the runtime of the project.

WP2 : Climate Model Evaluation and Analysis

Introduction

The WP2 of EUCLIPSE entitled “Climate Model Evaluation and Analysis” has three main objectives: (1) to evaluate the climate models that will participate in the CMIP5 model intercomparison project, focusing on the representation of cloud processes, (2) to better understand the role of clouds in climate, both in present-day and in climate change, and (3) to better interpret inter-model differences in climate projections.

In the second period of the EUCLIPSE project has been focused on the deliverables of WP2 (and WP3). In this section summaries of the WP2 deliverables D2.1, D2.2, D2.4, D2.6 and D2.7 will be presented.

Evaluation of clouds, radiation and precipitation in ESMs using COSP, clustering and compositing techniques

Deliverable 2.1

1. Introduction

This section reports on several activities focused on the evaluation of the simulation of clouds and radiation in state-of-the-art climate models using the Cloud Feedback Model Intercomparison Project (CFMIP) Observation Simulator Package [COSP; *Bodas-Salcedo et al.*, 2011]. The document is split into three sections, with contributions from three different modelling centres. Section 2 is the contribution from the Met Office Hadley Centre, and focuses on the role of clouds in the radiation budget of the Southern Ocean. Section 3 documents the contribution from Stockholm University, and presents an evaluation of Arctic clouds and their impact on the surface radiation budget. Section 4 is the contribution from the Laboratoire de Meteorologie Dynamique/Institut Pierre Simon Laplace, and evaluates the vertical distribution of tropical lowlevel clouds and their optical properties. These three studies cover a very wide range of cloud types in different climatic regions, and therefore present a first step towards a comprehensive evaluation of the simulation of clouds in the latest generation of climate models.

2. Role of cyclones in the Southern Ocean shortwave bias

i) Introduction

We study the top-of-atmosphere (TOA) outgoing shortwave radiation (OSR) biases in the Southern Ocean in the atmosphere-only models of the Coupled Model Intercomparison Project phase 5 [CMIP5, *Taylor et al.*, 2012] models. The reduction of these biases in the atmosphere-only versions of these climate models is important to minimise sea-surface temperature biases when these models are coupled to dynamic oceans. We apply a recently developed methodology based on clustering and compositing that allows us to study the contribution of each cloud regime to the total error in the TOA radiative fluxes, and to relate that with the typical meteorological conditions in which these regimes occur. This methodology can then be used to inform parameterisation developments in the different modelling centres and eventually lead to a reduction of these biases.

Recently, *Bodas-Salcedo et al.* [2012] study the role of clouds in the Southern Ocean shortwave bias in the latest version of the atmosphere-only version of the Met Office model. They apply clustering and compositing techniques to identify the cloud regimes that are responsible for the bias and assess whether the recent changes in the model's parameterisations have targeted the right cloud regimes. Here we apply the same methodology to the CMIP5 ensemble. *Bodas-Salcedo et al.* [2012] combine the clustering methodology developed by *Williams and Webb* [2009] and the cyclone compositing from *Field and Wood* [2007]. *Williams and Webb* [2009] obtain 7 mid-latitude cloud 'regimes' by spatio-temporal clustering of daily ISCCP histograms of cloud top pressure (CTP) versus cloud optical thickness (τ). Then, the mean cloud albedo (α), CTP and cloud fraction (CF) is obtained for these regimes. Daily mean model outputs of α, CTP, and CF from the ISCCP simulator are then projected onto the observational clusters to assign model grid points to one of 7 cloud regimes. These regimes are labelled as 'shallow cumulus', 'cumulus-stratocumulus transistion', 'stratocumulus', 'mid-top', 'thick frontal', 'cirrus' and 'thin cirrus'. These names are intended to indicate the typical characteristics of the majority of cloud which makes up the regime. Once the model data are projected onto the observational regimes, we composite the results around cyclone centres following *Field and Wood* [2007] over the latitudes 40^{o}S-70^{o}S. A box covering 60 degrees in longitude and 30 degrees in latitude is centred on each cyclone. The cyclone centres are identified using minima in daily mean sea level pressure. Then, the relative frequency of occurrence of each regime at each gridbox around the cyclone centre is calculated by analysing all the cyclones in a two year period. This allows us to identify the typical synoptic conditions in which the cloud regime biases occur. This could be potentially used to develop hypothesis of model changes that target the meteorological conditions that prevail in those regions of the cyclones that are mostly responsible for the radiation bias.

Model	Institution	References
CanAM4	CCCma (Canadian Centre for Climate Modelling and Analysis, Victoria, BC, Canada)	
CNRM-CM5	CNRM (Centre National de Recherches Météorologiques, Météo-France, Toulouse,France) and CERFACS (Centre Européen de Recherches et de Formation Avancée en Calcul Scientifique, Toulouse, France)	*Voldoire et al.* [2012]
CSIRO-Mk3-6-0	Australian Commonwealth Scientific and Industrial Research Organization (CSIRO) Marine and Atmospheric Research (Melbourne, Australia) in collaboration with the Queensland Climate Change Centre of Excellence (QCCCE) (Brisbane, Australia)	*Rotstayn et al.* [2010]
INM CM4	INM (Institute for Numerical Mathematics, Moscow, Russia)	*Volodin et al.* [2010]
IPSL-CM5A-LR	IPSL (Institut Pierre Simon Laplace, Paris, France)	*Hourdin et al.* [in pressa]
IPSL-CM5B-LR	IPSL (Institut Pierre Simon Laplace, Paris, France)	*Hourdin et al.* [in pressb]
FGOALS-s2	LASG,IAP,CAS (Institute of Atmospheric Physics, the Chinese Academy of Sciences,Beijing,China	
GFDL-HIRAM-C180	GFDL(Geophysical Fluid Dynamics Laboratory, Princeton, NJ, USA)	
GFDL-HIRAM-C360	GFDL(Geophysical Fluid Dynamics LaboratoryPrinceton, NJ, USA)	
HadGEM2-A	Met Office Hadley Centre (Exeter, UK)	*Collins et al.* [2011]; *Martin et al.* [2011]
MIROC5	AORI (Atmosphere and Ocean Research Institute, The University of Tokyo, Chiba, Japan), NIES (National Institute for Environmental Studies, Ibaraki, Japan), JAMSTEC (Japan Agency for Marine-Earth Science and Technology, Kanagawa, Japan)	*Watanabe et al.* [2010]
MPI-ESM-LR	Max Planck Institute for Meteorology (Hamburg, Germany)	
MPI-ESM-MR	Max Planck Institute for Meteorology (Hamburg, Germany)	
MRI-AGCM3-2H	MRI (Meteorological Research Institute, Tsukuba, Japan)	*Mizuta et al.* [2012]
MRI-AGCM3-2S	MRI (Meteorological Research Institute, Tsukuba, Japan)	*Mizuta et al.* [2012]
MRI-CGCM3	MRI (Meteorological Research Institute, Tsukuba, Japan)	*Yukimoto et al.* [2011]

Table 1. *Models used in Section 2 of this study.*

ii) Model and Observational data

We use data from the AMIP experiment of the CMIP5 archive. Table 1 shows the list of models that had submitted data from the AMIP experiment to the CMIP5 archive at the time of conducting this study. These models are used to provide an overview of the climatological biases in a relatively large ensemble of models in Section 2.2. The Cloud Feedback Model Intercomparison Project phase 2 (CFMIP2), which is part of CMIP5, requests additional diagnostics to be produced from a subset of the CMIP5 experiments. In particular, it requests diagnostics from the COSP to produce diagnostics from the models similar to the ones provided by the observational datasets. In the analysis presented in this section we use the ISCCP simulator in COSP [*Klein and Jakob*, 1999; *Webb et al.*, 2001]. Future work will use a wider range of simulators. We use data from the D series of the International Satellite Cloud Climatology Project [ISCCP, *Rossow and Schiffer* , 1999] and TOA radiative fluxes from the same database [*Zhang et al.*, 2004]. We use daily α, CTP, CF and TOA radiative fluxes from the ISCCP-D1 and ISCCP-FD products. We also use the 10-year monthly climatology of TOA radiative fluxes from the Clouds and the Earth's Radiant Energy System [CERES; *Wielicki and Coauthors*, 1996], Energy Balanced and Filled (EBAF) dataset [*Loeb et al.*, 2009].

iii) Climatological bias of the CMIP5 AMIP ensemble

Figure 2 shows the annual OSR climatology over the southern hemisphere from the CERESEBAF observations (top-left), and the model differences with respect to this observational dataset. Another set of observations (ISCCP-FD), is also included as an additional model. ISCCP-FD shows the smallest biases with respect to CERES-EBAF, which suggests that absolute model differences greater than 10W m^{-2} are outside the observational uncertainty. Eight out of fifteen models show moderate/strong negative biases in OSR in the south of 40°S, six of them show a mixed pattern with positive and negative regional biases, and only one shows a strong positive bias. This suggests that most models tend to underestimate the OSR in the Southern Ocean, in line with the results from *Trenberth and Fasullo* [2010], although there is certainly a substantial spread within the model ensemble, as clearly shown in the zonal mean plot in Figure 2. This is consistent with the behaviour of a five-member ensemble of models run in forecast mode for the transpose-AMIP phase 2 experiment [T-AMIP2; *Williams et al.*, 2012], implying that these biases develop quickly during the first few days of evolution in most models.

iv) Cyclone compositing

At the time of conducting this study, the following seven models had submitted CFMIP2 daily diagnostics: CanAM4, CNRM-CM5, IPSL-CM5B-LR, HadGEM2-A, MIROC5, MPI-ESM-LR, and MRI-CGCM3. We focus only on these models for the rest of this section.

Figure 2 shows the composites of OSR around cyclone centres over the Southern Ocean [40°S, 70°S]. These composites have been constructed from two years of daily data (1985/6), both for the models and the observations. The axes show latitude and longitude relative to the cyclone centre, in degrees. The orientation of these plots is such that negative(positive) latitudes define the poleward (equatorward) side of the cyclone. The schematic at the bottom right hand side of Figure 2 depicts a typical position of the fronts in this frame of reference, consistent with the observational analysis of *Govekar et al.* [2011]. The frontal region, dominated by high, thick, highly reflective cloud, typically lies in the NE quadrant, with larger values of OSR. The frontal region is a region of strong large-scale ascent [*Bauer and Del Genio*, 2006]. *Bauer and Del Genio* [2006] also show that the cold-air sector behind the cold front is a region of large scale subsidence. This subsidence is relatively strong just behind the cold front, and weak or close to neutral in the rest of the cold-air sector. This cold-air sector is dominated by a smaller cloud coverage and less reflective clouds, and hence the OSR is significantly smaller than in the frontal region. All models analysed conform to this picture to a certain degree of approximation, with the exception of IPSL-CM5B-LR, which shows a very symmetric distribution of OSR around the cyclone centre. Figure 2 also shows difference plots with respect to ISCCP FD. Most models show a negative bias across the entire domain, with the smallest biases occurring in the frontal region, and the largest biases in the cold-air side of the cyclone. IPSL-CM5B-LR is the only model that shows a mixture of positive and negative biases.

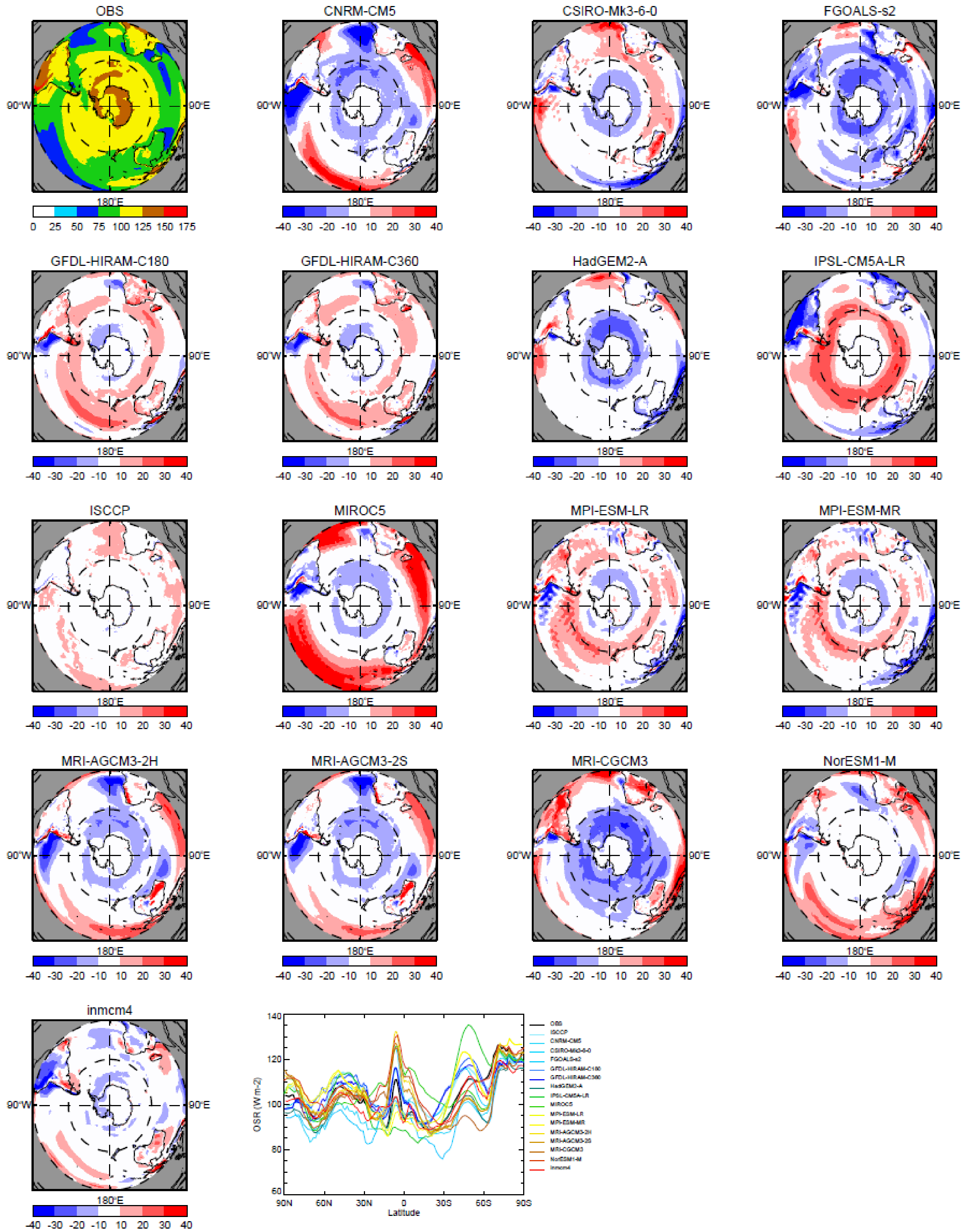

Figure 1:. *Southern Hemisphere annual climatology of TOA upwelling shortwave radiation. The top-left figure shows the CERES-EBAF observations, and the others the model biases with respect to CERES. ISCCP-FD is also shown as an additional model. The line plot shows the climatological zonal mean averages.*

In order to relate these radiative biases with the different cloud regimes, we compute the average properties of each regime within the cyclone composite domain. This allows us to calculate the contribution of each cloud regime to the total error in OSR (model minus ISCCP-FD) in that domain (Figure 3). This figure also shows the decomposition of the error in each regime into contributions from errors in the relative frequency of occurrence the radiative properties of the regime when simulated, and a co-variation term following, following [*Williams and Webb*, 2009]. It shows that there is a large degree of consistency among model biases in four cloud regimes. The mid-top regime is the dominant source of the deficit in OSR, with some contribution from the cirrus regime. Most models tend to compensate part of this deficit by producing too much frontal cloud. The errors in the thin cirrus regime are very small, which is not surprising because these clouds have very little impact in the shortwave radiation. As far as low-level regimes are concerned, the models show a consistent, albeit small, positive bias for shallow cumulus. Only MRI-CGCM3 shows a large positive bias in this regime. Two models show a large contribution from stratocumulus to the deficit in OSR, HadGEM2-A and MRI-CGCM3, and MIROC5 to a lesser extent. The behaviour of CNRM-CM5 in the stratocumulus regime, and to some extent IPSL-CM5B-LR and MPI-ESM-LR, is also interesting; it shows a negligible error in this regime due to a substantial cancellation of errors. It simulates this regime too frequently, but the clouds are not reflective enough.

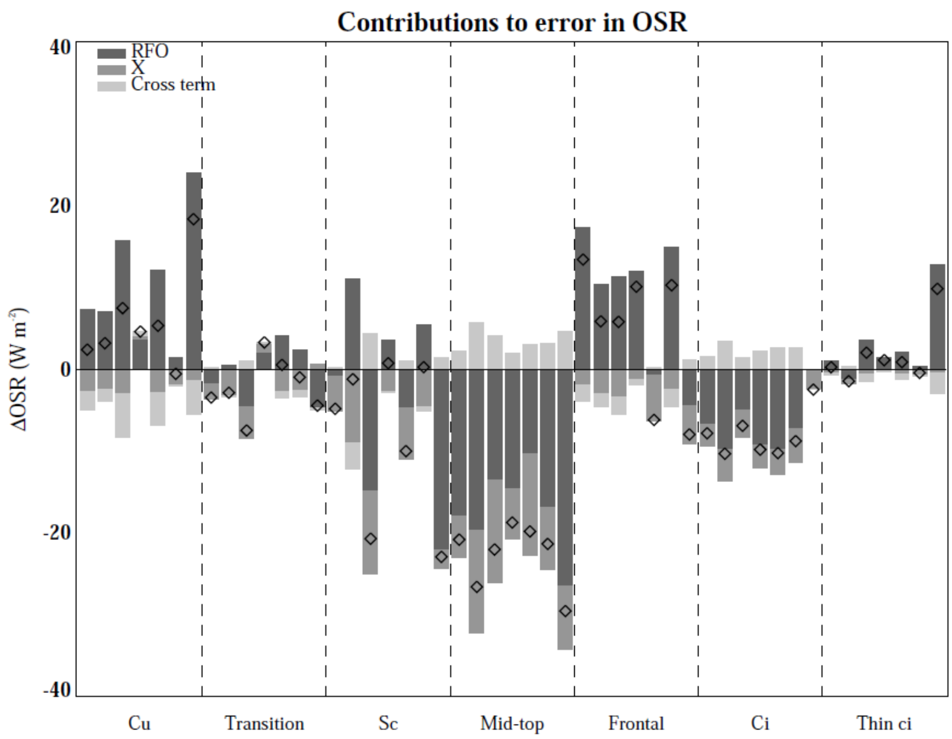

Figure 3. *Contribution of each cloud regime to the total error in the simulation of TOA outgoing shortwave radiation (model minus ISCCP-FD). The seven bars in each regime show results for each model, in the following order from left to right: CanAM4, CNRM-CM5, IPSL-CM5B-LR, HadGEM2-A, MIROC5, MPI-ESM-LR, and MRI-CGCM3. The total error in each regime is represented by the diamonds. The bars show a decomposition of the total error into contributions from errors in the relative frequency of occurrence (RFO), the radiative properties of the regime when simulated (X), and a co-variation term (Cross term) [Williams and Webb, 2009].*

Following *Bodas-Salcedo et al.* [2012], we plot cyclone composite maps of the RFO of each cluster. These maps help establishing links between the contributions to the OSR bias from each regime and the meteorological conditions in which the regimes occur. Figure 4 shows the results from the ISCCP data. It is reassuring to notice that the names assigned by *Williams and Webb* [2009] purely based on the radiative properties of the clusters are physically consistent with the area within the cyclone composite where those cloud types are expected to occur more frequently. The cold-air sector of the cyclone is dominated by the stratocumulus regime, with contributions also from the other two low-level cloud regimes (shallow cumulus, transition), and mid-level cloud. The frontal region is dominated by the frontal and mid-level regimes. The cirrus regime is mainly observed ahead of the leading edge of the frontal region, and the contribution from the thin cirrus regime is negligible.

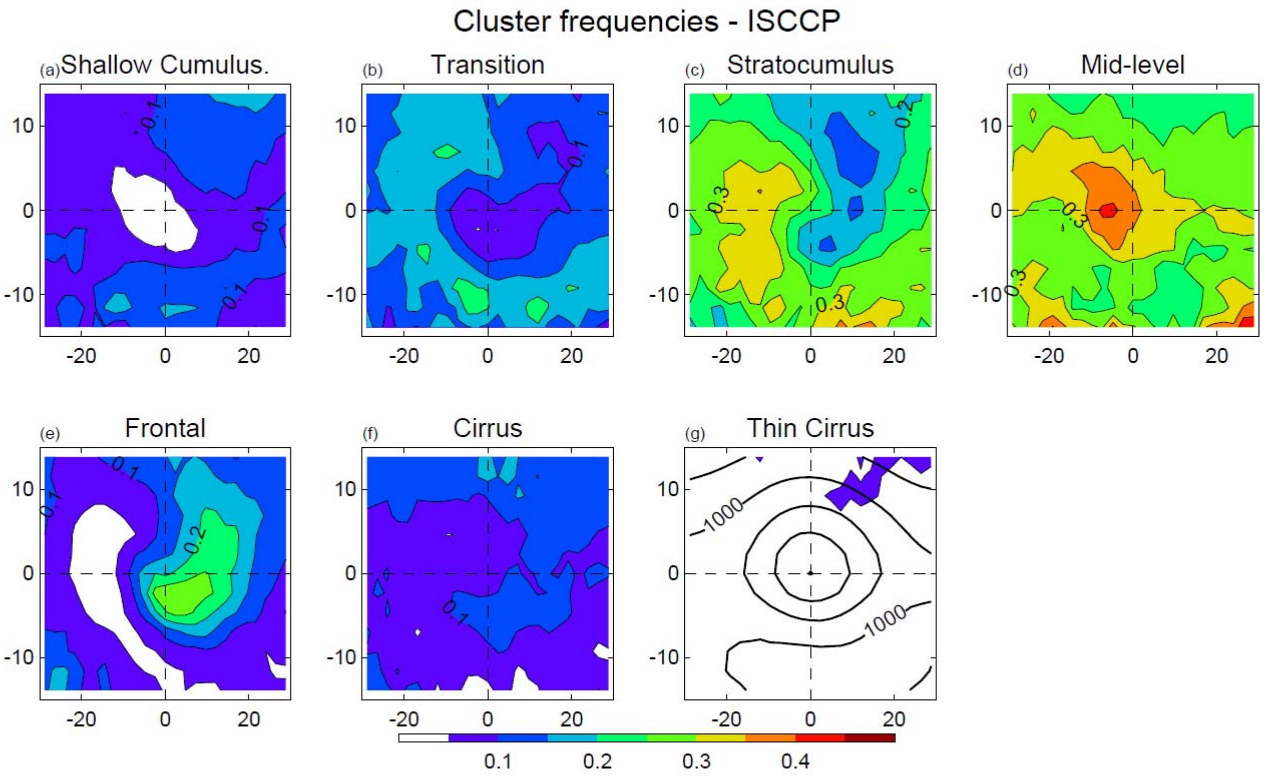

Figure 4. *Relative frequency of occurrence of ISCCP derived cloud regimes composited on a cyclone centred reference framework obtained from ERA-40 daily mean sea level pressure. The thick contours in figure (g) show the mean sea level pressure. The space between pressure contours is 8hPa, with the 1000hPa contour being labelled.*

Figures 5 to 7 show the model results, grouped by cloud regime, for the three low-level cloud regimes. All models overestimate the RFO of the shallow cumulus regime. In particular, CanAM4, HadGEM2-A, MIROC5, and MRI-CGCM3 (and to some extent, MPI-ESM-LR) show a strong overestimation of this regime in the cold-air side of the cyclone. Despite this excess of RFO, the impact in the OSR error is not large, except for MRI-CGCM3 (see Figure 3). This is due to the fact that the albedo and cloud fraction of this regime are low. Three models (IPSLCM5B- LR, MIROC5, and MPI-ESM-LR) also tend to overestimate the RFO of the transition regime in the cold-air side of the cyclone. It is interesting to notice that this is not clearly shown in Figure 3, where these models seem to show a very small error. This is due to some compensation of errors in the spatial distribution of this regime, with too much RFO of this regime in the cold-air side and too little in the frontal region. HadGEM2-A and MRI-CGCM3 underestimate the RFO of this regime in the cold-air side of the cyclone, and CanAM4 and CNRM-CM5 show a very good simulation of this regime. In the stratocumulus regime, CNRM-CM5, IPSL-CM5BLR, and MPI-ESM-LR simulate this regime too frequently, whereas HadGEM2-A, MIROC5, and MRI-CGCM3 do it too infrequently. CanAM4 shows again a good simulation of this regime.

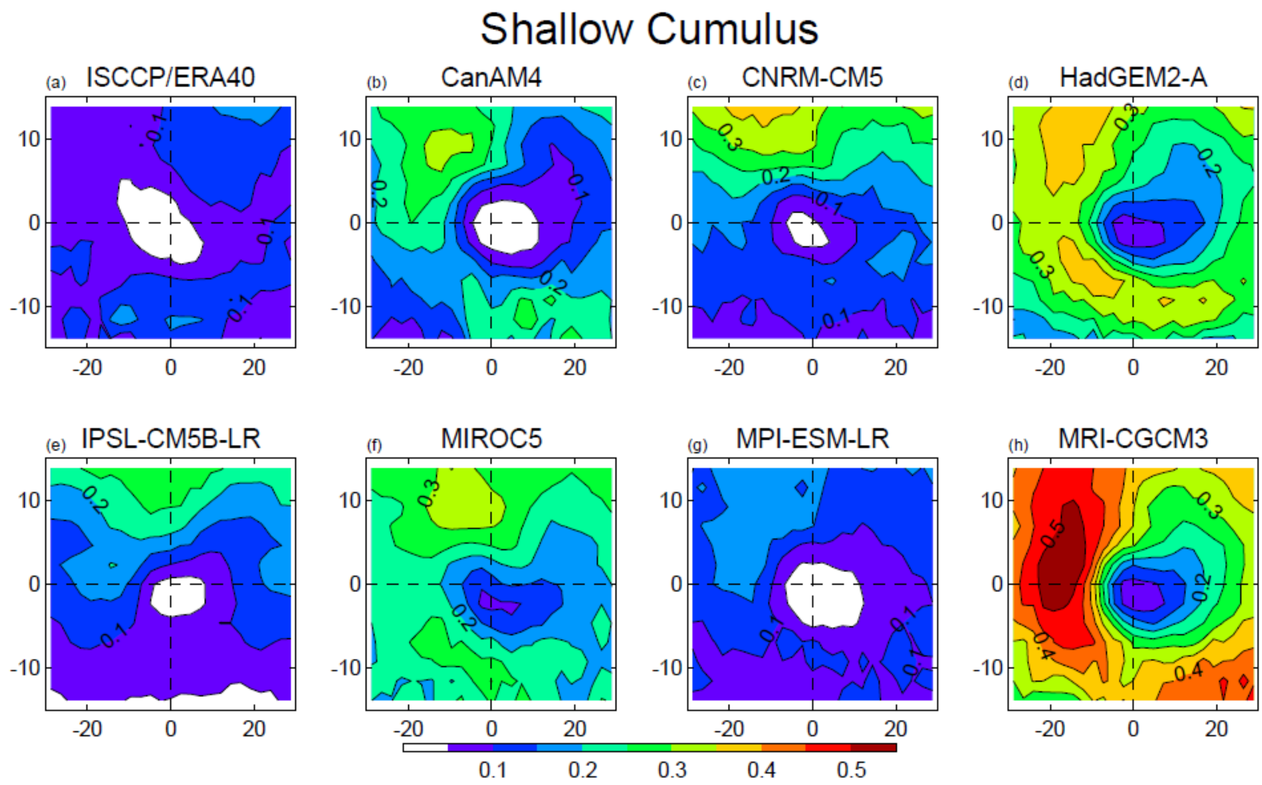

Figure 5. *Cyclone composite of the relative frequency of occurrence of the shallow cumulus cluster. (a) ISCCP observations, (b-h) model results.*

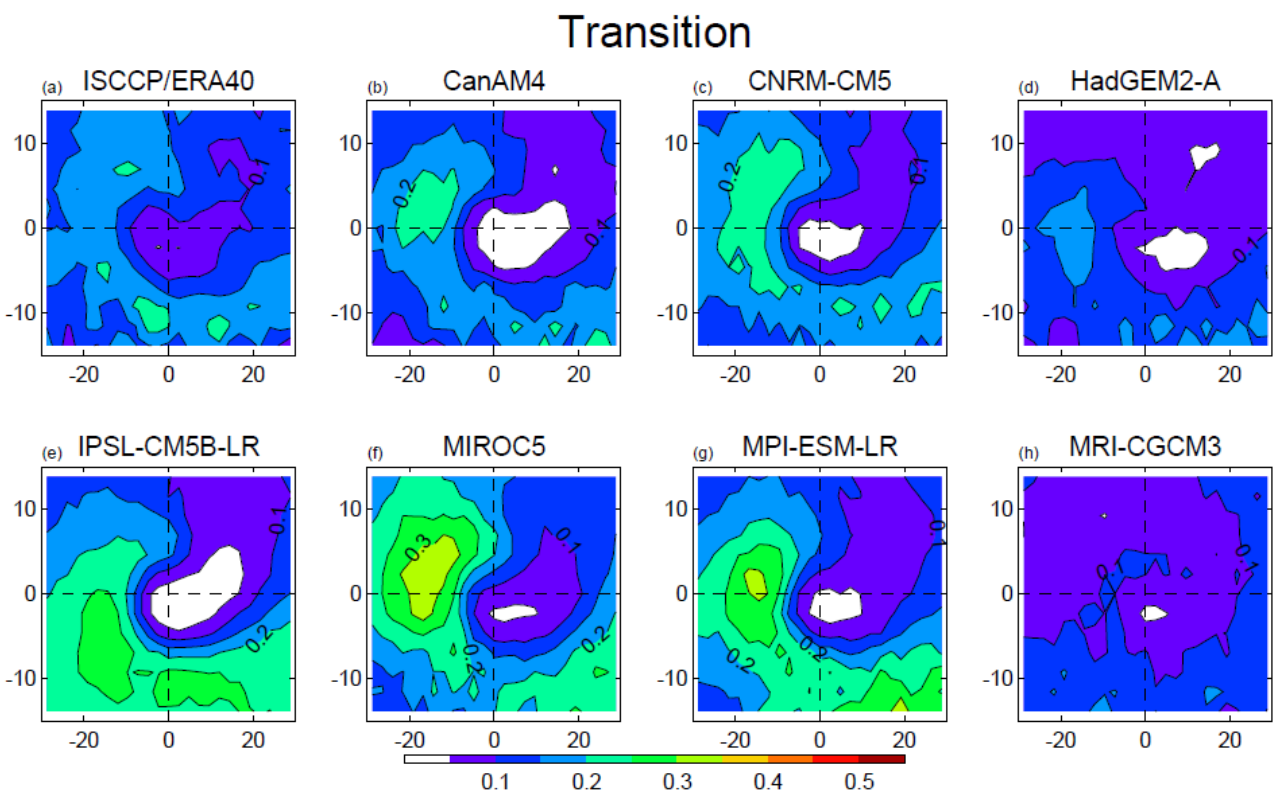

Figure 6. *As Figure 5 but for the transition cluster.*

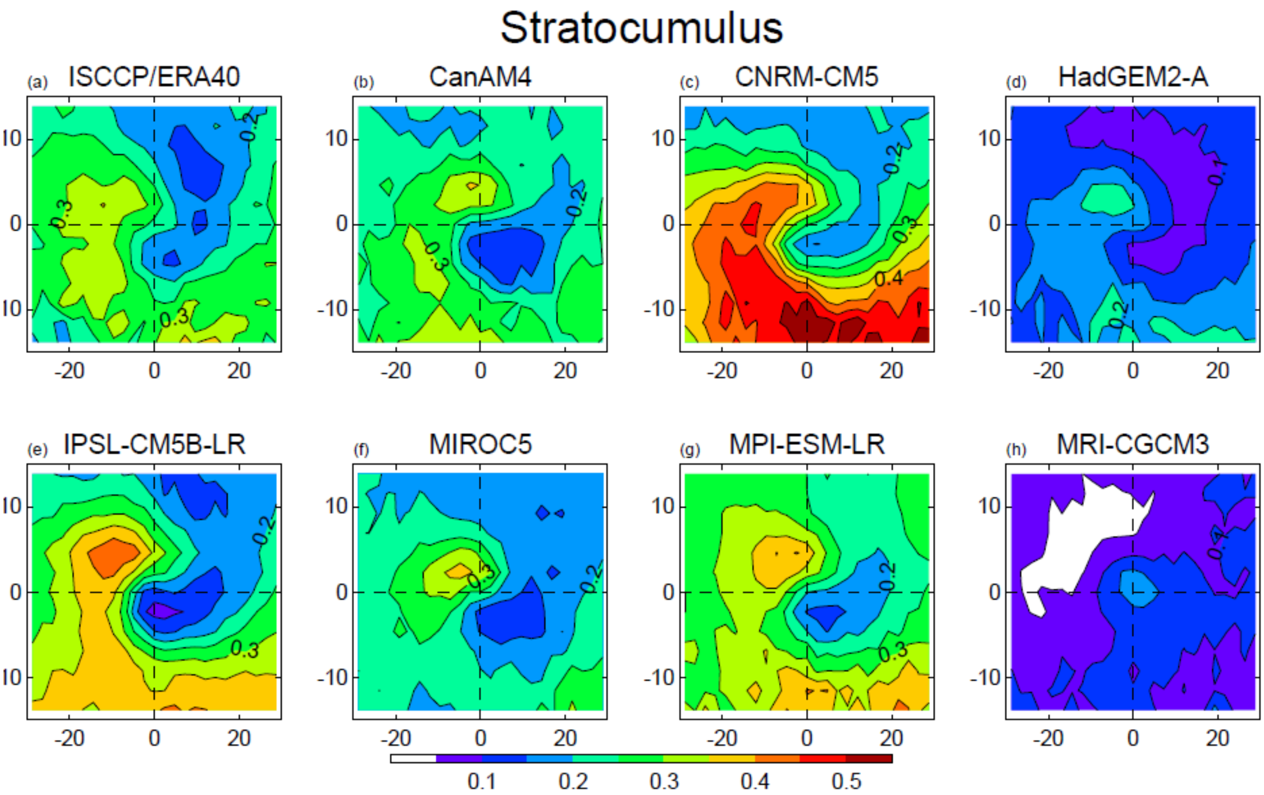

Figure 7. *As Figure 5 but for the stratocumulus cluster.*

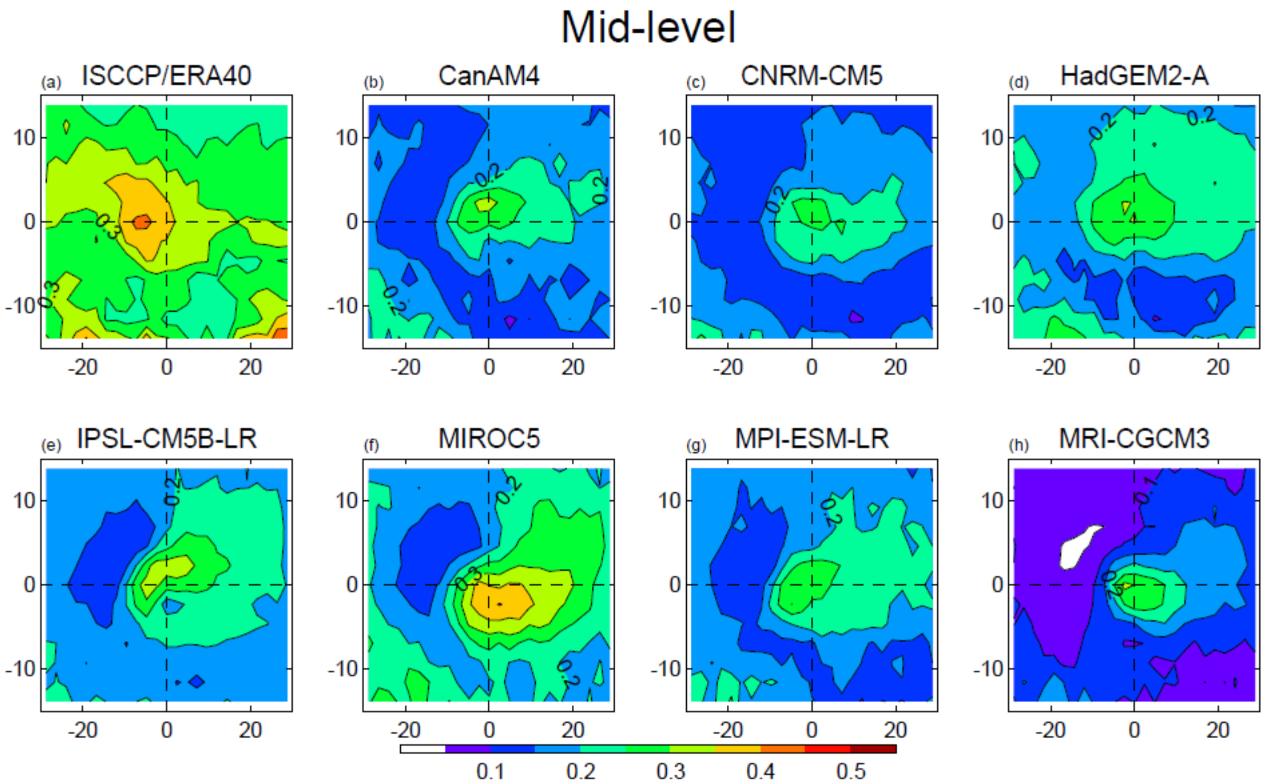

Figure 8. *As Figure 5 but for the mid-level cluster.*

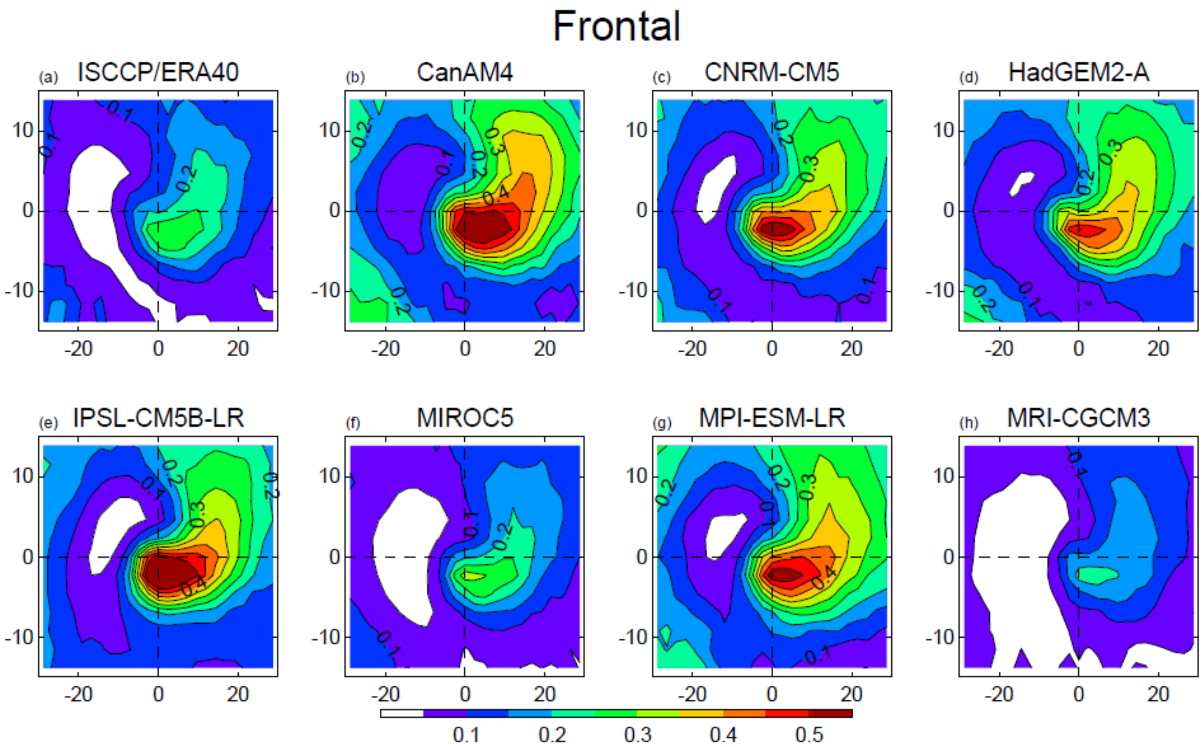

Figure 9. *As Figure 5 but for the frontal cluster.*

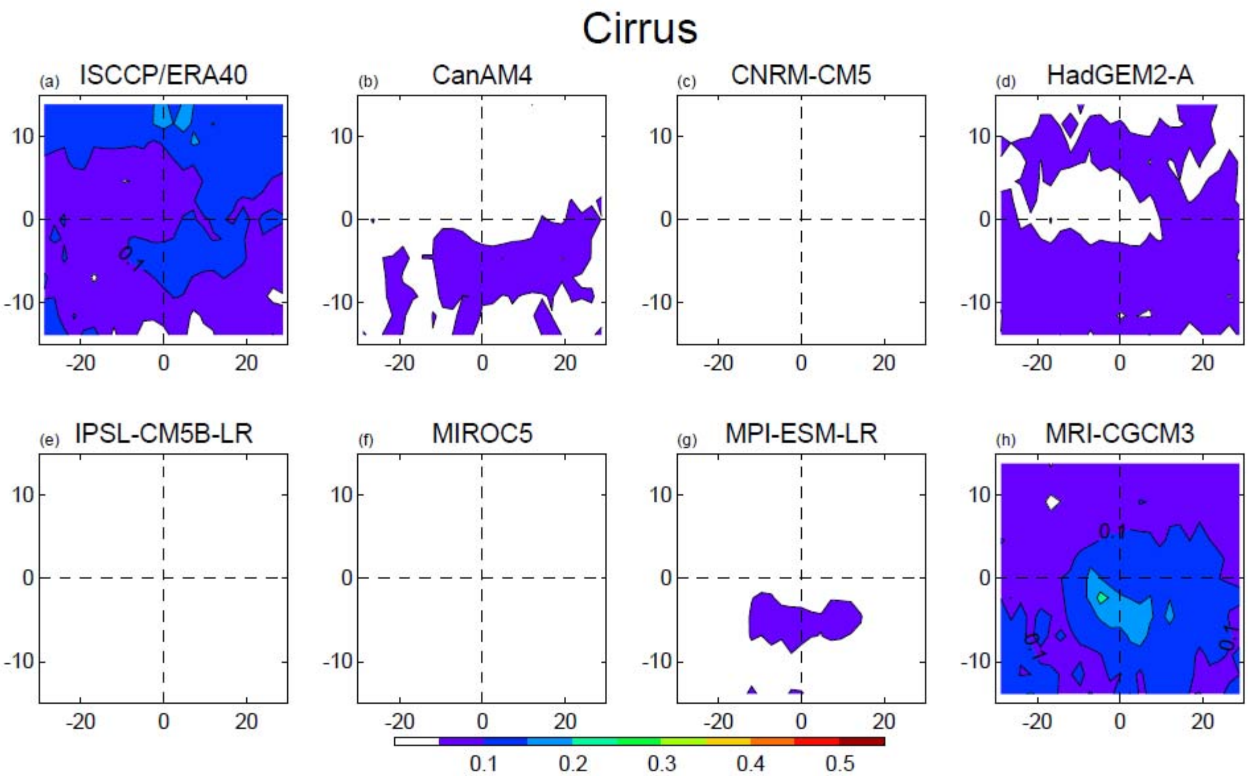

Figure 10. *As Figure 5 but for the cirrus cluster.*

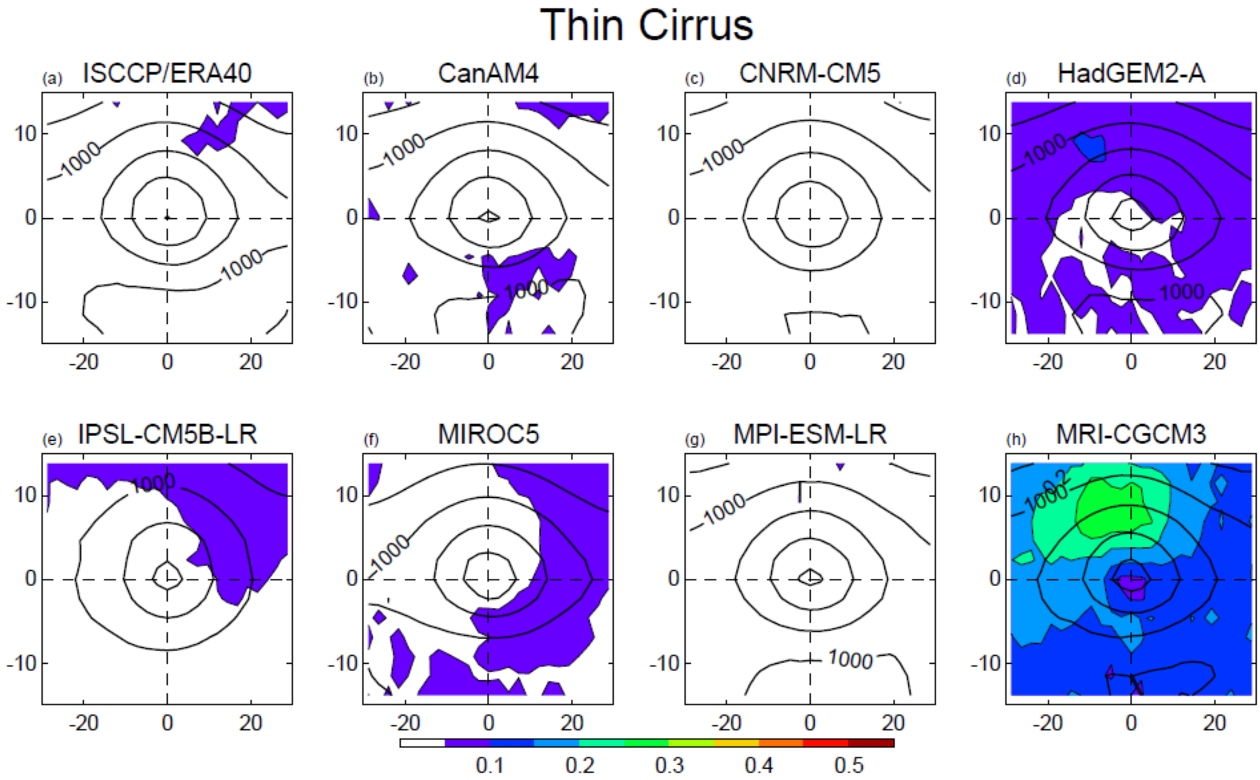

Figure 11. *As Figure 5 but for the thin cirrus cluster. The thick contours show the average mean sea level pressure in the cyclone composite domain. The space between pressure contours is 8 hPa, with the 1000 hPa contour being labelled.*

Models generally show a lack of mid-level cloud, this deficit being more severe in the cold air sector of the cyclone (Figure 8). A typical error of 10% absolute difference in the RFO of this regime would produce an approximate bias of 10W m^{-2}, consistent with the results in Figure 3. HadGEM2-A and MRI-CGCM3 are the models with the strongest OSR bias in the cold-air sector. They both share a consistent simulation of too much shallow cumulus regime, and too little transition and stratocumulus. This, added to the common lack of mid-level cloud makes the OSR bias to be larger in the cold air sector in these two models. Most models tend to simulate the frontal cloud regime too frequently (Figure 9) which explains its positive contribution to the OSR bias, which compensates for the negative contribution of other regimes. MIROC5, and especially MRI-CGCM3 show the opposite behaviour, with too little frontal cloud (Figure 3). Generally, models show a lack of cirrus (Figure 10), which contributes significantly to the total OSR deficit. Very little thin cirrus are observed by ISCCP, and most models capture this (Figure 11). Only HadGEM2-A and MRI-CGCM3 show some tendency to overestimate their population. Only in the case of MRI-CGCM3 the excess RFO of thin cirrus is radiatively relevant.

v) Summary and future work

It has been shown that the mid-top level regime is responsible for most of the OSR bias in models. However, due to the limitations of the ISCCP retrievals, this regime may contain a mixture of mid-level cloud and low-level cloud with thin, high cloud above. The results from Haynes et al. [2011] suggest that both situations contribute to the RFO of this cluster. We plan to extend this analysis to include cloud vertical distribution information from CloudSat and CALIPSO. This should help elucidate the relative contribution of these two different situations to the mid-level regime, and hence inform parameterisation developments that may help reducing the biases.

3. Evaluation of Clouds in the Arctic

i) Introduction

The Arctic is a region associated with extensive cloudiness [e.g. *Karlsson and Svensson*, 2011]. Due to commonly low cloud tops and relatively small insolation, in combination with the highly reflective surface, the net cloud radiative effect (CRE) at the TOA is small. However, for the surface energy budget, the Arctic clouds play a crucial role. Thus when evaluating how the Arctic clouds are simulated by climate models, it is appropriate to take on a surface perspective on the analysis as was done in previous studies of the CMIP3 model suite [*Karlsson and Svensson*, 2011; *Svensson and Karlsson*, 2011]. Results from these two studies are included in the analysis reported below for comparison. The Arctic region, due to harsh environmental conditions and due to challenges for remote sensing, is lacking long-term reliable observations with high spatial coverage. The aim of the analysis is to identify common structural problems in the climate models guided by the observations available.

ii) Annual Cycles

Figure 12 shows the climatologically averaged annual cycles of cloud parameters over the sea-ice covered ocean north of the Arctic circle (66.6N) in 16 CMIP5 models, the CMIP3 model ensemble, the INTERIM reanalysis and APP-x retrievals. Although CMIP5 and CMIP3 ensemble model medians show good agreement both with each other and with the observations (APP-x) in terms of total cloud fraction (Figure 12a), the across model spread is substantial. This is especially true wintertime when the CMIP5 model ensemble shows a range in total cloud fractions from 30% to 95%. There is no obvious over-all improvement in the simulation of total cloud cover between CMIP3 and CMIP5. In winter the across-model spread is unchanged while it is even larger in the CMIP5 ensemble compared to the CMIP3 ensemble in summer. A smaller number of members in the CMIP3 ensemble may partly explain this result.

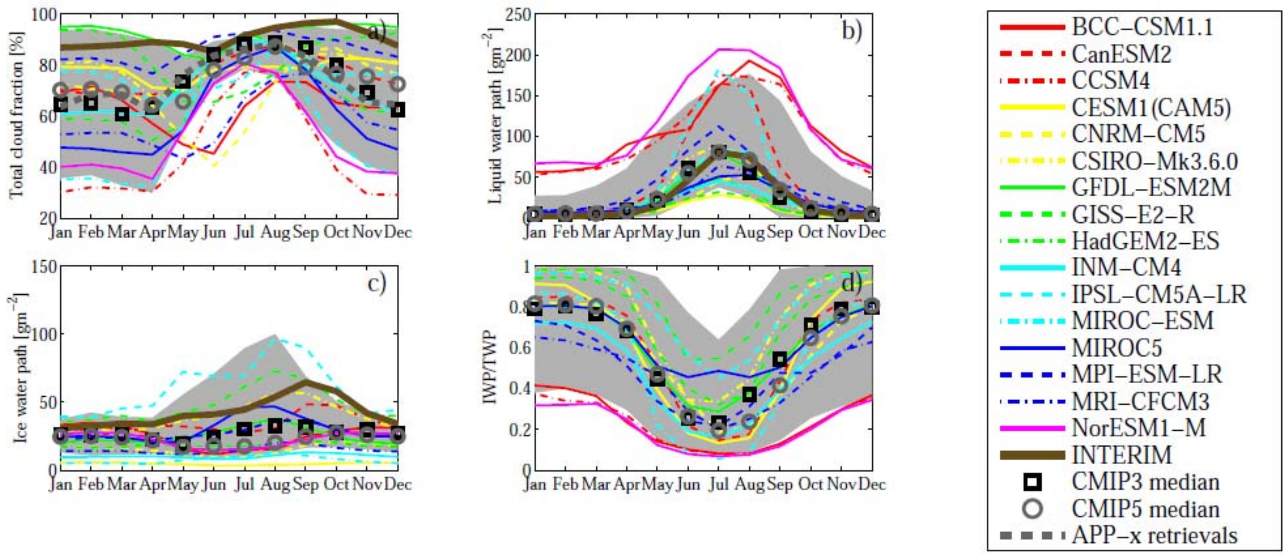

Figure 12. *Climatological seasonal cycles, area averaged over sea-ice covered ocean north of the Arctic circle (66.6N), of a) total cloud fraction, b) liquid water path, c) ice water path and d) the ice fraction of the total cloud water in CMIP5 models, ERA-INTERIM and observations. Period considered is 1980- 2004. The grey envelope indicates the range of the CMIP3 models evaluated in Karlsson and Svensson [2011].*

Neither has the across-model spread in the vertically integrated liquid and ice condensate (LWP and IWP) improved from the CMIP3 (Figure 12b and c). Three models (BCC, CCSM4 and NorESM) simulate substantial amounts of liquid condensate during the winter. Considering that CCSM4 and NorESM are in the lower end of winter total cloud fraction, this indicates that the clouds present are optically thick. The feature that clouds in the Arctic, although well below freezing, contain liquid condensate [e.g. *Verlinde et al.*, 2007], has previously not been well simulated [*Prenni et al.*, 2007; *Tjernstrom et al.*, 2008]. The presence of liquid condensate can substantially change the emissivity of the cloud and thus have large influence on the surface energy budget. In a regional model, by perturbing the number of ice nuclei available, *Prenni et al.* [2007] showed that maintaining liquid in the clouds could lead to large changes in the surface radiative budget (up to 100W m^{-2}). During winter in the CMIP5 model ensemble, a majority of the models simulate more than four times solid over liquid condensate (Figure 12d). To our knowledge, there is no long term record of typical LWP and IWP in the inner Arctic. However, measurements during the SHEBA campaign (winter 1997-1998) indicate an ice- to total water path ratio of about 0.6 for single layer mixed-phase, all-ice and all-liquid clouds combined [*Shupe et al.*, 2006].

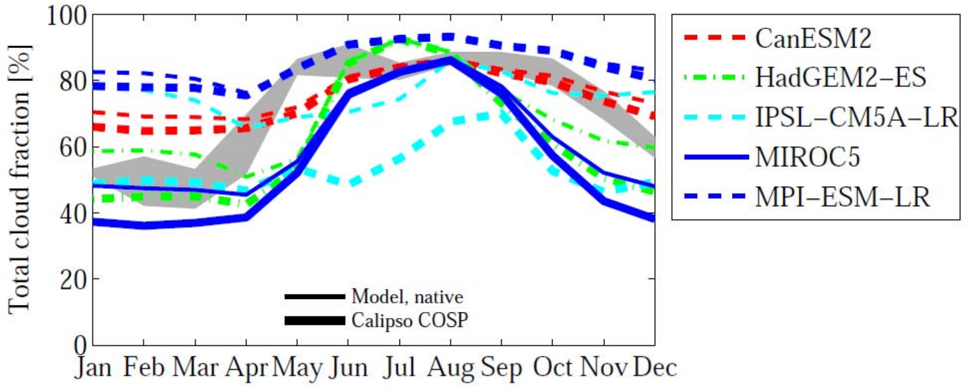

Figure 13. *climatological seasonal cycles, area averaged over sea-ice covered ocean north of the Arctic circle (66.6N), of total cloud fraction. Thin lines represent models native cloud fraction, thick lines represent the total cloud cover from the Calipso-simulator. Period considered is 1980-2004. The grey envelope indicates the inter-annual range in CALIPSO-GOCCP observed total cloud fraction (June 2006 - Dec 2010).*

The large across-model spread in models native total cloud fractions can potentially be attributed to differences in the frequency of occurrence of optically thin clouds between the models. By the use of satellite simulators, which mimics the retrieval algorithms of the sensors, but on the simulated atmospheric state, a more fair model-to-model and model-to-observation comparison can be done. Figure 13 shows the climatological annual cycle of models native total cloud cover along with the total cloud cover from the CALIPSO simulator for the subset of the models in Figure 12 that until now have delivered this variable to the CMIP5 archive. The grey envelope indicates the observed range in monthly averaged CALIPSO total cloud cover. In summer, all models, except IPSL, show negligible differences between the native and the simulator's total cloud cover. In general, the simulated summer clouds are thus optically thick enough to be detected by the simulator. In winter, all models, to various degrees, show differences between the native and simulator's total cloud fraction, the native cloud fraction always being larger. The annual cycle is therefore more pronounced in terms of the simulators' total cloud fraction. Comparing Figure 12a with Figure 13 it is evident that the subset of models that have the CALIPSO simulator total cloud fraction available, to a large extent, represents the across-model winter spread in total cloud fraction.

iii) Winter

To further investigate the consequences of the substantial across-model spread in Arctic winter cloud simulation for the surface energy budget we will use the concept of surface CRE. The surface CRE is defined as the difference in surface net radiative fluxes between all-sky and clear-sky conditions [e.g. Ramanathan et al., 1989; Karlsson and Svensson, 2011]. In the Arctic winter the sun is absent, thus the surface CRE boils down to only be in the longwave. Figure 14 shows the density scatter plot of surface longwave CRE and total cloud fraction (CALIPSO simulator) for the subset of models analyzed in Figure 13. The foundation of the scatter plots are all monthly averaged December, January and February sea-ice covered grid points north of the Arctic circle for the years 1980-2004. The shape of the density surfaces show large differences. HadGEM2 and MIROC5, which are the models with the most pronounced annual cycle in total cloudiness (Figure 13), also have the most confined scatter fields. This indicates these models have less variability in cloud altitude and emissivity, which results in strong correlation between the cloud fraction and the radiative influence at the surface. The three remaining models show larger spread of the scatter field, indicating larger variability. In these model overcast conditions can be associated with a wider range of surface CRE values, implying higher sensitivity to cloud microphysics (e.g. hydrometeors of liquid or solid phase) and/or cloud base temperatures.

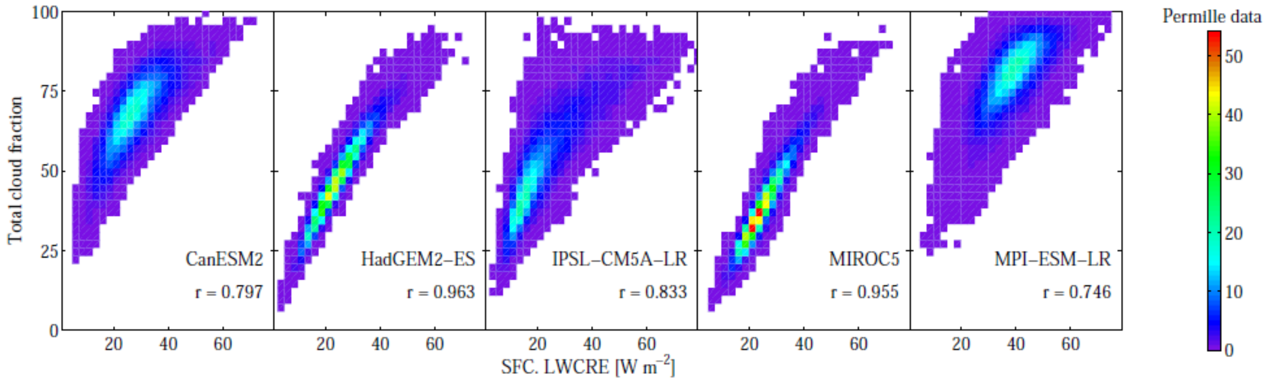

Figure 14. *Density scatter plots of monthly mean surface cloud forcing versus CALIPSO COSP total fraction for all wintertime (DJF) sea-ice covered grid points north of 66.6N during the period 1980-2004. The density is given as per mille data in each histogram bin. The bin size is 2.5 Wm^{-2} x 2.5 %. The correlation coefficient (r) between the parameters is given in each panel.*

In Figure 15 average values of the vertical integrated ice-to-total condensate ratio, vertical total condensate and near surface temperature are projected onto the density scatter fields of Figure 14. All models show an overall dependence such that smaller IWP fractions (i.e. more LWP) are associated with stronger surface CRE (Figure 14, upper panels). HadGEM and MPI show relatively small variability of the IWP fraction over the scatter field. In terms of total water path (TWP), all models have higher values associated with larger surface CRE (Figure 15, middle panels). The amount TWP in fully overcast conditions does differ substantially between the models, still these conditions are associated with more or the less the same surface CRE. This suggests that all models manages to have clouds with low cloud base that also are saturated in the longwave. Only MPI and IPSL (and to a minor extent CanESM) show fully overcast conditions associated with low surface CRE, which indicate the presence of high-level clouds and/or optically thinner clouds. This also suggests that, in overcast conditions, these kinds of clouds are absent or are at least are not responsible for the surface CRE signature in HadGEM and MIROC5. The averaged surface air temperature projected on the 2D-histograms is shown in the bottom panels of Figure 15. For overcast conditions, as expected, grid points with large surface CRE are also showing the highest temperature. In the full range of total cloud fraction, MPI, IPSL and CanESM show this dependence. The temperature results of HadGEM and MIROC5 in the low surface CRE/small cloud cover range, showing larger surface CRE to be associated with lower temperatures are surprising and need further investigation.

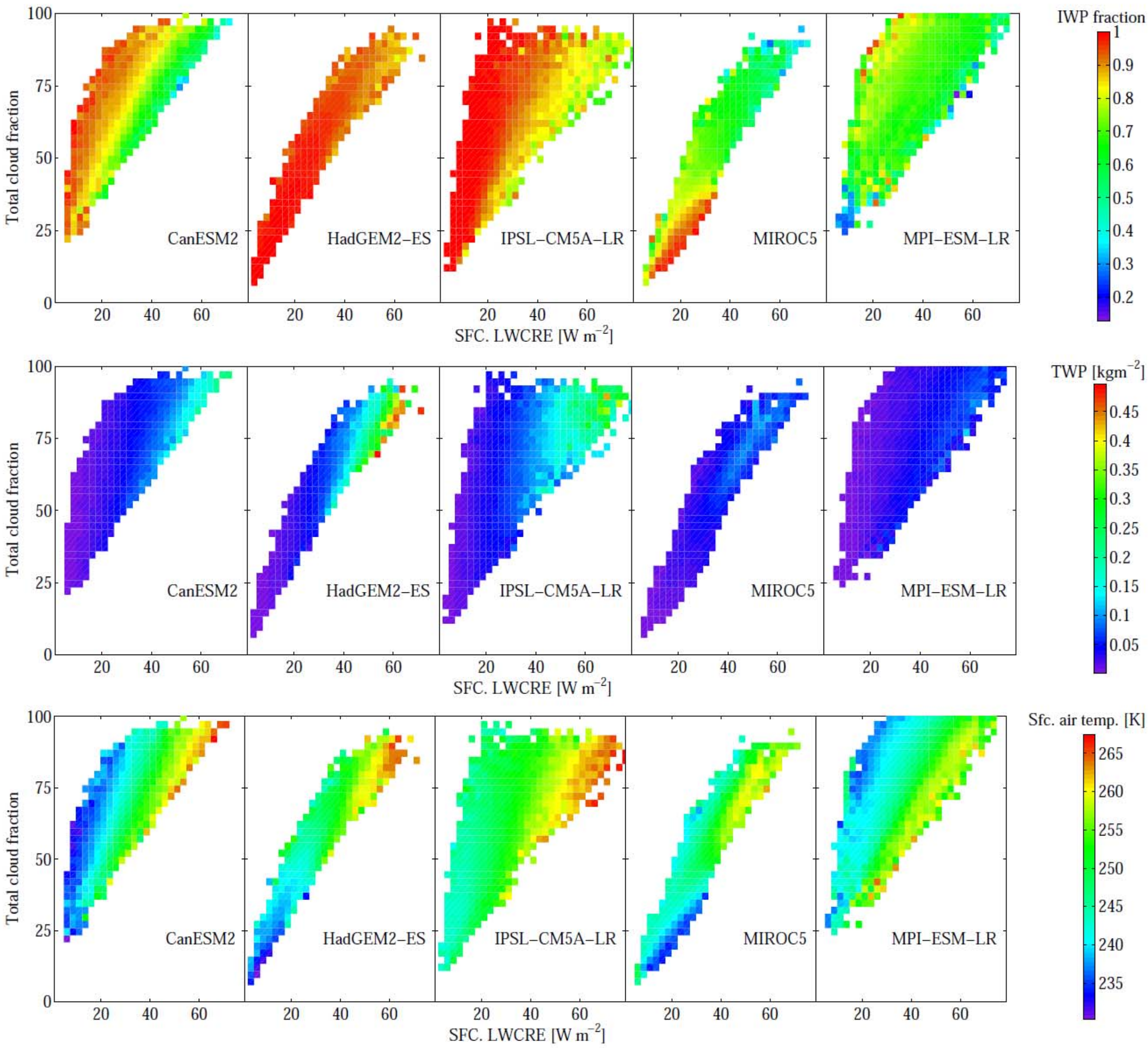

Figure 15. *projections of average ice condensate fraction, total water path and near surface temperature on the 2D-histogram of Figure 14.*

4. Vertical Distribution of Tropical Low-level Clouds and their Optical Properties

i) Introduction

The representation of tropical low-level clouds in several CMIP5 models is evaluated against those observed by the CALIPSO and PARASOL satellites. The CALIPSO and PARASOL satellite simulators from the COSP have been used to facilitate the comparison. Combining state-of the- art active and passive satellite instruments retrievals alongside their simulator counterparts allows for new techniques of evaluating the vertical distribution of low-level clouds, as well as their optical properties, in each model listed in Table 2. This work strives to answer the question: How well do models represent the vertical distribution of clouds and their optical properties in tropical low-level clouds?

Institute	*ModelName*	*Version*	
		Amon	cfMon
IPSL	IPSL-CM5A-LR	2011.04.27	2011.11.19
IPSL	IPSL-CM5B-LR	2012.05.26	2012.05.26
CNRM	CNRM-CM5	2011.10.06	2011.10.06
MPI-M	MPI-ESM-LR	2011.10.05	2012.02.15
MOHC	HadGEM2-A	2011.08.03	2011.08.09
CCCma	CanAM4	2011.10.20	2011.10.20

Table 2. *List of CMIP5 models used in Section 4 of this study. AMIP Experiment from 200606-200812.*

The simulator outputs are compared to both PARASOL and CALIPSO GOCCP data sets which are part of the Cloud Observations for Model Evaluation (CFMIP-OBS). CALIPSO GOCCP is based on the CALIOP Level 1B NASA Langley Atmospheric Sciences Data Center CALIPSO data sets. The Level 1B lidar Scattering Ratios (SR) instantaneous profiles are averaged onto a GCM grid resolution of 2°x2°) and 40 vertical levels from which cloud diagnostics are inferred [Chepfer et al., 2008, 2010]. The CALIPSO GOCCP data referred to as CALIPSO data hereafter. The satellite observations are combined with ECWMF ERA-Interim reanalysis data [Dee et al., 2011] to determine the large-scale environment.

ii) Vertical Distribution of Low-level Clouds

A study of the vertical distribution of stratocumulus and shallow cumulus clouds in the Tropical band (30N to 30S) was performed. Stratocumulus and shallow cumulus cloud regimes were identified according to large-scale environment as defined by *Klein and Hartmann* [1993]; *Bony et al.* [2004], and *Medeiros and Stevens* [2011]. Regions of large-scale subsidence are first identified using the vertical velocities (ω) at 500 hPa and 700 hPa. Low-cloud regimes are defined as having $\omega_{500hPa} \geq 10$ hPa day^{-1} and $\omega_{700hPa} \geq 10$ hPa day^{-1}. Next, the lower tropospheric stability (LTS $=\theta_{700hPa}-\theta_{sfc}$), where ($\theta$) is potential temperature, is used to distinguish between stratocumulus and shallow cumulus cloud regimes. When LTS $\geq$ 18.55 K, stratocumulus prevail; whereas if LTS = 18.55 K, shallow cumulus prevails [*Medeiros and Stevens*, 2011]. Within these two dynamically and thermodynamically defined cloud regimes, points of 'only' low-level cloud conditions are identified. Only low-level cloud conditions are defined as having high- and mid-level (< 680 hPa) cloud covers < 0.05, as determined by CALIPSO GOCCP and the lidar simulator. At each point identified, the vertical distribution of clouds from CALIPSO or the lidar simulator are taken. The frequency of occurrence of clouds of a given fraction, at a given altitude, is presented in Fig. 16 for each model.

Stratocumulus Clouds Distributions

The CALIPSO 3D low-level cloud profiles for tropical stratocumulus clouds are presented in Fig.16a. The observed 3D cloud profiles show clouds with fractions above 50% reaching frequencies >0.01 below 2 km. The greatest frequency of clouds, occur between 0.5 km and 2 km with fractions ≤ 20%. Above 2 km, clouds generally have smaller fractions.

The IPSL-CM5A model significantly underestimates the cloud fraction and frequency of clouds above 0.5 km. As such, the IPSL-CM5A misses the greatest frequency of clouds found in observations. Below 1 km, the lack of clouds is partially due to the frequent production of optically thin clouds (3<SR<5) in IPSL-CM5A discussed earlier. Below 0.5 km, however, the frequency of low-level clouds with fractions greater than 60% are overestimated. The stratocumulus clouds are much too close to the surface.

IPSL-CM5B shows improvement to clouds in the lowest 1 km of the atmosphere, although large cloud fractions still occur much too frequently. The frequency of clouds between 1 km and 3 km frequently have cloud fractions less than 20 %.

The CNRM-CM5 model produces a range of cloud fractions less than 20% at all altitudes; and cloud fractions ≤40% up to 2.5 km. Beyond 40%, however, very few low-level clouds are produced. As previously described, the CNRM-CM5 lack stratocumulus clouds; hence the lack of large cloud fractions at the lowest levels.

The MPI-ESM, CanAM4 and HadGEM2-A models all produce a distribution of cloud fractions throughout the atmosphere. Both MPI-ESM and CanAM4 frequently produce cloud fractions greater than 50%, however, these clouds mainly occur below 1 km. Cloud fractions above 50 %, from 1 to 2 km in these two models are distinctly lacking. HadGEM2-A produces cloud fractions greater than 50% for altitudes up to 2 km, and as such, best captures the distribution of low-level stratocumulus clouds seen in CALIPSO observations despite a slight overestimate in the frequency of clouds with fractions greater than 80%.

Shallow Cumulus Cloud Distributions

CALIPSO 3D low-level cloud profiles show tropical shallow cumulus clouds as having a greater frequency of smaller cloud factions compared to the stratocumulus regime (Fig. 16). Clouds with fractions greater than 40% rarely exceed frequencies of 0.01. The greatest frequency of clouds occur between the surface and 3 km; and clouds with fractions greater than 50% most frequently occur between 1.5 km and 2 km. Clouds above ~2 km, indicative of deeper cumulus clouds, naturally occur more frequently compared to the stratocumulus regime.

The IPSL-CM5A model shows a greater frequency of clouds with fractions less than 20% between 0.5 and 2 km. Clouds with fractions greater than 20% remain below 0.5 km and occur less frequently compared to the stratocumulus regime. Unlike the observations, IPSL-CM5A neither decreases the frequency of clouds in the lowest layer, nor increases the frequency of clouds greater than 20% above 1 km. The IPSL-CM5B model shows a decrease in the frequency of all cloud fractions below 1 km, however, they still have a distribution similar to the stratocumulus regime.

IPSL-CM5B also improves the frequency of clouds with fractions >20% between 1 km and 3 km. The 3D vertical distribution of clouds in the CNRM-CM5 model are very similar between the shallow cumulus and stratocumulus regime. As seen in observations, there is an increase in the frequency of higher altitude clouds. The peak of occurrence ranges from 1 km to 1.5 km; similar, though slightly lower, than found in CALIPSO.

Interestingly, the MPI-ESM, CanAM4 and HadGEM2-A models all show a considerable amount of clouds with fractions greater than 50% below 1.5 km. The overestimation of clouds below 1.5 km combined with an underestimation of clouds with fractions of 30% to 60% between altitudes of 1.5 km and 3 km give the impression clouds are bounded to surface, similar to that seen in the stratocumulus regime. In the following section, the impact of the vertical distribution on the optical properties of low-level clouds is discussed.

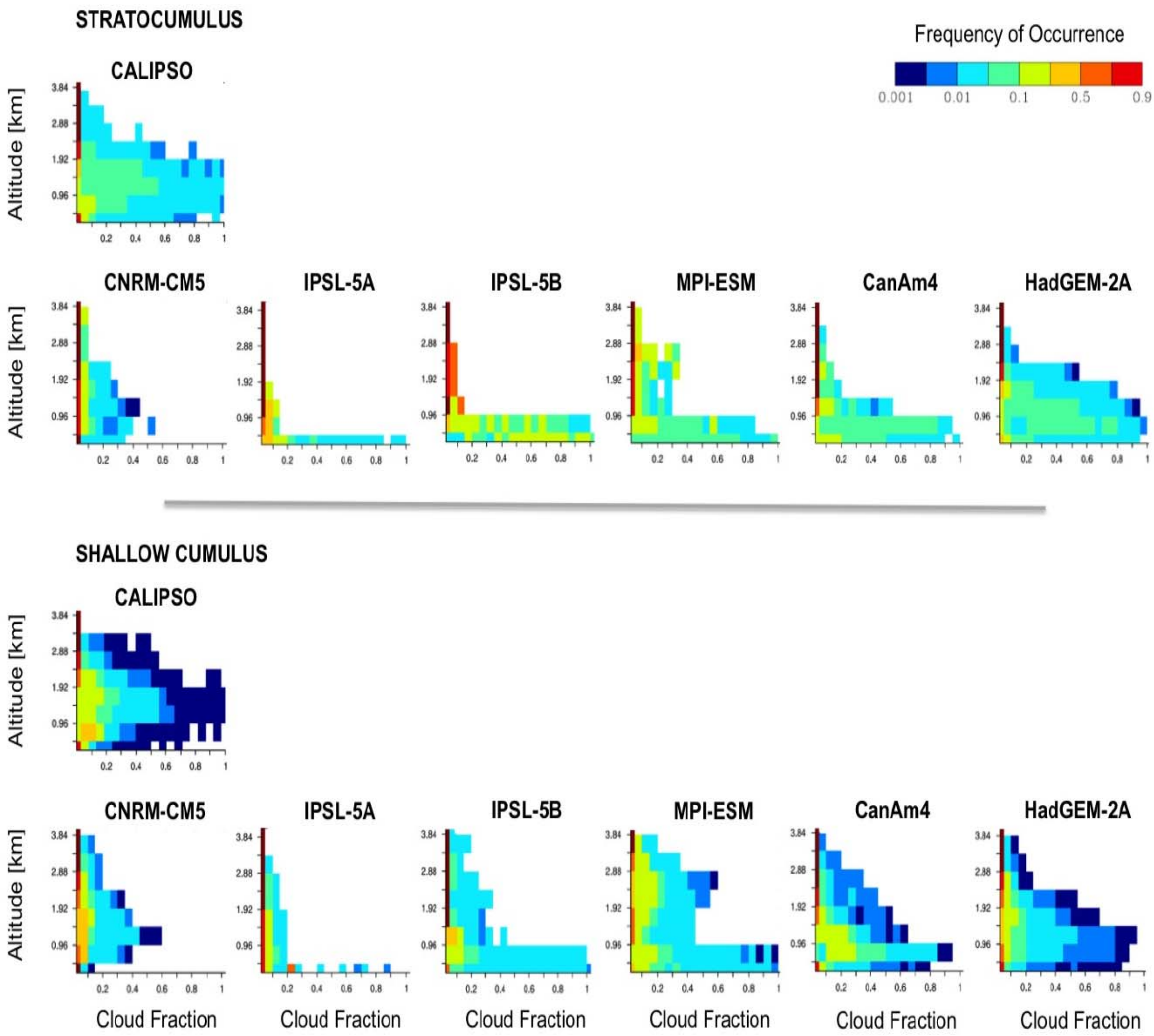

Figure 16. *Frequency of occurrence of clouds of a given fraction at a given altitude in the lowest 4 km of atmosphere under only low-level cloud conditions for (a) stratocumulus and (b) shallow cumulus cloud regimes.*

Parasol Reflectance

Above each column of only low-level tropical stratocumulus and shallow cumulus clouds identified in the previous section, the average PARASOL reflectance is calculated. In the models, the PARASOL simulator provides reflectances for five solar zenith angles which are linearly interpolated to derive a single PARASOL reflectance corresponding to the solar zenith angle each month and latitude. This PARASOL reflectance is directly comparable to the observed PARASOL reflectances [Konsta et al., submitted]. Alongside the PARASOL reflectances, the probability density function (PDF) of only low-level clouds, for a given interval, is presented in Fig. 17.

Over the stratocumulus regime, observed PARASOL reflectances increases with increasing cloud cover, ranging from approximately 0.10 to 0.25 (Fig.17a). All models have similar reflectances for cloud covers less than 10%, which are all lower than observed. As cloud cover increases, differences between the modelled reflectances themselves and the observations becomes greater. Modelled reflectances range from ~0.4 to ~0.5 for a cloud cover of 100%, which is double the observed values in some cases. Interestingly, modelled reflectances of MPI-ESM and HadGEM2-A, and of IPSL-CM5B and CCCma, are similar despite having a very different vertical distribution of clouds.

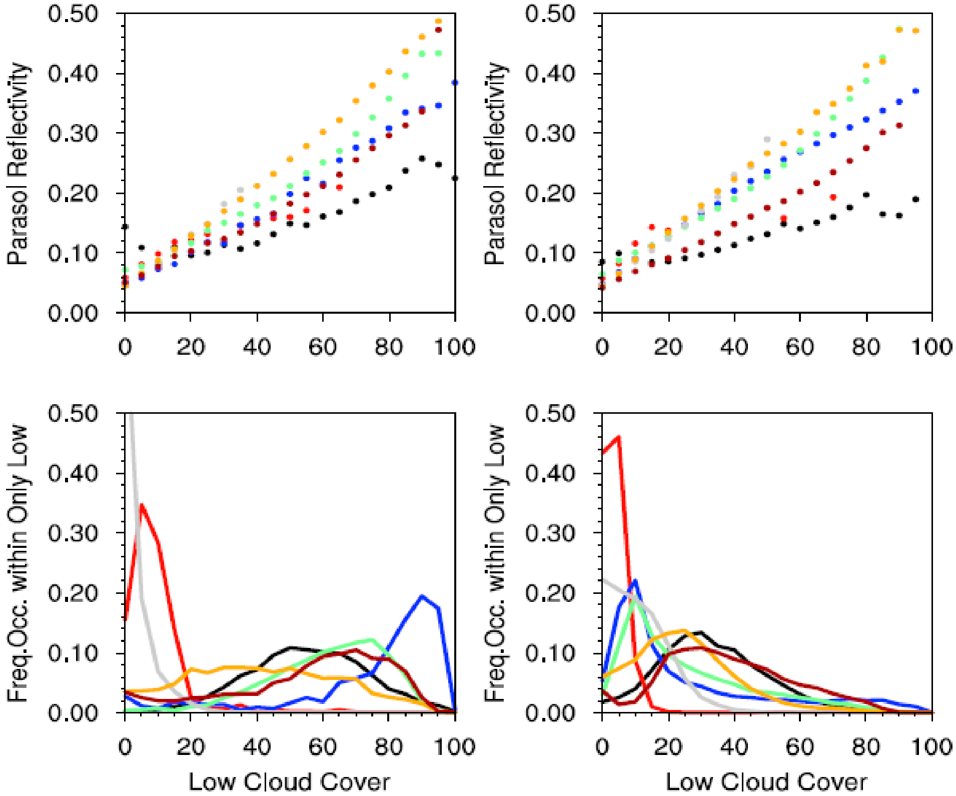

Figure 17. *Parasol reflectance and probability density function for a given only low-level cloud cover for tropical stratocumulus regimes (a,b) and shallow cumulus regimes (c,d).*

Combining the PARASOL reflectances in Fig.17a with the PDF distributions in Fig.17c, one can determine the frequency in which modelled cloud optical depth diverges from observations. For example, models with negatively skewed distributions and overestimated reflectances for large cloud covers, as is the case for HadGEM2-A and IPSL-CM5B, often overestimate the cloud optical depth of low-level clouds. Models with platykurtic or positively skewed distributions and similar reflectances as observations, such as CNRM and IPSL-CM5A, rarely have large differences between modelled and observed reflectances.

Observed PARASOL reflectances over the shallow cumulus regime range from approximately 0.08 to 0.18; showing a dimming in optical depth compared to the stratocumulus regime (Fig.17b). The models, however, produce similar reflectances in shallow cumulus regimes as in stratocumulus regimes. This may be the result of having very similar vertical distributions of low-level cloud regimes as seen in Fig. 16.

Observations show shallow cumulus regimes have slightly positively skewed distributions (Fig.17d). The models capture this positive skewness. The IPSL-CM5A, IPSL-CM5B, CNRM and MOHC models, however, are much too positively skewed; overestimating the frequency of low-level cloud covers less than 20% while underestimating the peak frequency of low-level cloud covers between 20 and 60%. The MPI and CCCma models are able capture the distribution of shallow cumulus clouds well.

As distributions of low-level clouds in CMIP5 models improve, shifting towards a greater frequency of large cloud covers, errors in the optical brightness of stratocumulus and shallow cumulus clouds will have a greater impact on the radiation budget.

iv) Conclusions

In pursuit of the question: 'How well do models represent the vertical distribution of clouds and their optical properties in the present climate?' we have identified both systematic biases and compensating errors amongst the models.

Evaluation of stratocumulus and shallow cumulus clouds in the lowest 4 km of the atmosphere found few models were able to produce a vertical distribution of throughout the boundary layer. Few models produced tropical stratocumulus and shallow cumulus cloud fractions greater than 50% above 1 km as found in CALIPSO observations. Modelled clouds greater than 50% mostly remain below 1 km; for both stratocumulus and shallow cumulus cloud regimes.

The modelled 3D distribution of tropical stratocumulus and shallow cumulus yielded Parasol reflectances which were generally greater than observed. The differences between modelled and observed reflectances systematically increased with increasing cloud cover. Combined with the distributions of only low-level clouds, one could determine the frequency which models diverged from observations. In the stratocumulus regime, models show a great spread in the frequency in which modelled reflectances diverged from observations due to the different distribution skewness modelled cloud fraction. The modelled skewness range from positively to negatively skewed, as opposed to the gaussian distribution observed. Comparably, in the shallow cumulus regime, models often have more positively skewed distributions than observed, implying the reflectances in models do not differ as often from observations. As model distributions of low-level clouds improve, the significance of errors in optical brightness will increase unless parameterizations improve. The analysis of 3D cloud fraction and parasol reflectances, of only low cloud fraction, may be a way of testing new boundary layer parameterizations.

Assesment of cloud-aerosol-radiation interactions in CMIP5

Deliverable 2.2

1. Introduction

The radiative forcing by anthropogenic aerosol due to their effect on clouds and radiation is the main uncertainty in climate change forcing. This hampers our ability to quantify climate sensitivity (Schwartz, 2008). One reason for the simulated spread in aerosol indirect radiative forcings is the large diversity of Earth System Models (ESMs) in their representation of cloud and aerosol processes. Some ESMs neglect aerosol-cloud interactions entirely (Stevens, 2012), while others include complex aerosol cycles and comprehensive cloud microphysics and parameterise aerosol-cloud interactions to various degrees of sophistication (Boucher, 2012).

A previous model intercomparison study in the AEROCOM initiative that evaluated the aerosol-cloud interactions in ten different atmospheric general circulation models (GCMs) using satellite data has demonstrated some skill of the models in simulating the effect of aerosols on cloud droplet number, but substantial problems in parameterising the effect on precipitation formation (Quaas et al., 2009). Since this AEROCOM study, some ESMs later used in the 5th Coupled Model Intercomparison Project (CMIP5) evolved to include more detailed aerosol and cloud processes (e.g., the GFDL and NCAR GCMs), while others reduced the complexity of aerosol-cloud interactions (MPI-ESM). The study by Quaas et al. (2009) thus is not representative for the interpretation of the CMIP5 results.

Consequently, the present report aims at analysing the representation of cloud-aerosol-radiation interactions in the CMIP5 simulations. From the set of simulations carried out within CMIP5 (Taylor et al., 2009), three are selected for this analysis, namely the

- Historical simulation (1850 – 2005, using observed emissions of greenhouse gases and aerosols); experiment 3.2 in the definition of Taylor et al. (2009)
- SSTClim simulation (climatological sea surface temperature, SST, and sea ice cover as well as greenhouse gas and aerosol emissions for pre-industrial conditions); experiment 6.2a
- SSTClimAerosol simulation (as SSTClim, but with aerosol emissions for the year 2000); experiment 6.4a.

The Historical simulation is generally used to evaluate and assess the skill of the simulations of each of the ESMs, based on which the reliability of projections of future climate change is often judged. In this report, we aim to understand the aerosol forcing imposed to this simulation by comparing the difference between the last period (2001 – 2005) and the earliest period (1861 – 1865) to the idealised simulations (SSTClimAerosol minus SSTClim). We further compare the simulation results for the recent period in the Historical simulations to satellite observations.

2. Idealised simulations to infer aerosol forcing

In this section, the effect of anthropogenic aerosols on individual parameters is analysed by comparing a five-year average of the SSTClimAerosol simulation with the SSTClim simulation. The geographical distributions of aerosol optical depth (AOD), cloud-top droplet number concentrations (CDNC), cloud-top droplet effective radii (CDR), cloud albedo, planetary albedo and finally reflected solar radiation are examined. The change in AOD is a primary metric for the aerosol direct forcing by scattering. The changes in CDNC and CDR, respectively, reflect the aerosol indirect forcing with a particular focus on the first aerosol indirect effect. The change in cloud albedo, defined as the change in all-sky minus clear sky albedo, is a metric for the total aerosol indirect effect. The change in planetary albedo is a latitude-independent picture of the total solar aerosol effect. The change in reflected solar radiation, finally, is the adjusted forcing of the total aerosol effect.. For a more detailed discussion of these results and the corresponding maps we refer to the full report on this deliverable which can be found at http://www.euclipse.eu/products.html.

All models show a general increase in AOD. Particularly MIROC and CSIRO show large increases over Europe, China and Central Africa, IPSL in the same regions, but a smaller increase. MRI shows smaller changes than the other models. Analysing CDNC all models give an overall global increase, CSIRO having the strongest increase and IPSL the smallest. The increase of AOD over Europe, China and Central Africa simulated by MIROC and CSIRO is also clearly visible in CDNC for these models, with especially CSIRO showing strong increases up to 150 – 200 cm^{-3} over large areas of the Northern Hemisphere. For MRI, the maritime stratocumulus decks show a large sensitivity to the anthropogenic aerosols as expressed in a strong signal in increased CDNC. All these changes to a large extent mirrored by decreases in simulated CDR, although in CSIRO, the changes in CDR are less strong relative to the changes in CDNC compared to the other models, which may hint to a substantial simulated increase in cloud liquid water path. For cloud albedo, planetary albedo, and adjusted forcing, the results are rather noisy in all simulations. MRI, MIROC and HadGEM show increases in cloud albedo and subsequently in planetary albedo which reflect the spatial pattern of CDR decreases. For the other models, it is difficult to clearly distinguish consistent patterns. The same conclusions can be drawn for the simulated adjusted forcing.

3. Historical simulations

It is interesting to investigate to which extent these findings from the idealised simulations can be extracted also from the historical simulations, because the aerosol forcing, and its historical evolution, in these simulations is important to potentially assess climate sensitivity (Schwartz, 2008). The changes for the same parameters are compared for the periods 2001 – 2005 and 1861 – 1865 from the historical simulations. Despite the varying ocean surface condition in these simulations, the main characteristics of the geographical distribution of the AOD increase are very similar between the idealised and historical simulations. The same is found for CDNC (Fig. 19). For CDR (Fig. 20), the patterns are similar, but in general, in all models, either the decrease in CDR is less pronounced, or even an increase is simulated, in the historical simulations compared to the idealised simulations. This hints to an increase in cloud liquid water path in response to the increasing greenhouse gas concentrations in the historical simulations.

Analysing the cloud albedo and planetary albedo, for those models that showed distinct patterns of aerosol forcing (MRI and MIROC), the geographical distributions of this forcing can also be found in the historical simulation. A slightly less strong increase, or locally at some places even a decrease, in cloud albedo is simulated in the historical compared to the idealised simulations. Again, the pattern of cloud albedo change and planetary albedo change are mostly consistent. IPSL, which did not show a pronounced aerosol effect in any metric, simulates a widespread decrease in planetary albedo, different from the other models. This decrease may be attributable to a positive cloud feedback to greenhouse-gas warming. MRI and MIROC simulate a strong decrease in planetary albedo, but not in cloud albedo, over the Arctic region in the historical simulation which is not found in the idealised simulation. This is probably a strong snow/ice albedo feedback in these models, which is not equally pronounced in IPSL and CSIRO.

4. Comparison of historical simulations to satellite observations

For the recent period in the historical simulations (2001 – 2005), a comparison to satellite observations from the MODerate Resolution Imaging Spectroradiometer (MODIS) for AOD, CDNC and CDR, and from the Clouds and the Earth's Radiant Energy System (CERES) for planetary albedo is possible. The results are presented in Fig. 18-21. Simulated AOD patterns compare well to MODIS, especially for CSIRO. The other models tend to simulate less AOD than retrieved, especially over the Northern Hemisphere mid-latitudes. CDNC is generally substantially lower in the models compared to the MODIS retrieval, except for CSIRO which shows larger values. Most models show the land-sea contrast with larger concentrations over land than over ocean, which is also found in the retrievals. IPSL, however, simulates even lower CDNC over land than over ocean, where it already is quite low compared to the retrievals. MRI also rather shows larger CDNC over land compared to ocean – perhaps a reason for the large susceptibility of oceanic clouds to anthropogenic aerosols discussed above. Also for CDR, the models do not compare very well to MODIS, and have very large discrepancies compared to one another. HadGEM and MIROC results are rather close to MODIS, but substantially lower over land, perhaps pointing at a too strong aerosol indirect effect. MIROC, CSIRO and especially IPSL simulate much smaller CDR than MODIS retrieves, while MRI diagnoses very large droplets and only a small land-sea contrast. Planetary albedo in general compares comparatively well among models and CERES retrievals. However, the meridional gradient in the models is much lower than in CERES, with substantially larger albedos simulated compared to the retrievals.

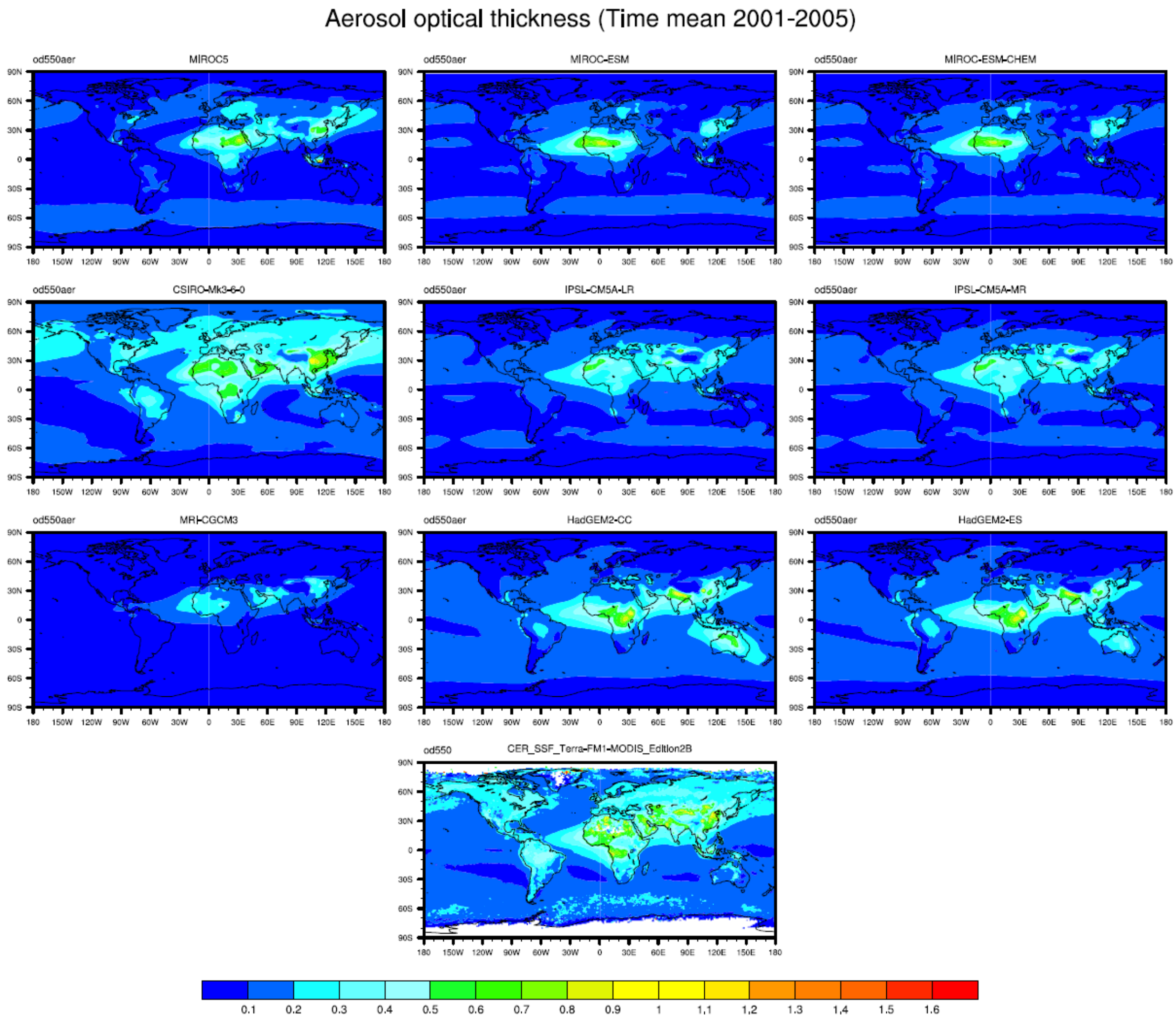

Figure 18: *Comparison of the period 2001-2005 for the historical run with MODIS satellite observations for AOD.*

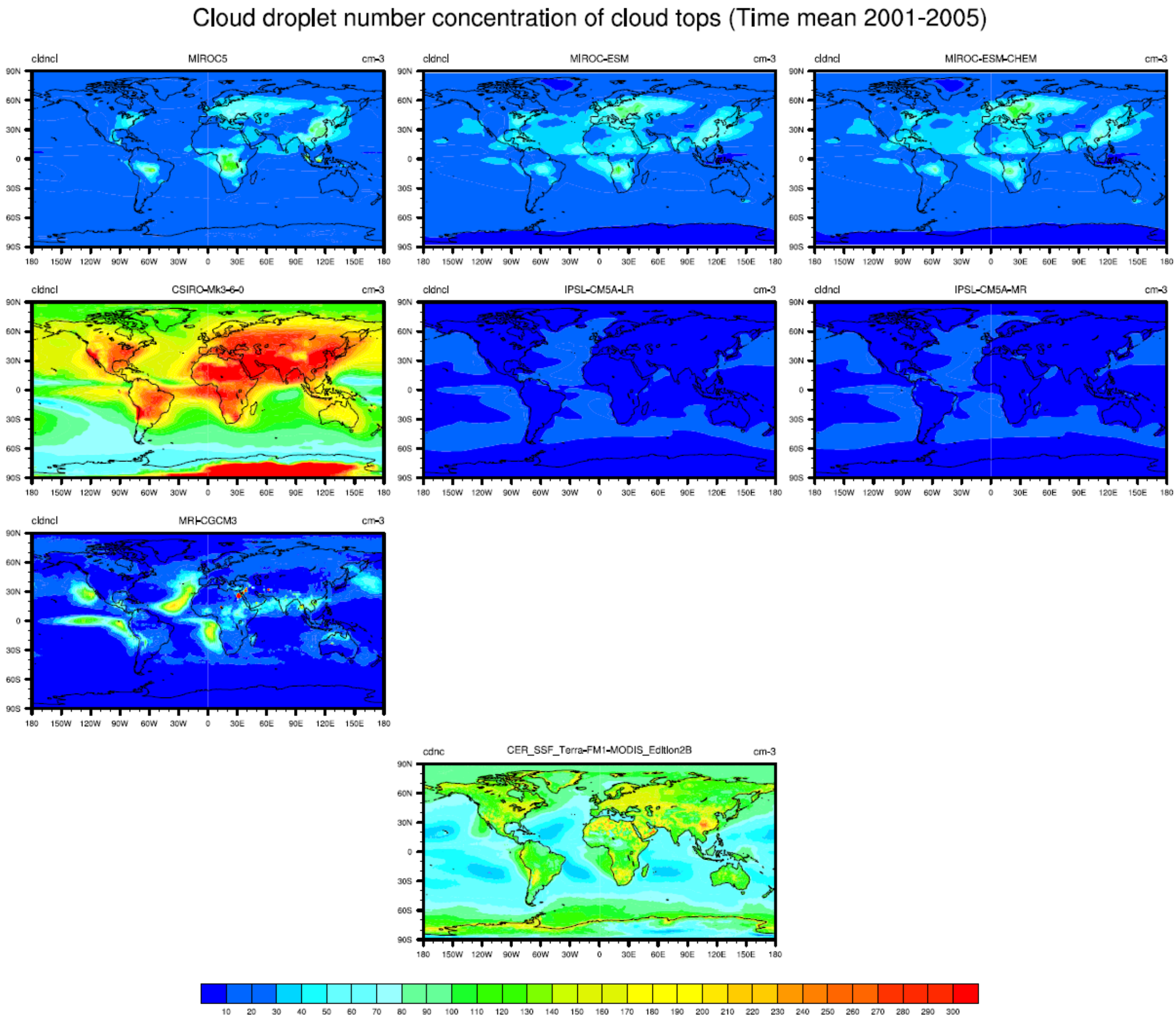

Figure 19: *Comparison of the period 2001-2005 for the historical run with MODIS satellite observations for CDNC.*

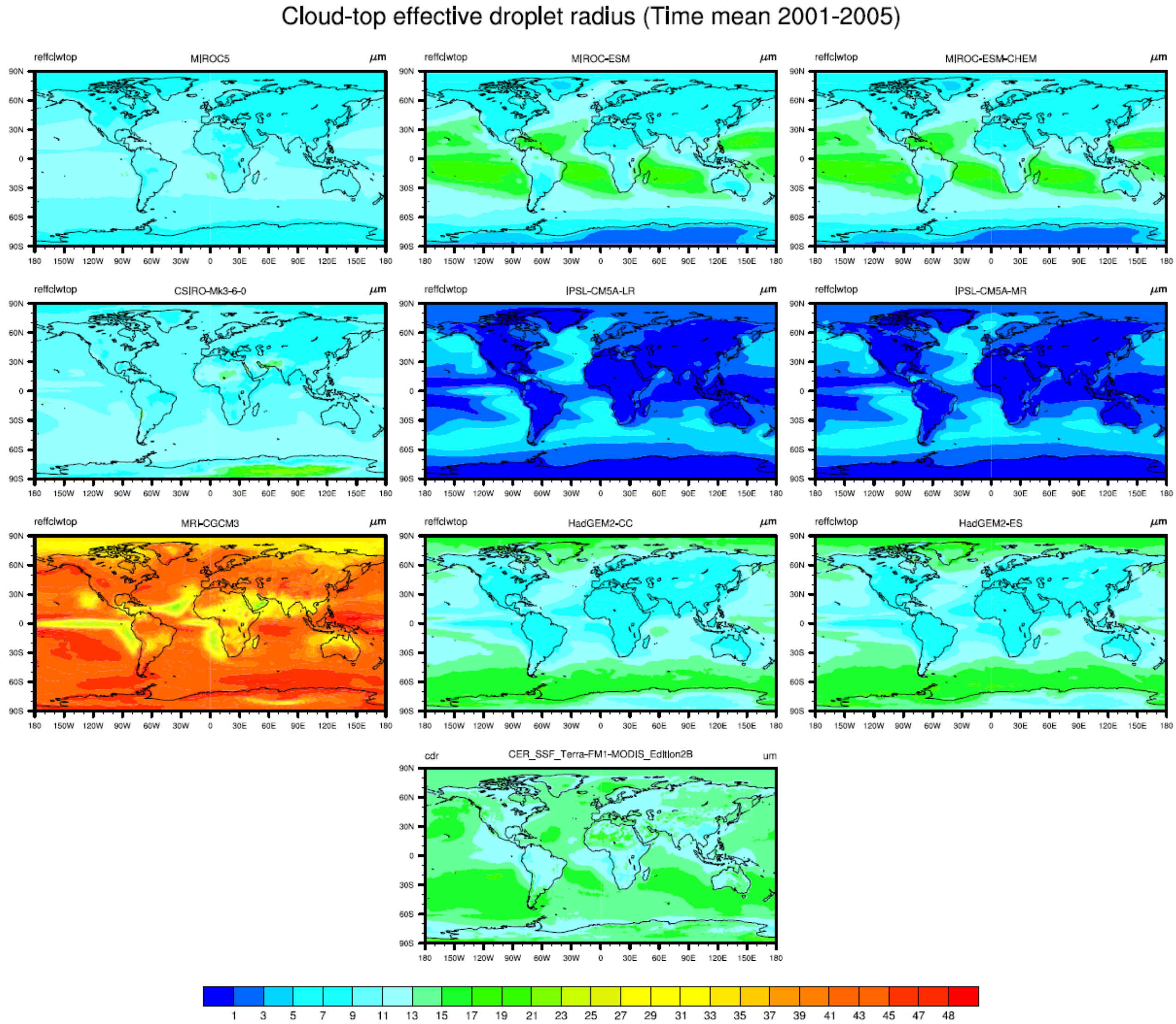

Figure 20: *Comparison of the period 2001-2005 for the historical run with MODIS satellite observations for CDR..*

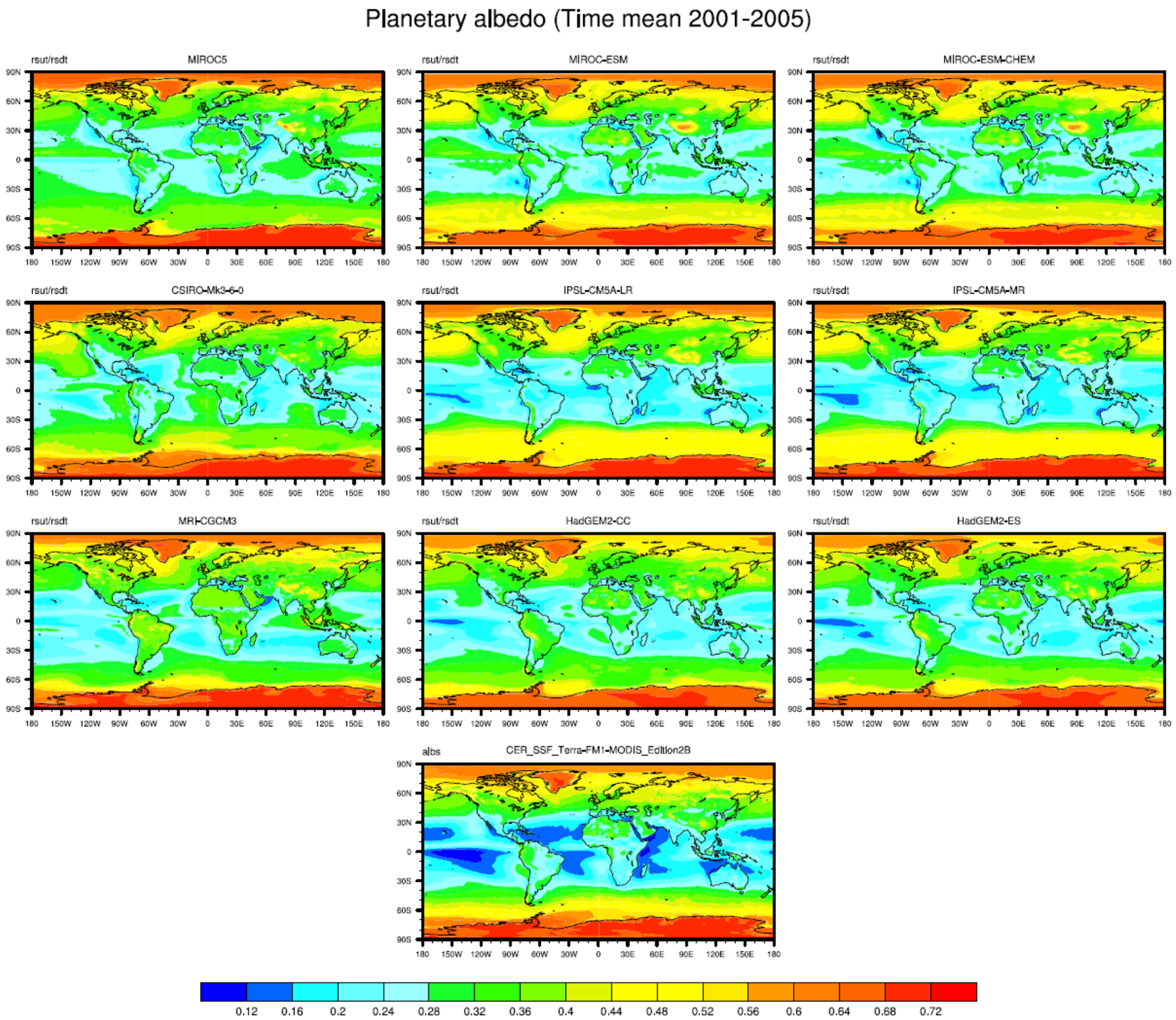

Figure 21: *Comparison of the period 2001-2005 for the historical run with MODIS satellite observations for AOD.*

Ability of climate models to simulate the ITCZ, the intra-seasonal and inter-annual variability of the tropical atmosphere, and temperature extremes over Europe using a new set of diagnostics

Deliverable 2.4

1. Introduction

WP2 is focused on the analysis and the evaluation of climate simulations from CMIP5 (the 5th Phase of the Coupled Models Intercomparison Project), and the Task 2 of this WP aims at understanding how cloud and moist processes affect the simulation of the tropical atmosphere and temperature extremes in the current climate. This report presents an early analysis of the ability of CMIP5 climate models to simulate the Inter-Tropical Convergence Zone (ITCZ) and the Madden-Julian Oscillations (MJO, section 1), the tropical inter-annual variability (the El-Niño Southern Oscillation or ENSO, section 2), and temperature extremes over Europe (section 3). Climate model outputs have been available on the CMIP5 data archive (Earth System Grid) later than anticipated at the time of the writing of the EUCLIPSE proposal. For this reason, the focus of this deliverable is put on the evaluation of a subset of CMIP5 models, especially those developed by EUCLIPSE participants (CNRM-CM5, HadGEM2, IPSL-CM5A, MPI-ESM; unfortunately, EC-Earth and IPSL-CM5B outputs are not yet available for analysis). By the end of the project, additional models will be considered, and the role of the representation of cloud and moist processes in the models' ability to reproduce the observed tropical variability and European extremes will be examined in more details.

2 ITCZ and MJO in the CMIP5 models

i) Introduction

Some of the models show some improvement in the simulation of the seasonal and intraseasonal variability of tropical precipitation. The double ITCZ bias is still present in most of the models. This bias is reduced in most models participating to EUCLIPSE compared to the previous generations of the same models. In particular, it appears that the double ITCZ bias has become small in atmosphere-only simulations, and that coupled feedbacks account for a large part of this bias in coupled simulations. Some improvement can be found in the simulation of intraseasonal variability, in particular in models whose previous generation already performed better. Among these models, the role of the ocean-atmosphere coupling seems to be quite different from one model to the other.

ii) Seasonal cycle of the precipitation

Figure 22 shows the annual average of precipitation in the ocean-atmosphere models participating to EUCLIPSE. Most of the models simulate too strong oceanic ITCZ's. All of them also exhibit the well-known double-ITCZ bias, with a spurious longitudinal rainband south of the equator in the East Pacific. Some also simulate a double ITCZ in the tropical Atlantic.

But except for the HadGEM-ES model, all the models participating to EUCLIPSE reduced their double ITCZ biases compared to the previous version, as shown in Figure 23 by a metric proposed by Bellucci et al. (2010), the Southern ITCZ index (average annual precipitation between 100W and 150W, 0 and 20S).

Indeed, the seasonal cycle of the precipitation in the East Pacific (80W-120W) has improved in coupled models, as shown in Figure 24, compared to Dai (2006) and de Szoeke and Xie (2008). In particular, the CNRM-CM5 no longer simulates a double ITCZ all year round, but simulates a single ITCZ that moves across the equator following the solar forcing, similarly to the IPSL-CM5A and MPI-ESM. Only the HadGEM-ES simulates the observed March-April double ITCZ but the Southern ITCZ is then much more intense than in the observations (the increase of the SI index from CMIP3 to CMIP5 is actually due to this enhanced precipitation).

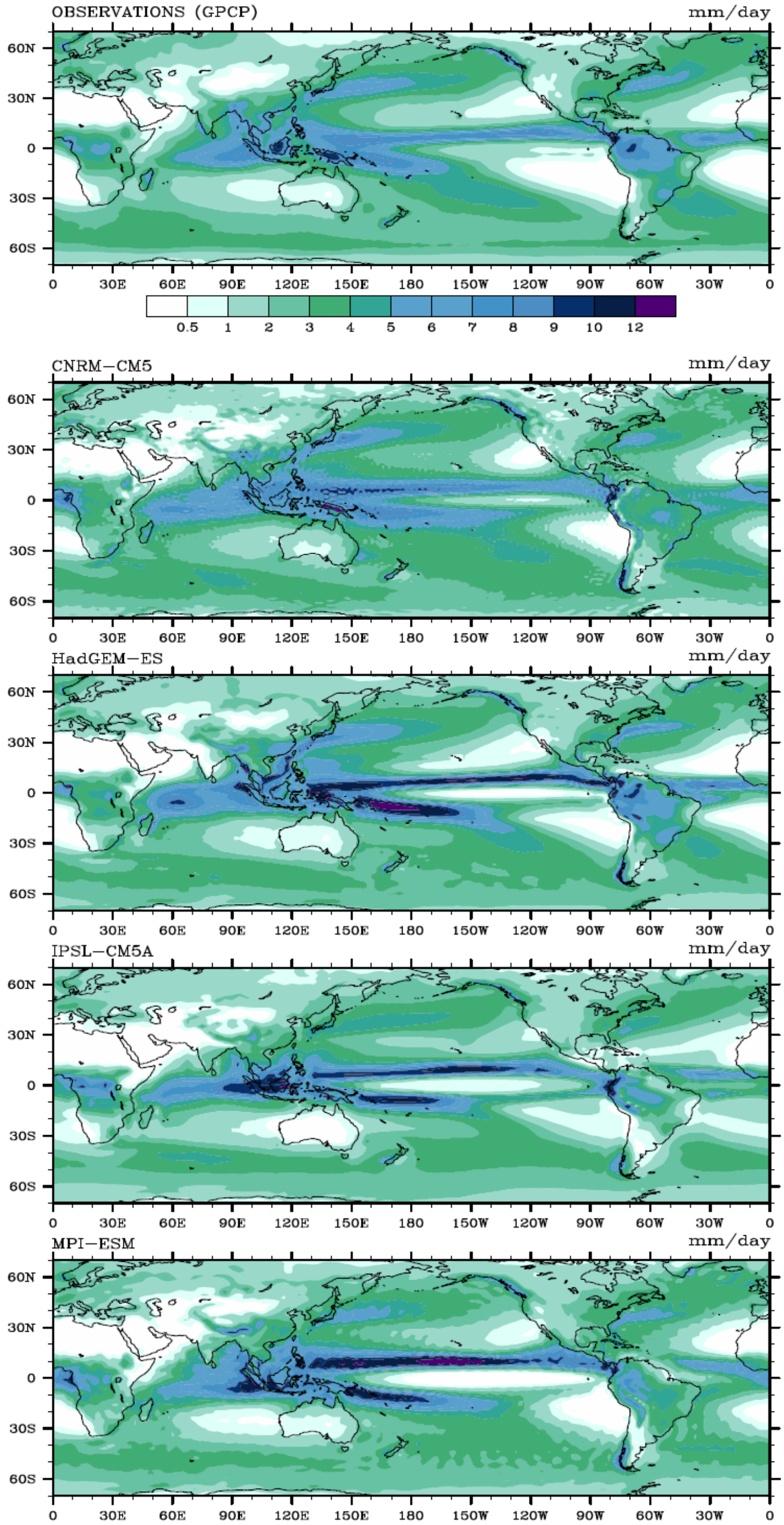

Figure 22: *Mean annual precipitation as observed (GPCP) and simulated by some CMIP5 models (CNRM-CM5, HadGEM-ES, IPSL-CM5A, MPI-ESM).*

Figure 25 shows the seasonal cycle of precipitation in the East Pacific in the atmosphere-only simulations. Compared to the ocean-atmosphere coupled simulations, the precipitation biases are much reduced, and the biases of the atmospheric models do not easily relate to those of the coupled models. In the East Pacific, the MPI model ECHAM and the CNRM model ARPEGE even underestimate the precipitation in the March/April Southern ITCZ. It shows that the coupled ocean-atmosphere feedbacks are responsible for most of the double ITCZ bias in the East Pacific, maybe more so than in the previous generation of models (Lin 2007). Coupled feedbacks are also essential in modulating the double ITCZ bias, and they are responsible for a large part of the inter-model differences.

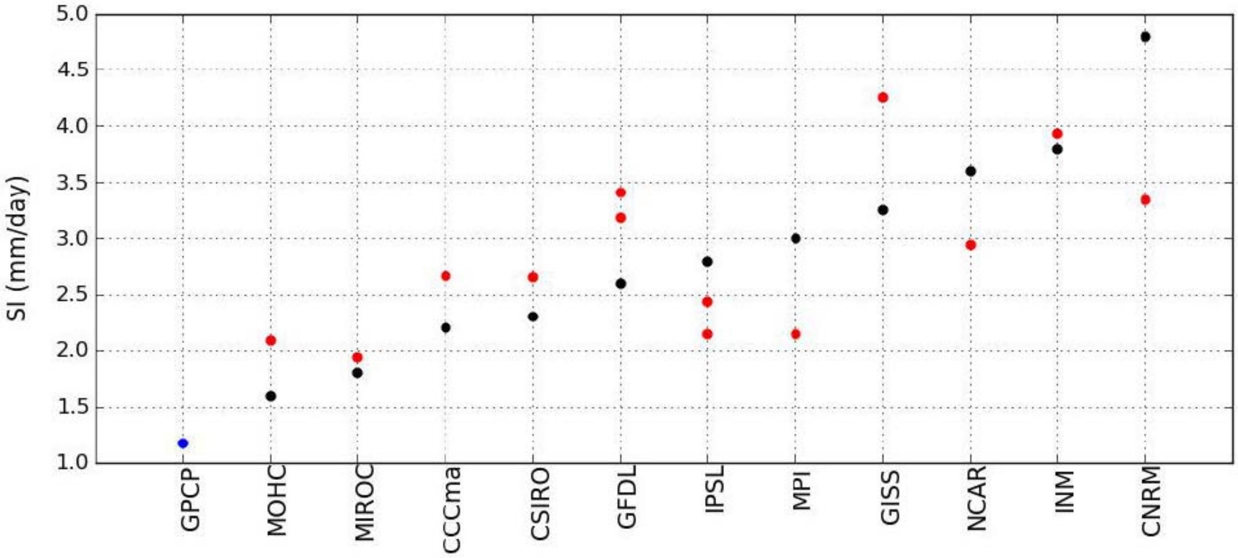

Figure 23: *Southern ITCZ index for CMIP5 (red dots) and CMIP3 (black dots) models (adapted from Bellucci et al., 2010).*

ii) Intraseasonal Variability

Figure 26 shows the symmetric and asymmetric (with respect to the equator), space and time cross-spectra of tropical OLR and zonal wind at 850 hPa, that is a classical diagnosis of subseasonal tropical variability (see Wheeler and Kiladis 1999). The Madden Julian Oscillation appears as a maximum of the symmetric spectrum between wavenumbers 1 and 2, in the 30-50-day range. Eastward-propagating (positive wavenumbers) Kelvin waves appear in the symmetric spectrum along the straight lines, while westward-propagating (negative wavenumbers) Equatorial Rossby waves appear on the same spectrum in the 10-80-day range. Mixed Rossby-Gravity wave can be seen in the center of the asymmetric spectrum.

The CMIP5 models exhibit contrasting skills at simulating the subseasonal variability. The IPSL-CM5A simulates a very weak subseasonal variability. The CNRM-CM5 exhibits subseasonal variability close to the observation in terms of power, but the dispersion of gravity (Kelvin and Mixed Rossby-Gravity) waves differs from the observations. It corresponds to a deeper equivalent depth of the troposphere in that model. The MPI-ESM simulates a very realistic subseasonal variability, but with underestimated power (recent analyses suggest that the OLR variation on intraseasonal scales in this model is not simulated with a consistent phase with respect to the wind and precipitation signals, reducing the cross-spectrum power). The MPI and CNRM models simulate an MJO variability that is enhanced, closer to the observed intensity compared to the previous generation of models (Lin et al. 2006). In the previous generation of models, the IPSL model simulated more kelvin-wave variability, and the CNRM model did not simulate much of these waves. The MPI model kept most of the characteristics of the previous generation.

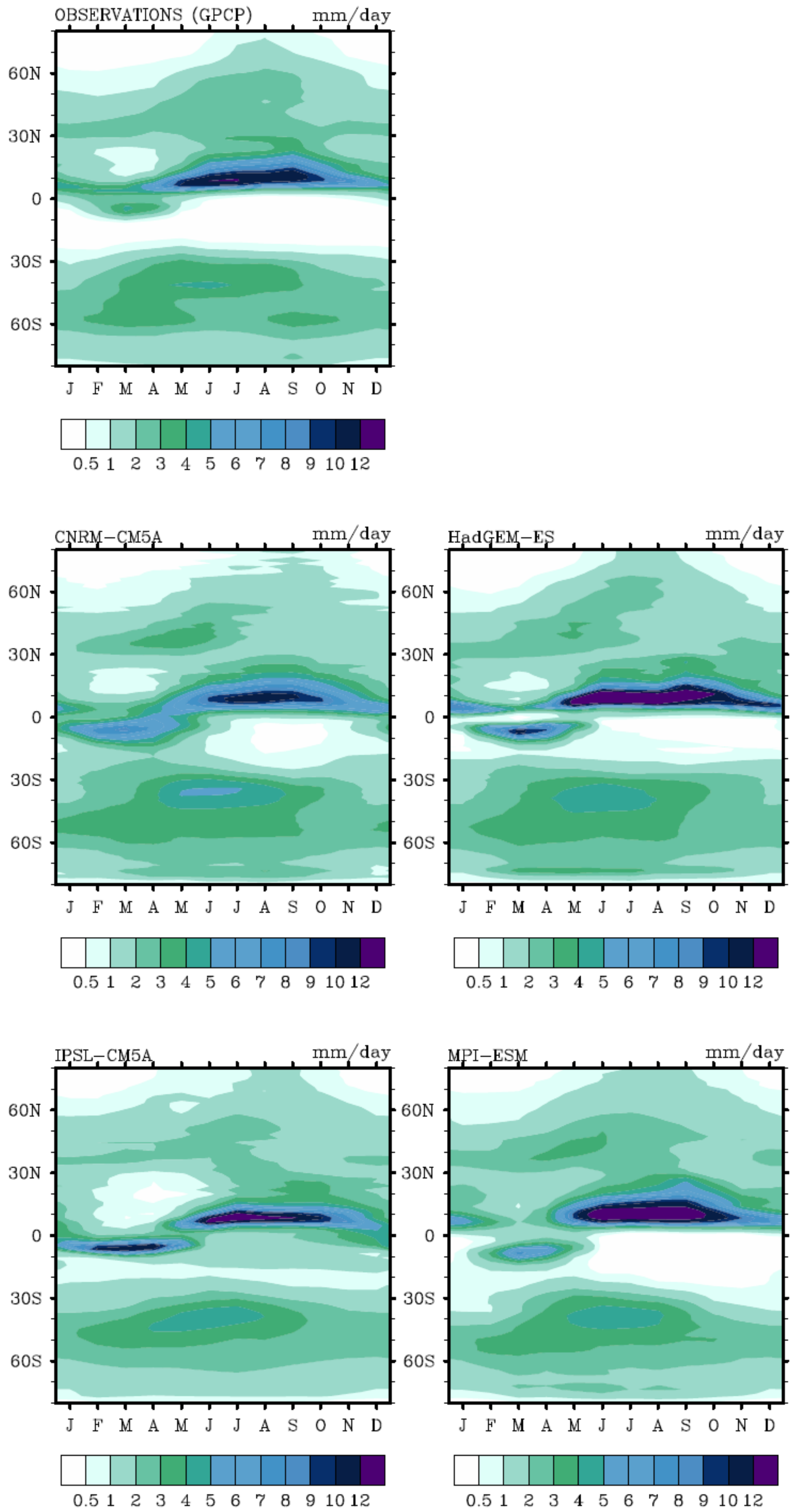

Figure 24: *Seasonal cycle of the precipitation in the Eastern Pacific (80W-120W) as observed (GPCP) and simulated by CMIP5 ocean-atmosphere coupled models (CNRM-CM5, HadGEM-ES, IPSL-CM5A, MPI-ESM).*

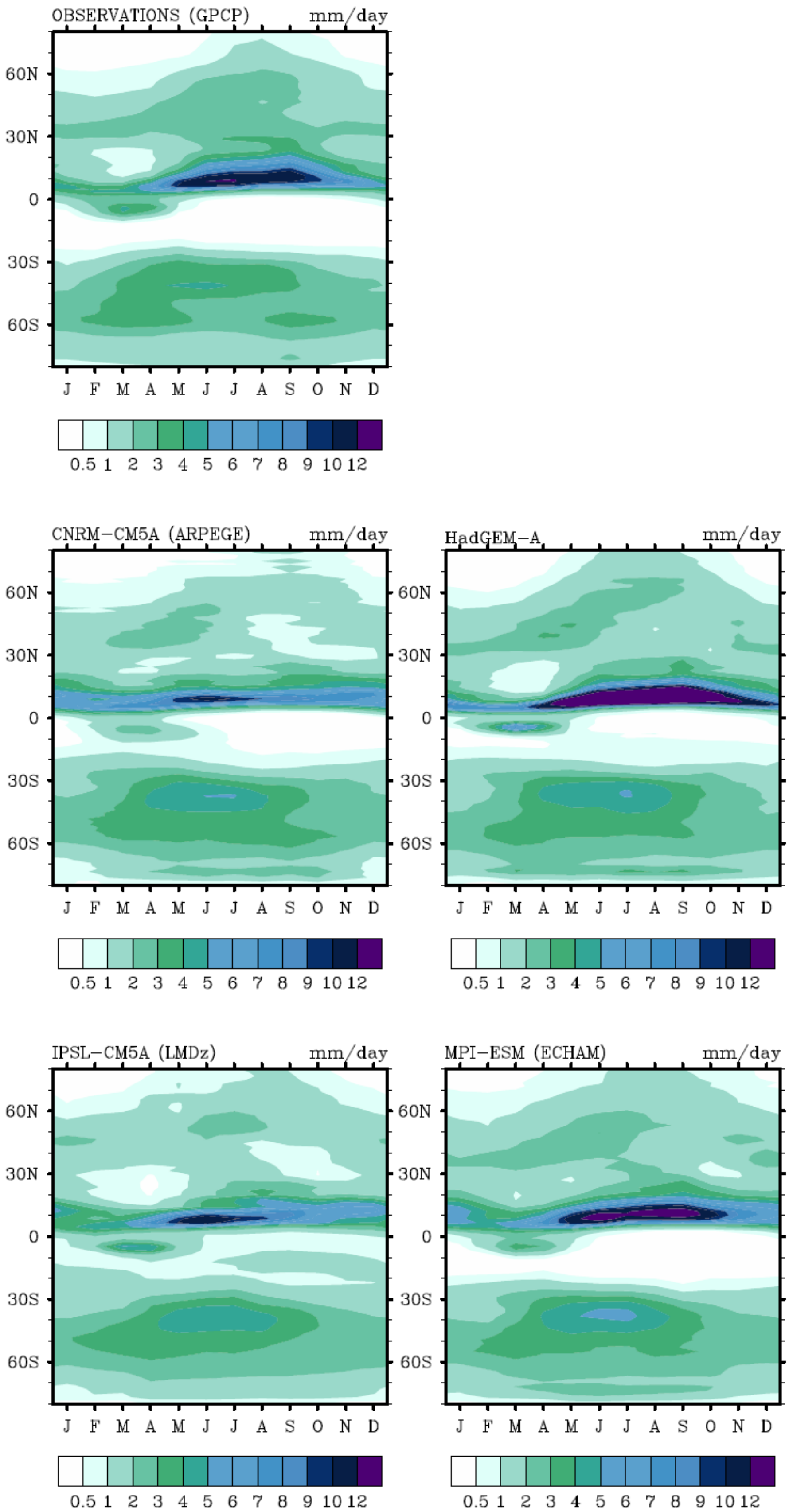

Figure 25: *Seasonal cycle of the precipitation in the Eastern Pacific (80W-120W) as observed (GPCP) and simulated by CMIP5 atmosphere-only models (CNRM-CM5, HadGEM-A, IPSL-CM5A, MPI-ESM).*

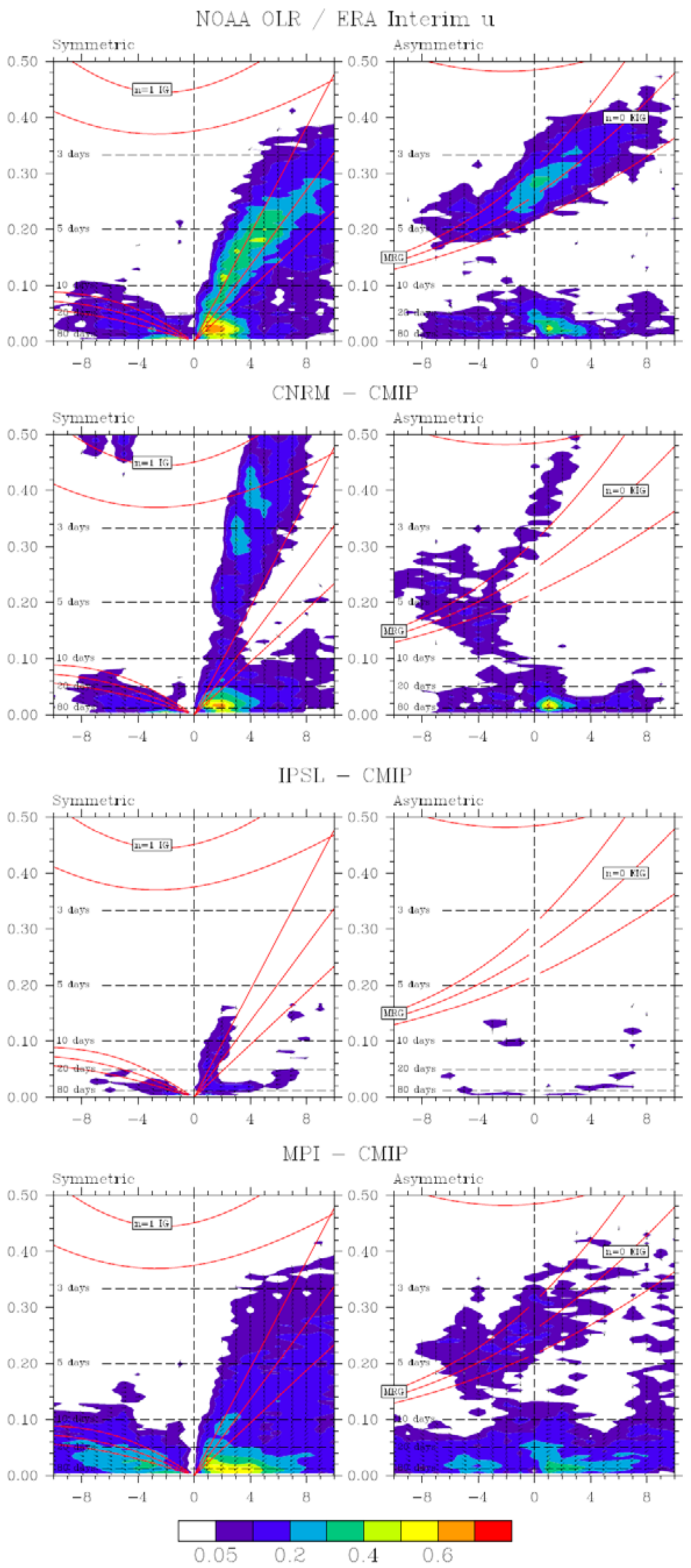

***Figure 26*:** Space and time symmetric and asymmetric spectra of intraseasonal variability as observed (NOAA OLR and ERA Interim) and simulated by the CMIP5 coupled models (CNRM-CM5, IPSL-CM5A, MPI-ESM).

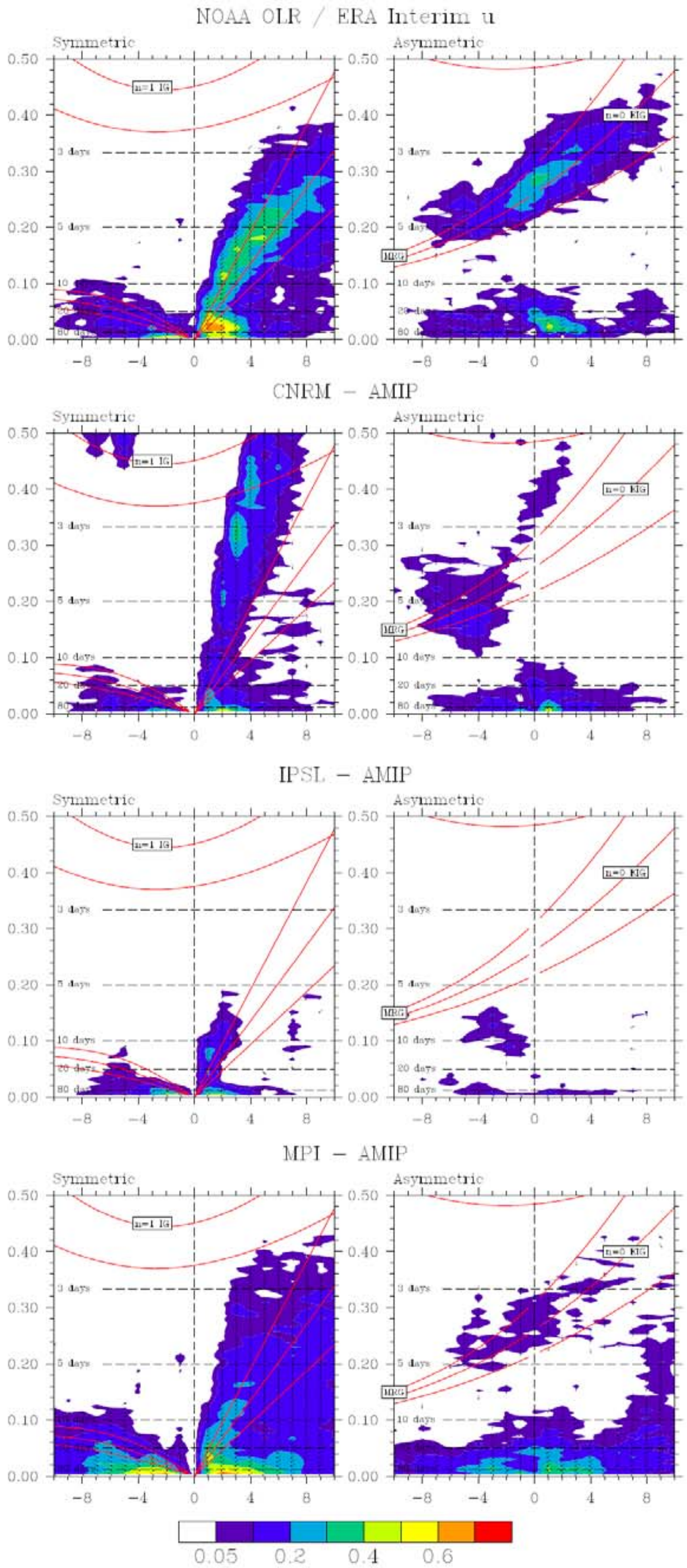

***Figure 27*:** Space and time spectrum of intraseasonal variability as observed (NOAA OLR and ERA Interim) and simulated by the CMIP5 atmosphere-only models (CNRM-CM5, IPSL-CM5A, MPI-ESM).

The contrast between coupled models is even more pronounced in terms of the role of the ocean-atmosphere coupling. Figure 27 shows the same spectra as in figure 5, but for the corresponding atmosphere-only models. The coupling clearly enhances the MJO in all the models, but much more so in CNRM-CM5 than in the MPI-ESM. The convectively-coupled gravity waves are fairly insensitive to the coupling, except maybe in the IPSL-CM5A model in which the subseasonal variability is larger in the atmosphere-only model.

3. A first assessment of ENSO in CMIP5

i) Introduction

CMIP5 as a multi-model ensemble does not exhibit a quantum leap in ENSO performance or sensitivity, compared to CMIP3 as a multi-model ensemble. Looking at individual modeling centres, about half show an improvement in ENSO amplitude. The multi-model mean state does not exhibit significant changes from CMIP3 to CMIP5, but a slight degradation of surface heat fluxes, although a number of individual centres saw an improvement. Very few models score better for all metrics and most have pluses and minuses. Examination of a selection of physical feedbacks highlights that there is still the potential for the cancellation of errors and that a process-based analysis is fundamental to properly assess ENSO in CGCMs.

The first assessment of basic ENSO properties in control simulations of CMIP5 and a comparison with CMIP3 has been performed. We use the metrics as developed within the CLIVAR Pacific Panel, which assess both the tropical Pacific mean state and interannual properties. We use multi-century pre-industrial simulations for both CMIP3 and CMIP5 as required to ensure statistical robustness. Simulation lengths are 300 years (but for MIROC-ESM-CHEM, 255 years and HadGEM2CC, 240 years). The analysis in Figures 28 and 29 is presented per modelling centre to also assess progress (see Table 3 for official CMIP model names). Precise CMIP5-variables used in the analysis are detailed in the figure captions. Observations or reanalysis used for reference include HadISST1.1 (years 1900-1999), ERA40 (years 1958-2001), CMAP (years 1979-2005) and OAFlux (years 1958-2006 for turbulent and 1984-2006 for radiative).

Modelling centre	CMIP3 model(s)	CMIP5 model(s)
BCC	n/a	BCC-CSM-1
CCCma	CGCM3.1	CanESM2
CNRM	CNRM-CM3	CNRM-CM5
CSIRO	CSIRO-Mk3.0	CSIRO-Mk3.6
GFDL	GFDL2.0	GFDL-ESM2M
	GFDL2.1	
GISS	GISS-AOM	GISS-E2-H
	GISS-EH	GISS-E2-R
	GISS-ER	
IAP	FGOALSg1.0	n/a
INM	INM-CM3.0	INM-CM4
IPSL	IPSL-CM4	IPSL-CM5A-LR
		IPSL-CM5A-MR
MIROC	MIROC3.2-MR	MIROC5
	MIROC3.2-HR	MIROC-ESM
		MIROC-ESM-CHEM
MOHC	HadCM3	HadGEM2-CC
	HadGEM1	HadGEM2-ES
MPI	ECHAM5/MPI-OM	MPI-ESM-LR
MRI	MRI-CGCM2.3.2	MRI-CGCM3
NCC		NorESM1-M

***Table 3*:** CMIP3 and CMIP5 official model names per modelling centre.

ii) ENSO Metrics

Under the guidance of the CLIVAR Pacific Panel a set of ENSO metrics has been proposed to facilitate the comparative analysis and understanding of ENSO in CGCMs. These contribute to a wider effort to set up standard metrics for the routine evaluation of CGCMs, as for instance organised for CMIP5. It is key to document the background systematic errors in the tropical Pacific (mean annual cycle and mean state). Indeed, ENSO is defined as an anomaly to these and ENSO errors can often be traced back to these systematic errors. Hence the set of metrics used here include both ENSO and mean state diagnostics (Figure 28). The 4 ENSO metrics encompass ENSO amplitude (Nio3 SST std dev), structure (Nio3 vs. Nio4 amplitude), frequency (RMSE of Nio3 SSTA spectra) and heating source (Nio4 precipitation std dev). The other metrics deal with SST, zonal wind stress, precipitation and surface heat flux mean state and annual cycle (Guilyardi and Wittenberg 2010). The specific averaging regions were chosen after correlating different regions to ensure independent metrics are chosen. More details can be found at http://www.locean-ipsl.upmc.fr/ENSOmetrics/index:html.

iii) Has ENSO performance in CGCMs improved since CMIP3 ?

ENSO properties

A preliminary analysis of the metrics in Fig 28 first shows that the range of modelled ENSO amplitude in CMIP5 (red dots in Figure 28a) is reduced by about half compared to CMIP3 (blue dots). This is a clear improvement over the CMIP3 ensemble where this diversity was larger than could be explained by observational variability/uncertainty. Although we note that this is a preliminary result as not all modelling groups have submitted output at this stage and the spread of the CMIP5 models could still go up.

The ENSO amplitude, as measured by SST standard deviation, was too large in the central/west Pacific in CMIP3 CGCMs (Nio4 region, 0.8oC compared to 0.65oC in observations) and this has also improved in CMIP5 (0.6oC). Nevertheless there is still the occasional model with spuriously more variability in the west than in the east Pacific (CSIRO-Mk3.6 in CMIP5, CCCma-CGCM3.1 in CMIP3). About half of the centres for which data is available for both CMIP3 and CMIP5 (11 centres) show an improvement in ENSO amplitude while the rest show no change or degradation.

The ENSO spectra metric (Figure 28g) also shows an improved picture in CMIP5 when compared to CMIP3 even at the individual model level. As this metric is sensitive to slight shifts in modelled ENSO spectraand the realworld spectra may not be well constrained by the short observational record this result much be taken with caution. The heating source associated with ENSO, as measured by the Nio4 precipitation standard deviation (Figure 28d), still exhibits large errors in most CMIP5 models with mixed improvements for individual centres.

Mean state in Tropical Indo-Pacific

The multi-model mean state metrics (Figures 28c,e,f,h,i) do not exhibit significant changes from CMIP3 to CMIP5, but for a slight degradation of surface heat fluxes (Figures 28i), albeit in the presence of significant observational uncertainty in surface fluxes. At the individual level, half of the centres show some improvements, mostly marked for the mean zonal wind stress at the Equator in the Pacific (Figure 28h) while the net surface heat flux in the east Pacific is almost always degraded (Figure28i).

Atmosphere response during ENSO

Several studies point out the central role of the atmosphere general circulation model (GCM) response during ENSO in shaping the modelled ENSO (see for instance Guilyardi al. 2009b and Lloyd et al. 2011). The Bjerknes and heat flux response are computed in Figure 29. There is no qualitative change in the multi-model mean Bjerknes feedback (Figure 29a) although most centres exhibit an improvement in their models.

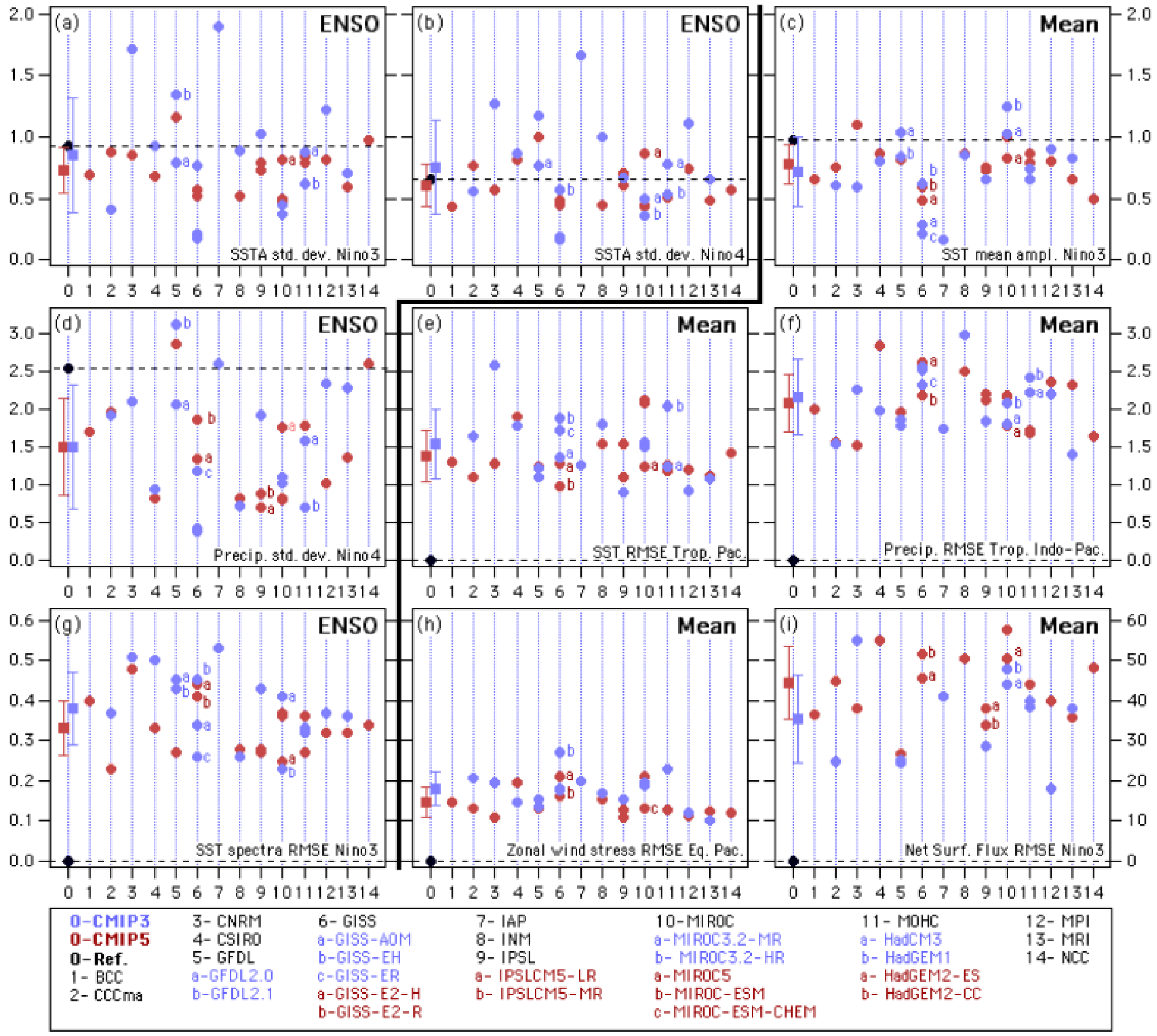

Figure 28: *ENSO and mean tropical Pacific metrics for pre-industrial control simulations - CMIP3 (blue) and CMIP5 (red). (a) and (b) SSTA std. dev. in Niño 3 and Niño 4 (C), (c) SST annual cycle amplitude in Nio3, (C), (d) precipitation response (std dev) in Nio4 (mm/day), (e) SST RMS error in tropical Pacific, (C), (f) precipitation spatial RMS error over tropical Indo- Pacific, 30N-30S (mm/day), (g) ENSO power spectrum (Nio3) RMS error, (C2), (h) zonal wind stress spatial RMS error over equatorial Pacific 5N-5S (103Nm2), (i) net surface heat flux RMS error in Niño 3 (Wm2). Reference datasets, shown as black solid circles and dashed lines: HadISST1.1 for (a), (b), (c), (e) and (g); ERA40 for (h); CMAP for (d)(f); OAFlux for (i). The CMIP3 and CMIP5 multi-model mean are shown as squares on the left of each panel with the wiskers representing the model standard deviation. Monthly atmosphere grid CMIP5-variable used: ts for (a), (b), (c), (e) and (g); tauu for ERA40 for (h); pr for (d)(f); hfls (latent), hfss (sensible), rlds (LW down), rlus, (LW up), rsds (SW down), rsus (SW up) to obtain qnet=-hflshfss+ rlds+rsds-rlus-rsus (i). All fields were interpolated onto a common 1degree grid and then time averaged for mean fields. See* http://www.locean-ipsl.upmc.fr/ENSOmetrics/index:html *for details of computation.*

The total heat flux response in Nio3 (Figure 29b) is improved for a few models (CNRM, MIROC5) although most see a degradation (also seen in the mean heat flux - Figure 29i) leading to more inter-model diversity than in CMIP3. Paradoxically, a number of centres have improved shortwave and latent heat flux response (Figures 29c-d) even though the multi-model mean value does not evolve much. Conversely a number of models have degraded shortwave heat flux response with more models having a positive feedback instead of the observed negative value of -7 Wm^{-2}/C.

While it would have been tempting to conclude from simply looking at the Nio3 anomaly standard deviations (Figure 28a) that the CMIP5 ensemble is converging on reality, examination of these physical feedbacks highlights that there is the potential for the cancellation of errors leading to such convergence. This shows the power of examining these process-based metrics.

With only part of the data available (20 models out of 30-40 planned), CMIP5 as a multi-model ensemble does not exhibit a quantum leap in ENSO performance or sensitivity, compared to CMIP3 as a multi-model ensemble. Looking at individual modeling centres, about half show an improvement in ENSO amplitude. The multi- model mean state does not exhibit significant changes from CMIP3 to CMIP5, but for a slight degradation of surface heat fluxes, although a number of individual centres saw an improvement. Very few models score better for all metrics and most have pluses and minuses. Examination of a selection of physical feedbacks highlights that there is still the potential for the cancellation of errors and that a process-based analysis is fundamental to properly assess ENSO in CGCMs.

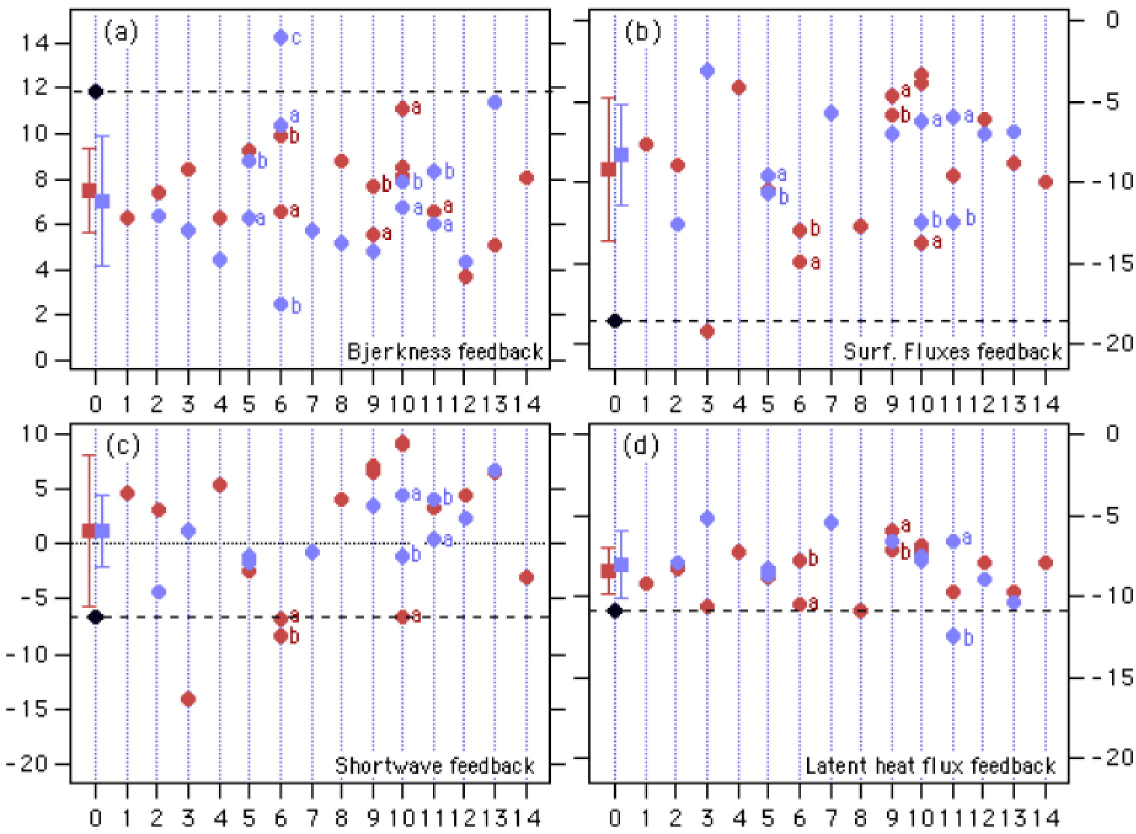

Figure 29: *Atmosphere feedbacks during ENSO for pre-industrial control simulations - CMIP3 (blue) and CMIP5 (red). (a) Bjerknes feedback, computed as the regression of Niño 4 wind stress over Nio3 SST (103Nm2/C); (b) heat flux feedback, computed as the regression of total heat flux over SST in Nio3 (Wm^{-2}/C); (c) Shortwave component of (b); (d) Latent heat flux component of (b). References: ERA40 for (a) and OAFlux for (b), (c) and (d).Monthly atmosphere grid CMIP5-variable used as described in Figures 7. See models and centres legend in Figure 7.*

We also note that many of the new CGCMs are simulating much more processes than they were in CMIP3 (aerosol indirect effect, strat/trop interactions, land ice, flowing rivers, carbon cycle, ecosystems, and driving by emissions rather than concentrations). This makes things tougher: there are new feedbacks to amplify biases, more uncertain model parameters to constrain and more constraints when finalizing the model set up. But this also holds promise: new avenues for improvement, better contact with observational and theoretical constraints, and new realms of ENSO impacts to be explored.

4. European temperature extremes in CMIP5 models

i) Introduction

CMIP5 models have difficulties to simulate observed frequencies of extremely hot/cold days. Most of these biases are present in CFMIP2 experiments, and are generally consistent with biases in mean temperatures. In 21st century projections, while the mean European warming tends to increase (decrease) the frequency of hot (cold) days in all models, high uncertainties remain concerning both amplitudes and patterns of these changes. In order to evaluate contributions of large-scale circulation and non-dynamical processes to simulated temperature extremes, we propose a methodology based on a weather-regime approach. While the dynamical contribution to mean biases and changes turns out to be minor, large-scale circulation seems to have a substantial contribution to future uncertainties in winter. In particular the future increase found in CMIP5 in wintertime NAO-, which limits the depletion of cold extremes in Northern Europe, is in noted contradiction with previous CMIP and CFMIP2.

ii) Evaluation in present-day climate

The representation of both summer (JJAS) and winter (DJFM) temperature extremes by 9 CMIP5 / CFMIP2 models, including 4 EUCLIPSE models (CNRM, IPSL, MOHC and MPI), has been evaluated by comparing both amip and historical runs to E-OBS observations over the period 1979–2008. At each point, extremely warm (cold) days are defined as days with a Tmax (Tmin) anomaly above the 90th (below the 10th) centile of the corresponding E-OBS distribution. With this definition, extreme temperatures are said well represented if the simulated frequency of extreme days equals 10%.

Figure 30 shows mean frequencies of summertime warm days for all models in amip runs. In general, models overestimate hot days in Central Europe (especially MIROC, CNRM) and underestimate them in Scandinavia (esp. CCCMA, MRI) and Western Europe (esp. IPSL, MPI). Figure 31 is similar but for wintertime cold days, showing a general underestimation of cold extremes in Scandinavia and South-Western Europe (except CNRM and MOHC) and an overestimation over North-Eastern Europe (except MPI and MRI). These biases are quasi-systematically amplified in historical runs, but with same spatial patterns. They often scale with mean biases, except in a few cases: for instance IPSL's summer cold bias is weak over Western Europe despite a high underestimation of hot extremes.

ii) Future changes and uncertainties

Future changes in extreme temperatures are assessed by considering for each model the mean frequency, in the rcp85 run over 2070–2099, to exceed the 90th or 10th centile of the historical run over 1979–2008. Given the mean European warming in climate change scenarios, the frequency of summertime warm extremes is projected to increase from 10% in recent period (by definition) to ~50% by late 21st century, with a large model spread (25% for MRI, 80% for IPSL). A meridional gradient is found in the model-ensemble response, with a higher (lower) increase in warm extremes in Southern (Northern) Europe. In winter, the frequency of cold extremes is projected to decrease from 10% to ~1%, again with a large model spread (0.3% for IPSL and MIROC, 2.5% for NCC). This depletion is generally higher in North-Eastern Europe. Patterns of changes in both summertime and wintertime extremes are consistent with mean temperature

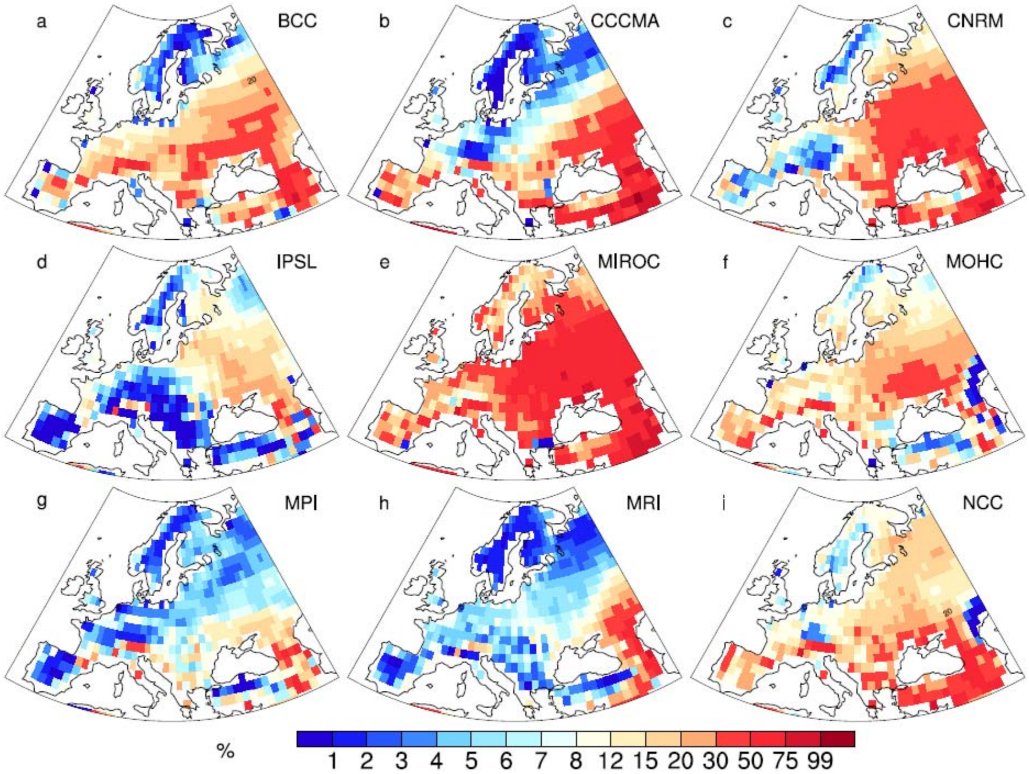

Figure 30*: *Frequencies of summertime extremely hot days in amip experiments.

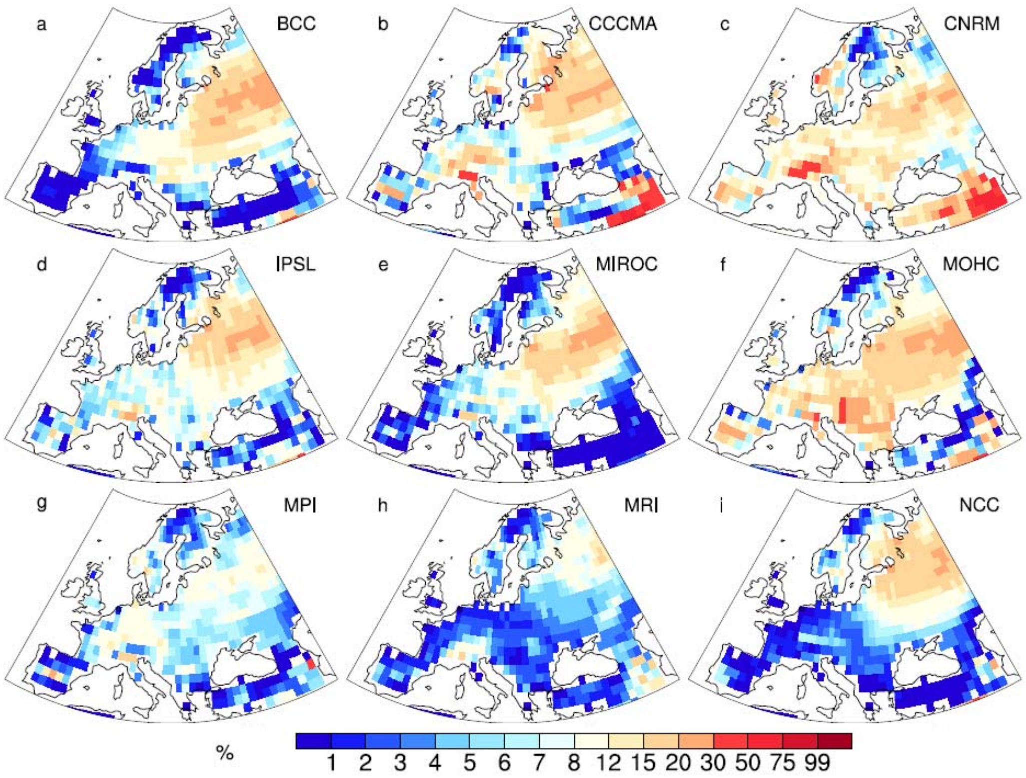

Figure 31*: *Frequencies of wintertime extremely cold days in amip experiments.

changes, but not necessarily scaled in amplitude: for instance the highest mean warming in summer occurs for CCCMA while the highest increase in hot extremes occurs for IPSL.

A similar diagnostic was made in CFMIP2 experiments by comparing amipFuture to amip run (only EUCLIPSE models available). Despite similarities in the main responses (increase in warm extremes, decrease in cold extremes), patterns and amplitude differ from CMIP5 experiments, which is likely due to the difference in SSTs. We therefore believe that an extra CFMIP2 experiment forced, for each model, by the native SST anomaly derived from the rcp85 run could be helpful.

iii) Separating dynamical vs. non-dynamical contributions

European temperatures are mainly driven by the North-Atlantic atmospheric dynamics. The attribution of both present-day biases and future changes to dynamical (i.e. large-scale circulation) and/or other processes (i.e. radiative fluxes, soil or cloud feedbacks) is therefore a key question. In order to separate the role of large-scale circulation we use a weather-regime approach that clusters daily anomalies of Z500 into preferred states. Regimes derived from NCEP2 reanalysis are taken as reference. We find 4 quasi-equiprobable regimes for both summer (Atlantic Low, Blocking, Atlantic Ridge and NAO-) and winter (NAO+, NAO-, Blocking and Atlantic Ridge), which can be described by their frequencies of occurrence f_k and their intra-class distributions of circulations d_k (or structures). Any mean variable $\overline{X}$ (e.g., frequency of extreme days) can be written as:

$$\overline{X} = \sum_k f_k \cdot \Phi(d_k)$$

with Φ a transfer function between circulations and X. Thus a difference between two values of $\overline{X}$ (e.g., model vs. observations or future F vs. present P) can be broken down into:

$$\Delta^{F-P}\overline{X} = \underbrace{\sum_k \Delta f_k \cdot \Phi^P(d_k^P)}_{BC} + \underbrace{\sum_k f_k^P \cdot \Phi^P(\Delta d_k)}_{WCd} + \underbrace{\sum_k f_k^P \cdot \Delta\Phi(d_k^F)}_{WC\Phi} + \epsilon$$

where BC + WCd is the dynamical contribution (differences in regimes' frequencies + structures) and WC Φ the non-dynamical contribution (see details in Cattiaux et al. 2011a, 2011b). Figure 32 shows biases and future changes in regimes' frequencies for both seasons. Present-day biases are contrasted, except for the winter Blocking which is underestimated by all models (a,c). As in previous CMIP, a robust increase in summer Blocking is found (b). Surprisingly, CMIP5 models exhibit an increase in winter NAO- to the detriment of NAO+ and Blocking (d), which is in noted contradiction with increases in NAO+ found in all previous CMIP and in CFMIP2 experiments (amipFuture vs. amip frequencies). Eventually, applying the linear breakdown methodology to mean frequencies of warm/cold extremes in the model-ensemble shows that:

- dynamical contributions to present-day biases and future changes are minor, especially in summer. The under-estimation of wintertime Blocking slightly contributes to the lack of cold extremes in Central Europe, while the future increase in wintertime NAO- tends to limit the depletion in cold extremes in Scandinavia.
- dynamical contributions to uncertainties (model-spread) are minor in summer, but substantial in winter, especially due to disagreements on changes in Atlantic Ridge frequency and NAO-/Blocking structures (Figure 33).

The next step will consist in understanding non-dynamical contributions, which seem to play a major role, especially in summer. In particular, contributions of radiative fluxes and potential roles of land surface and cloud feedbacks to present-day biases and future uncertainties in temperature extremes will be investigated.

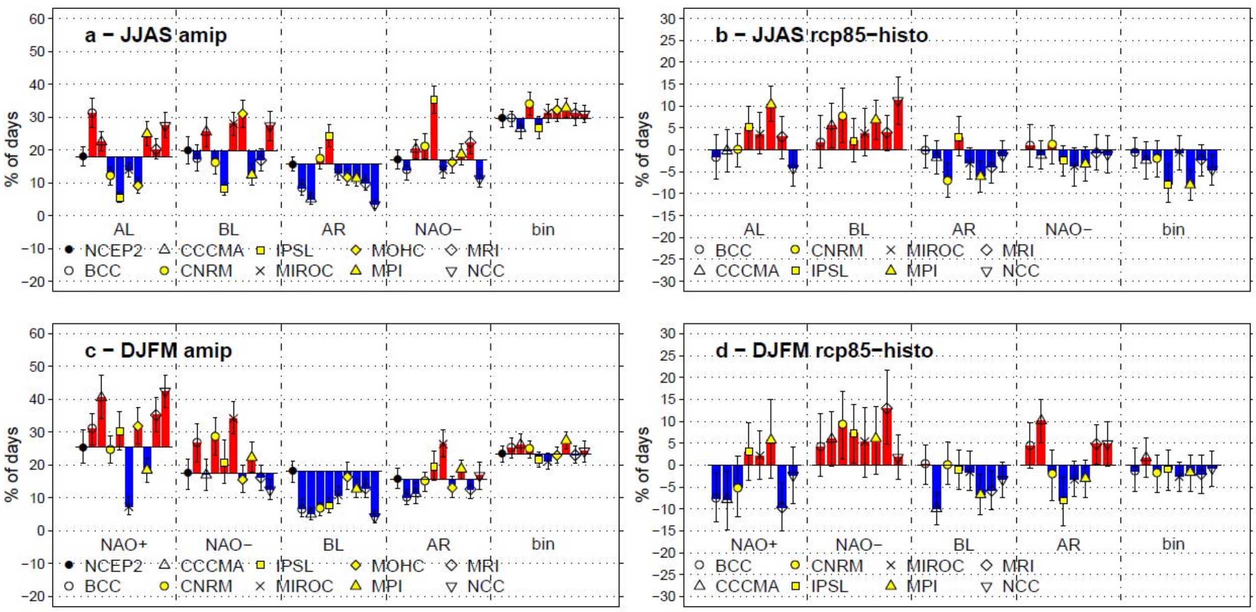

Figure 32**:** *Frequencies of occurrence of weather regimes. (a–b) Summer: (a) amip frequencies as departures from NCEP2 reference and (b) rcp85-historical differences. (c–d) Same for winter. EUCLIPSE models are highlighted in yellow. MOHC is missing in right panels (Z500 unavailable so far).*

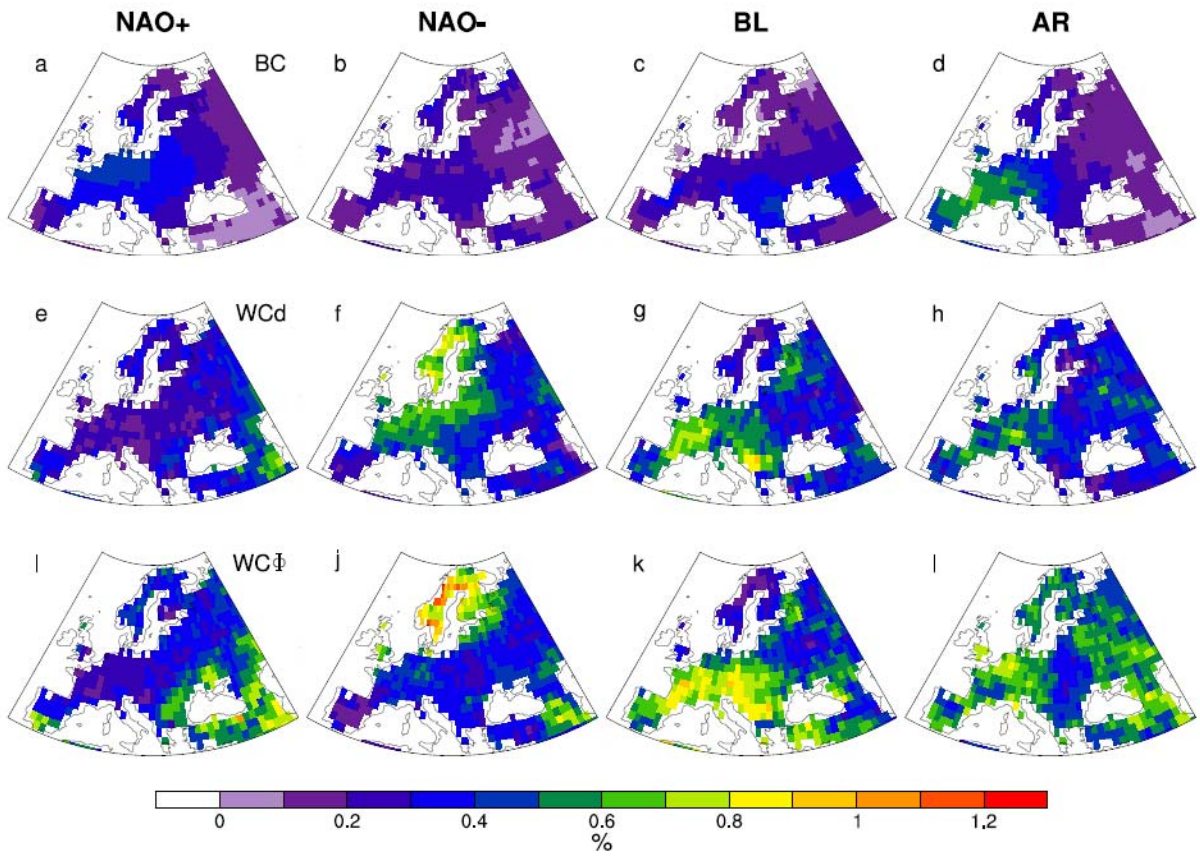

Figure 33: *Breaking-down methodology applied to future uncertainties in wintertime cold extremes: multi-model standard deviations of each term of the equation, sorted by regime (columns) and contribution type (rows).*

Diagnostic of the climate feedbacks produced by the different models in some CMIP5 simulations; Report on the spreads of feedbacks and of cloud and precipitation responses to climate change and their comparison with estimates from the CMIP3 models

Deliverable 2.6

1. Analysis of climate sensitivity estimates from CMIP5 models

i) Introduction

We quantify forcing and feedbacks across available CMIP5 coupled atmosphere-ocean general circulation models (AOGCMs) using several methodologies. First, we analyze simulations forced by an abrupt quadrupling of atmospheric carbon dioxide concentration and apply the linear forcing-feedback regression analysis of Gregory et al. (2004) to the ensemble of AOGCMs. We show that the range of equilibrium climate sensitivity is 2.1-4.7 K, i.e. close to that derived from CMIP3 models, and that differences in cloud feedbacks continue to be important contributors to this range. Then, using the so-called kernel approach proposed by Soden and Held (2006) we assess the role of inter-model differences in climate feedbacks associated with water vapor, temperature lapse rate, clouds and surface albedo in the spread of climate sensitivity. This analysis confirms the role of cloud feedbacks in the climate sensitivity uncertainty. It also shows that fast tropospheric adjustments to CO2 contribute to the spread, but to a much lesser extent than climate feedbacks.

ii) Climate sensitivity estimates

Equilibrium climate sensitivity (ECS) is defined as the global equilibrium surface-air-temperature change in response to instantaneous doubling of atmospheric CO2 concentration. Although this is clearly not a realistic scenario, ECS is a convenient way of quantifying the joint effect of forcing and feedback, which are separately quantities of practical interest for understanding and predicting transient climate change. Recently, a new generation of climate models, participating in CMIP5, has been developed. Diagnosing the forcings, feedbacks and ECS in each of these models is a first step to identifying and understanding sources of uncertainty in their climate projections.

AOGCM	Radiative Forcing (Wm^{-2})		Climate Feedback Parameter $-\alpha$ ($Wm^{-2} K^{-1}$)				$2xCO_2$ Eqm Climate Sensitivity (K)
	Fixed-SST	Regression	Net	LW Clear-Sky	SW Clear-Sky	Net CRE	
CanESM2	7.35	7.67	−1.04	−1.88	0.71	0.13	3.69
CNRM-CM5	n.a.	7.43	−1.14	−1.73	0.78	−0.20	3.25
CSIRO-Mk3-6-0	6.20	5.17	−0.63	−1.70	0.84	0.23	4.08
GFDL-CM3	n.a.	5.98	−0.75	−1.94	0.70	0.48	3.97
GFDL-ESM2G	n.a.	6.18	−1.29	−1.65	0.61	−0.26	2.39
GFDL-ESM2M	n.a.	6.72	−1.38	−1.63	0.58	−0.33	2.44
HadGEM2-ES	6.99	5.85	−0.64	−1.66	0.65	0.37	4.59
INM-CM4	6.24	5.95	−1.43	−1.98	0.67	−0.12	2.08
IPSL-CM5A-LR	6.49	6.20	−0.75	−1.99	0.53	0.70	4.13
MIROC-ESM	n.a.	8.51	−0.91	−1.93	0.83	0.19	4.67
MIROC5	n.a.	8.25	1.52	1.85	0.84	0.51	2.72
MPI-ESM-LR	8.63	8.18	−1.13	−1.79	0.71	−0.04	3.63
MPI-ESM-P	n.a.	8.62	−1.25	−1.80	0.65	−0.10	3.45
MRI-CGCM3	7.19	6.49	−1.25	−1.99	0.83	−0.09	2.60
NorESM1-M	n.a.	6.21	−1.11	−1.86	0.86	−0.11	2.80
Model mean	7.01	6.89	−1.08	−1.83	0.72	0.02	3.37
Standard Dev.	0.85	1.12	0.29	0.13	0.11	0.32	0.83

Table 4: Forcing, feedback and equilibrium climate sensitivity values from CMIP5 models. The 4xCO2 adjusted radiative forcing has been diagnosed via two independent methods: regression and fixed-SST. The – and equilibrium climate sensitivity values are derived from ordinary least-squares regression. From Andrews et al. (2012).

For this purpose, we apply the regression method of Gregory et al. (2004) to an ensemble of AOGCMs using the CMIP5 so-called "abrupt4xCO2" experiment. Another estimate of the forcing is derived from CMIP5 4xCO2 equilibrium experiments.

The ECS of each model is given in Table 4 and shown in Figure 34, increasing from left to right. Based on the available CMIP5 model simulations, the ECS spans the range from 2.1 K to 4.7 K, which is similar to the 2.1-4.4 K range diagnosed from equilibrium 2xCO2 slab-ocean experiments performed with the earlier CMIP3 generation of models (Randall et al. 2007).

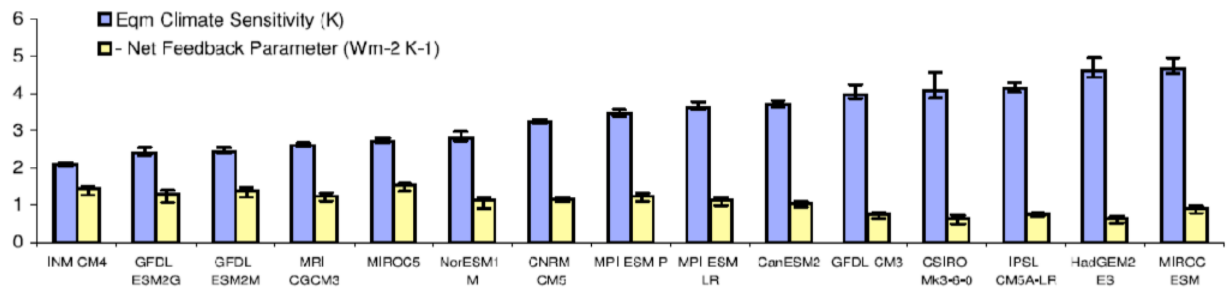

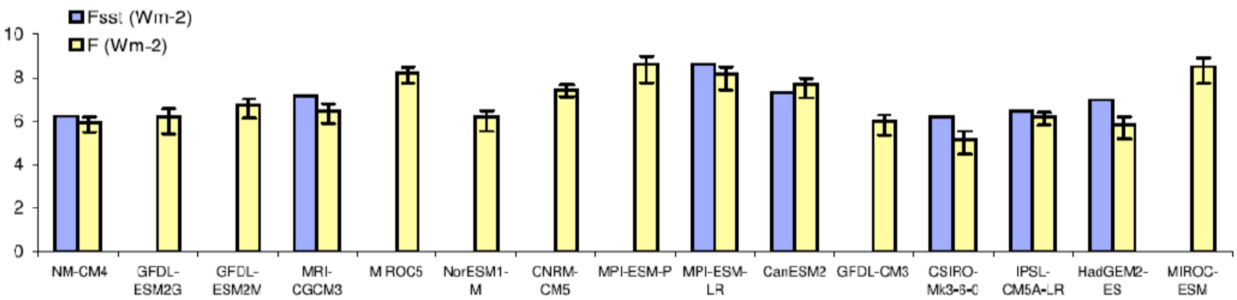

Figure 34: *Comparison of the 2xCO2 equilibrium climate sensitivity, 4xCO2 adjusted radiative forcing (from fixed-SST, Fsst, and regression, F) and various climate feedback terms. The models are ordered from left to right in order of their equilibrium climate sensitivity. Note that in the top panel,* α *is reported as the climate feedback parameter, rather than -*α*, to maintain the same scale. Errors bars represent 95% (2.5-97.5%) confidence interval on the fit. From Andrews et al. (2012).*

There are some differences in forcings across models, which might be expected from differences in their treatment of radiative transfer and differences across models in rapid tropospheric and land surface adjustment processes (e.g. Gregory and Webb, 2008). In the previous generation of models, differences in feedbacks contributed more to the uncertainty in ECS than forcing (Webb et al., 2006, 2012). This also appears to be the case in CMIP5.

Although the multi-model mean CRE (cloud-radiative effect) feedback is close to zero (Table 4), large differences between models are noticeable (Table 4). The models span a wide range (-0.5 to +0.7 W/m2/K), which explains most of the range in the net feedback parameter, as in CMIP3 (Ringer et al. 2006). Such values are consistent with near neutral or positive cloud feedbacks of CMIP5 models (like CMIP3 models) when defining cloud feedbacks relative to the Planck response and thus taking into account the cloud masking effects (Soden et al. 2008).

The spread of ECS can to a certain extent be explained by differences in CRE feedbacks, i.e., those models with a more positive CRE feedback tend to have a larger ECS. As with the older generation models (Webb et al. 2006), this spread mostly comes from inter-model differences in SW CRE feedback processes.

iii) Interpretation of the spread of climate sensitivity estimates

The spread of CMIP5 climate sensitivity estimates is analyzed further by using another methodology consisting in decomposing the global-mean surface temperature change into climate feedbacks associated with radiative forcing, water vapor, temperature lapse-rate, surface albedo and cloud changes (Dufresne and Bony 2008). For this purpose, we use the radiative kernel approach (Soden and Held 2006) to diagnose climate feedbacks and tropospheric adjustments from CMIP5 models (Vial et al., submitted). Recognizing that the increase of CO2 induces fast adjustments in the atmosphere and at the land surface (Gregory and Webb 2008), we define the radiative forcing of each model from atmosphere-only experiments in which the CO2 concentration is increased but sea surface temperatures are kept unchanged.

For each model (11 models have been considered so far, including 3 EUCLIPSE models), we compute the contributions to climate sensitivity associated with each feedback parameter and with the fast response to CO2 (Figure 2). From a methodological point of view, we find that considering the tropospheric adjustments to CO2 as part of forcings rather than feedbacks (like at the time of CMIP3) reduces the strength of cloud feedbacks by about 20%, but does not substantially affect their spread.

The contributions of the Planck response, tropospheric adjustments, and feedbacks to the multi-model mean estimate of climate sensitivity show than on multi-model average, the Planck response and the combined water vapor plus lapse rate feedback provide the largest contributions to the climate sensitivity (their sum contributes for two third of the multi-model mean climate sensitivity), and that the sum of the cloud feedback, surface-albedo feedback and CO2 adjustments contributes for about one third.

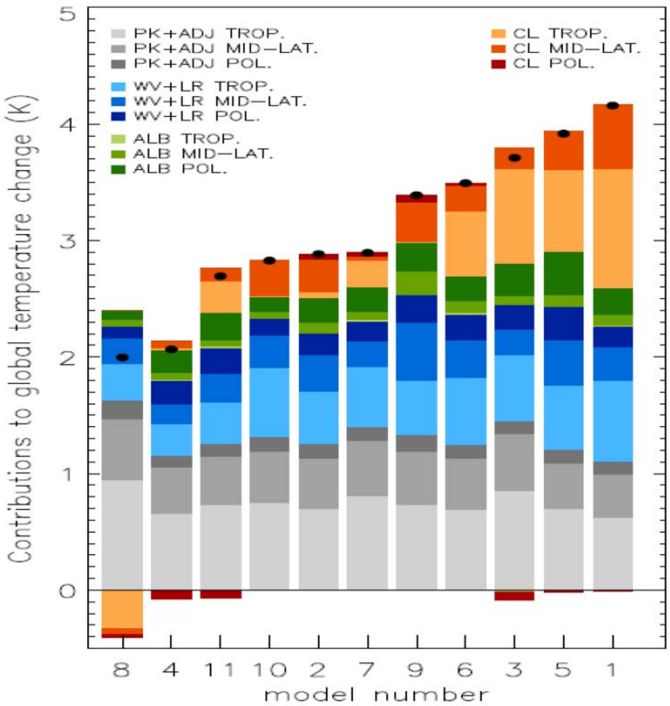

***Figure 35**: Decomposition of the climate sensitivity estimate (indicated by black dots) of each CMIP5 model into different contributions (the sum of all contributions equals the climate sensitivity): the Planck response to the non-adjusted forcing and the adjustments (PK+ADJ, in grey), the combined water vapour + lapse rate feedback (WV+LR, in blue), the albedo feedback (ALB, in green) and the net could feedback (CL, in red). Each contribution is also decomposed into the three different regions: the tropics (light shading), the mid-latitudes (medium shading) and the poles (dark shading). From Vial et al. (submitted).*

In terms of inter-model differences, on the other hand, the relative contributions of the different components is very different. Cloud feedbacks are responsible for about 70% of the spread of climate sensitivity estimates amongst models, with a large contribution from the tropics. The combined water vapor + lapse rate feedback is found to also provide a non negligible contribution to the spread of climate sensitivity.

This work will be updated in the next few months by adding models to the analysis, as soon as they become available on the CMIP5 multi-model archive.

2 Analysis of tropical cloud feedbacks

i) Introduction

In CMIP3, tropical cloud feedbacks exhibited a large spread amongst models, which primarily resulted from. We show that the spread of tropical cloud feedbacks has not narrowed among CMIP5 models (Vial et al, submitted), and that it is still dominated by inter-model differences in the (low) cloud response predicted by the models in regimes of weak subsidence and shallow convection. By analyzing the cloud response to global warming in a range of model configurations (coupled ocean-atmosphere, atmosphere-only, aqua-planet, single-column), we are able to interpret the physical mechanisms underlying the strongest positive cloud feedback estimate from CMIP5 models (predicted by the IPSL-CM5A-LR model).

ii) Spread of tropical cloud radiative responses

Figure 36 shows that the spread of tropical cloud-radiative responses amongst CMIP5 models has not reduced compared to CMIP3 (Bony and Dufresne 2005, Vial et al. submitted). CMIP5 experiments now allow us to assess the relative contributions of temperature-mediated responses (feedbacks) and tropospheric adjustments to the spread of cloud-radiative responses under climate change.

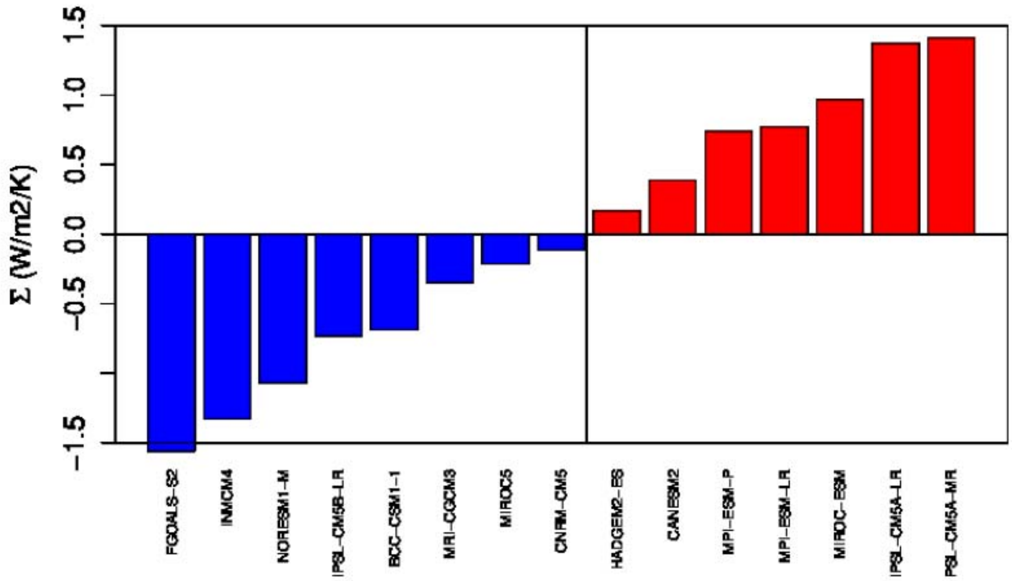

Figure 36*: Sensitivity (in W/m2/K) of the Net Cloud Radiative Forcing to Sea Surface Temperature changes predicted by 15 CMIP5 coupled ocean-atmosphere climate models over tropical ocean. Low-sensitivity models are shown in blue, and high sensitivity models in red. This figure is an update of Bony and Dufresne (2005).*

We find that both feedbacks and adjustments contribute to the spread, with however a much larger role of feedbacks. We find that the spread of tropical cloud-radiative responses and cloud feedbacks arises from a larger range of dynamical regimes in CMIP5 than in CMIP3, but that it remains dominated by inter-model differences in the SW component of cloud feedbacks and by the cloud response in regimes of weak subsidence and shallow convection (Vial et al submitted). Current analyses now focus on determining the role of different cloud types and physical processes in the inter-model spread of cloud radiative responses under climate change.

iii) Interpretation of the positive cloud feedback predicted by the IPSL-CM5A-LR model

The response of low-level clouds to climate change has been identified as a major contributor to the uncertainty in climate sensitivity estimates among climate models. Figure 36 shows that the IPSL-CM5A-LR coupled ocean-atmosphere model is the model that predicts the strongest positive cloud feedback in the tropics. By analyzing the behaviour of low-level clouds in a hierarchy of models (coupled ocean-atmosphere model, atmospheric general circulation model, aqua-planet model, single-column model) using the same physical parameterizations, we propose an interpretation of the strong positive low-cloud feedback predicted by this model under global warming (Brient and Bony 2012).

In a warmer climate, the model predicts an enhanced clear-sky radiative cooling, stronger surface turbulent fluxes, a deepening and a drying of the planetary boundary layer, and a decrease of tropical low-clouds in regimes of weak subsidence. We show that the decrease of low-level clouds critically depends on the change in the vertical advection of moist static energy from the free troposphere to the boundary-layer. This change is dominated by variations in the vertical gradient of moist static energy between the surface and the free troposphere just above the boundary-layer. In a warmer climate, the thermodynamical relationship of Clausius-Clapeyron increases this vertical gradient, and then the import by large-scale subsidence of low moist static energy and dry air into the boundary layer. This results in a decrease of the low-level cloudiness and in a weakening of the radiative cooling of the boundary layer by low-level clouds.

We are currently investigating the extent to which the energetic framework proposed in this study helps to interpret the spread of tropical cloud feedbacks exhibited by CMIP5 models (Figure 36) under climate change.

We also studied the influence of uncertain model parameters on the low-cloud feedback predicted by this model (Brient and Bony, submitted). For this purpose, sensitivity tests were carried out in a range of model configurations (atmospheric GCM, aqua-planet GCM, single-column model). We show that the physical mechanism and the sign of the IPSL-CM5A-LR feedback is robust, but that the strength of the feedback can vary considerably depending on the model tuning parameters. Moreover, the strength of the low-cloud response to climate change exhibits a strong correlation with the strength of the low-cloud radiative effects predicted in the current climate. We show that this correlation primarily results from a local positive feedback (referred to as the beta feedback) between boundary layer cloud radiative cooling, relative humidity and low-cloud cover. Based on this correlation and observational constraints, it is suggested that the strength of the tropical low-cloud feedback predicted by the IPSL-CM5A model in climate projections might be overestimated by about fifty percent.

We showed that CMIP5 models still exhibit a ”too few, too bright” low-cloud problem in the tropics and that the models systematically over-estimate the optical thickness of low-level clouds (Nam et al. 2012). This bias potentially over-estimates the strength of the ”beta feedback”. In the future, in collaboration between WP2 and WP4, we will investigate further the role that the beta feedback may play in the simulation of the current climate and in climate change cloud feedbacks, based on coordinated model experiments.

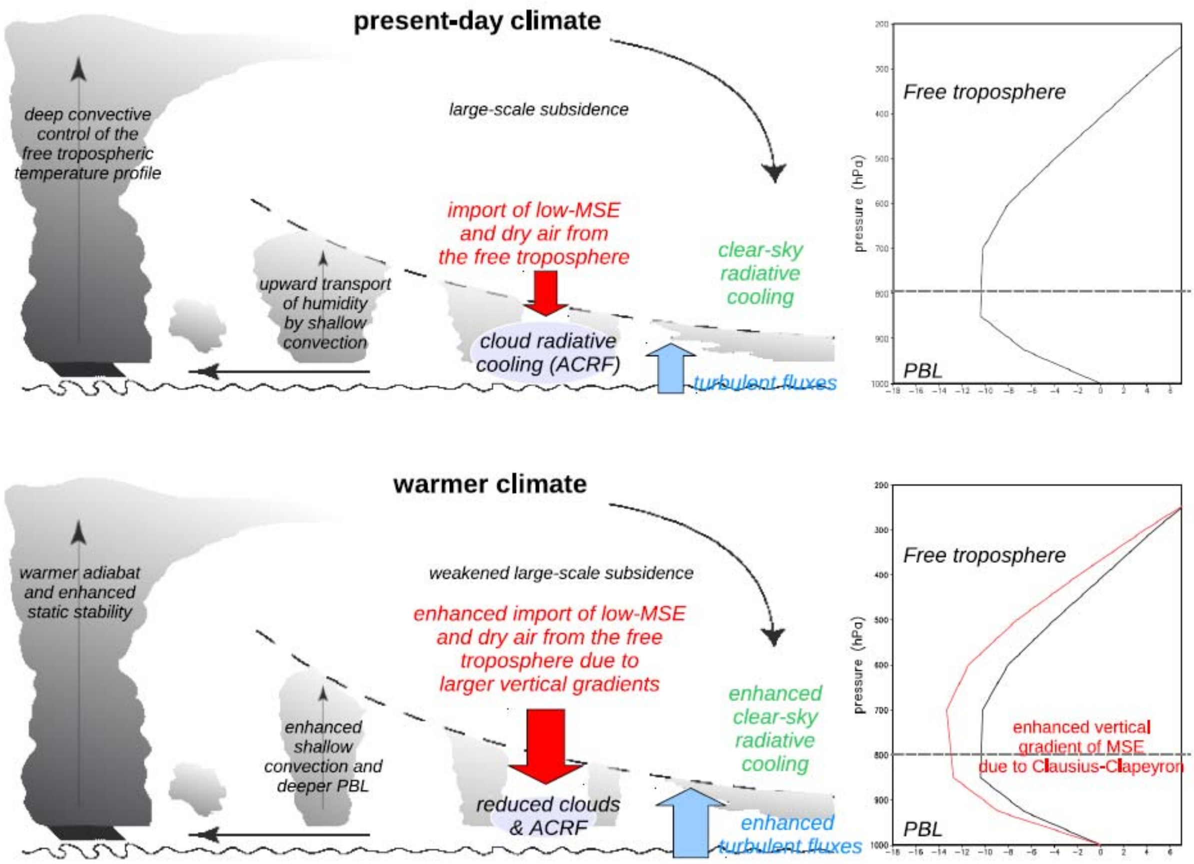

***Figure 37**: Schematic of the physical mechanisms controlling the positive low-cloud feedback of the IPSL-CM5A-LR OAGCM in climate change. In the present-day climate, tropical marine lowclouds primarily occur in regimes of large-scale subsidence. In these regimes, the moist static energy (MSE) of the PBL is increased by surface turbulent fluxes, and decreased by clear-sky radiative cooling, cloud-radiative cooling, and by the downward advection of low MSE from the free troposphere (the typical profile of MSE deficit on the right -defined as the difference between the MSE profile and the 1,000 hPa MSE- shows that the MSE minimum occurs around 700850 hPa in weak subsidence regimes). Shallow cumulus clouds contribute to the vertical transport of humidity from the PBL to the lower free troposphere, and deep convection controls the free tropospheric temperature profile of the tropical belt. In a warmer climate, the change in the moist-adiabatic stratification of the tropical atmosphere, the enhanced vertical transport of humidity by shallow convection and the deeper PBL due to enhanced surface fluxes all tend lead to a decrease of the vertical gradient of MSE. However, the non-linearity of the Clausius-Clapeyron relationship leads to a larger increase in specific humidity at high temperatures and low altitudes than at lower temperatures and higher altitudes. This leads to an enhanced vertical gradient of specific humidity and MSE between the PBL and the lower free troposphere, and thus an enhanced import of low-MSE and dry air from the free troposphere down to the PBL. This decreases the low-level cloud fraction and weakens the cloud radiative cooling within the PBL. From Brient and Bony (2012).*

3 Analysis of tropical precipitation projections

i) Introduction

Large uncertainties remain about the future evolution of rainfall, particularly in the tropics and at the regional scale. Understanding the factors that control the regional distribution of tropical precipitation and its response to anthropogenic activities would help to assess model projections and to inform policy decisions about adaptation and mitigation. In the original EUCLIPSE proposal, we had planned to analyze the spread of regional precipitation responses to climate change. However, when analyzing CMIP5 precipitation projections, we were struck by the resemblance of the regional pattern of tropical precipitation change predicted by CMIP5 models with that predicted by CMIP3 models under different scenarios. For this reason, we decided to understand first the reasons for this robustness before investigating the reasons for inter-model differences. In this report, we thus focus on the understanding of the CMIP5 multi-model mean pattern of tropical precipitation changes at the regional scale.

i) Analysis

The increase of carbon dioxide concentration in the atmosphere is expected to affect the hydrological cycle through surface warming (e.g. Held and Soden 2006). However, recent studies have shown that carbon dioxide could also impact the atmosphere through fast adjustments independent of surface temperature changes (e.g. Gregory and Webb 2008). To assess the actual dependence of tropical precipitation projections on surface warming, we analyze a large suite of CMIP5 model outputs from a range of experiments (realistic, idealized, RCP scenarios) and configurations (coupled ocean-atmosphere model, atmosphere-only, aqua-planet, single-column), and we decompose the regional precipitation changes into thermodynamical and dynamical components (Figure 38).

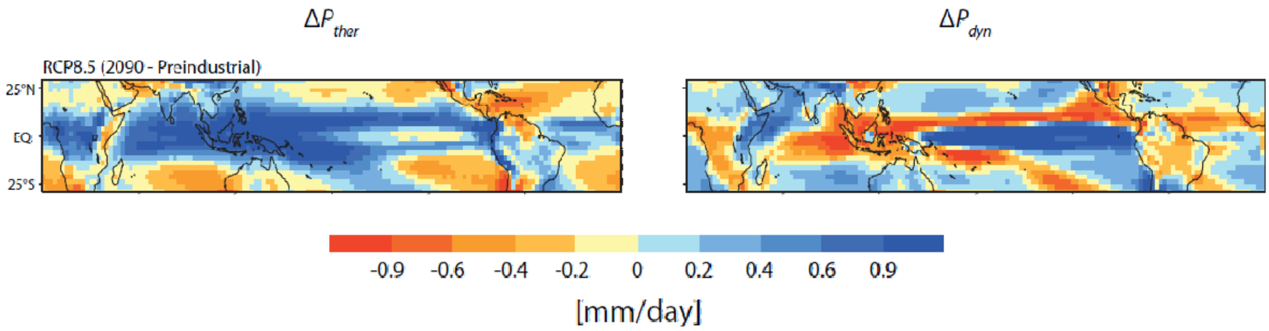

***Figure 38**: Interpretation of the multi-model mean regional pattern of tropical precipitation projections. The annual-mean precipitation change predicted by CMIP5 coupled ocean-atmosphere models in a non-mitigated climate change scenario (RCP8.5) at the end of the century (around 2090) is decomposed into thermodynamical (**Δ**Pther) and dynamical (**Δ**Pdyn) components (**Δ**P = **Δ**Pther + **Δ**Pdyn). The thermodynamical component is dominated by the Clausius-Clapeyron relationship and thus exhibits a "wet get wetter, dry get drier" regional pattern, while the dynamical component is related to the change in large-scale atmospheric vertical motions. From Bony et al. (submitted).*

We show that in the tropics, a substantial fraction of the long-term precipitation changes projected by climate models by the end of the century, and particularly the dynamical component, does not depend on surface warming but results from the fast and direct impact of increased carbon dioxide concentrations on the large-scale atmospheric circulation. This effect is explained by the radiative impact of greenhouse gases on the internal cooling of the atmosphere, which affects tropical convection and the strength of atmospheric vertical motions. It is predicted by multiple state-of-the-art climate models in a large spectrum of configurations, and by an operational Numerical Weather Prediction model (we performed weather forecasts in 4xCO2 conditions with the ECMWF-IFS model). These findings suggest promising strategies for improving the assessment of regional rainfall projections, and highlight the limitations of geo-engineering strategies that would aim at weakening global warming and regional precipitation changes without removing carbon dioxide from the atmosphere.

Over the next years, we plan to exploit these findings and this methodology to better understand inter-model differences in regional precipitation projections in the tropics.

WP3 : Process-Level Evaluation

1. Introduction

WP3 aims to evaluate and to understand how the large-scale forcing conditions control cloud cover, cloud amount, precipitation, and how these cloud properties influence the radiative budget and to what extend this is faithfully reproduced by the ESMs. Moreover WP3 aims to asses how these cloud properties and their associated radiative properties change if we apply perturbed large scale forcing conditions that are indicative for future climate conditions such as warmer SST's and weakened large scale subsidence. This way we can obtain guidelines how cloud feedback mechanisms operate and which are the underpinning physical mechanisms that can be used to critically test the realism of the parameterized cloud response in Earth System Models.

Since the largest source of uncertainty in cloud climate feedback in ESM's are due to their representation of low low clouds we concentrate in WP3 on stratocumulus (scu) and shallow cumulus clouds (shcu) and transition mechanisms between those clouds.

In order to achieve realistic representations of these cloud types, but also understanding and ultimately a comprehensive evaluation to what extend state of the art parameterizations in operational ESM's are capable of reproducing the essential cloud physics and dynamics in both present and future climate conditions, a suite of different model approaches have been used:

1 *Large Eddy Simulations* are applied as to establish the most reliable and most realistic estimates for the representation of stratocumulus cumulus and transitions between these regimes both in present and future climate conditions.

2 *Mixed Layer Models* are simplified models that are uses achieve understanding on the behaviour of the realistic but complex results of the Large Eddy Simulation

3 *Single Column Models* are used to asses to what extend the parameterization packages of the ESM's that are part of EUCLIPSE are capable of reproducing the responses that are found for the Large Eddy Simulations and that are subjected to the same large scale forcings and perturbations

4 *High Frequency Output data from selected gridpoints from 3d ESM simulations* are used to assess the climatologies for various cloud regimes (including Scu and Cu) for a much wider ranger of large scale forcings for both present and future climate conditions

In the remainder of this section we will systematically review our findings with all these different model approaches, from which, for the first time, a comprehensive picture will emerge how boundary layer clouds behave under present and perturbed climate conditions.

2. Description of the Eulerian steady state cases and the Lagrangian transition cases.

Deliverable 3.1

The steady states of Scu and Shcu are based on a study form a previous European FP5 project EUROCS. In that project a comprehensive evaluation was performed for a number of Numerical Weather Prediction (NWP) and climate models over a cross section as indicated in Figure 39. This cross section follows the trade winds in the Hadley Cell starting from subtropics near the Californian coast where the cold ocean and the strong inversion due to the subsiding dry air favours the existence of solid stratocumulus decks. Further upstream these stratocumulus decks break up into shallow cumulus clouds as a results of weakened subsidence and a warmer ocean surface and finally at the Intertropical Convergence Zone (ITCZ) frequent deep convective events are observed. Evaluations of ESM output for different periods along this transect have been reported in the literature (Siebesma et al. 2003, Teixeira et al. 2011) and have surfaced the basis of three LES cases that are indicative for solid stratocumulus (S12), cumulus under stratocumulus (S11) and Shallow Cumulus (S6) as part of CGILS project (CFMIP-GCSS Intercomparison of Large-Eddy and Single-Column Models).

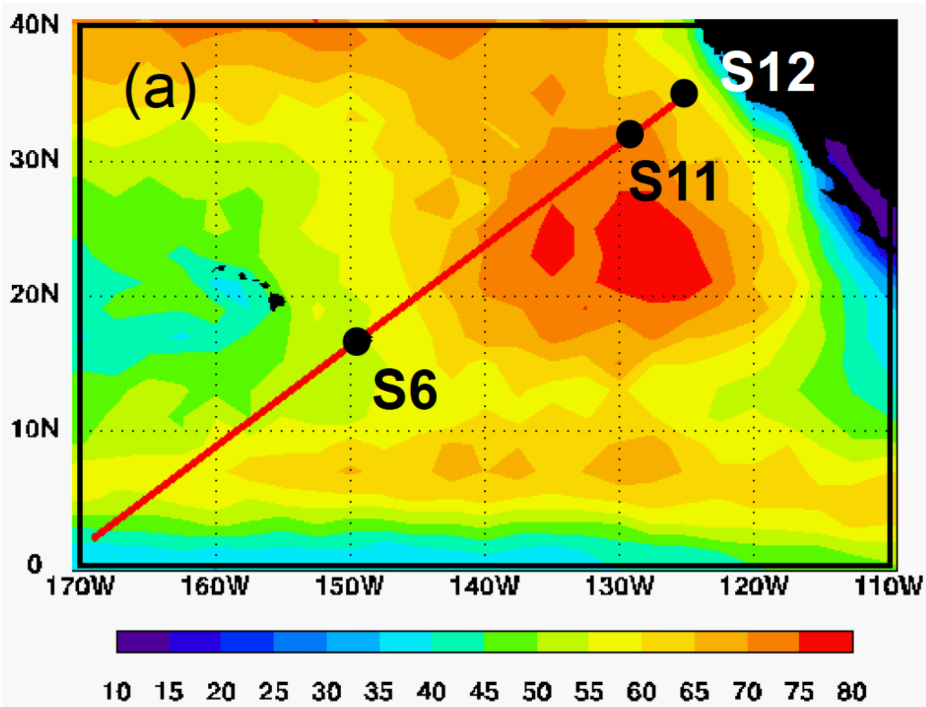

Figure 39. *Averaged amount of low clouds in June-July-August (%). The red line is the northern portion of the GPCI. The symbols 'S6', 'S11' and 'S12' are the three locations used in the CGILS experiments (From Zhang et al., 2012a).*

These 3 cases are also subjected to idealized future climate conditions in order to determine the cloud-radiative feedback by increasing the SST by 2K and through weakening the imposed subsidence. Details of the applied large scale forcings for the present and the future climate are displayed in Figure 40.

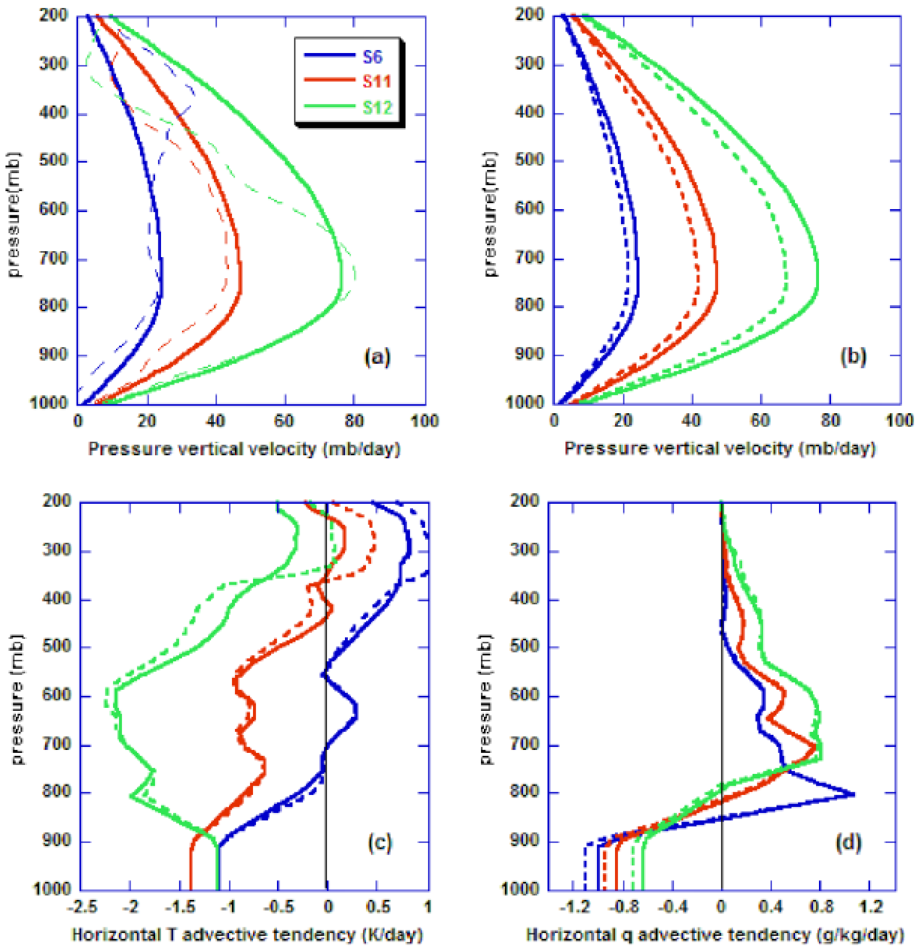

Figure 40. *(a) Large-scale pressure vertical velocity (subsidence) for the three locations in the control climate (solid lines), and in the ERA-Interim (dashed lines). (b) Same as (a) except that the dashed lines denote subsidence rates in the warmer climate. (c) Same as (b) except for horizontal advective tendency of temperature. (d) Same as (b) except for horizontal advective tendency of water vapor*

In addition to these three cases that aim to represent the steady states for three representative boundary layer clouds regimes in a Eulerian framework, there are additional Lagrangian cases constructed that follow the mean flow and thereby the transition from stratocumulus via cumulus under stratocumulus to a shallow cumulus regime. To this purpose observations collected during the First Lagrangian experiment of the Atlantic Stratocumulus to Cumulus Transition Experiment (ASTEX) (Albrecht et al., 1995; Bretherton et al., 1995; De Roode and Duynkerke, 1997) have been used to set up such a case. Figure 41 shows the schematics of the observed transition during ASTEX. The breakup of the stratocumulus cloud can be attributed to a weakening of the large-scale subsidence rate and a gradual decrease in the inversion stability and a subsequent increase in the entrainment rate. In addition to the ASTEX Lagrangian, we also consider a slow, intermediate and a fast transition based on composite observations as reported in Sandu and Stevens (2010). The initial conditions of the latter three cases differ mainly in terms of temperature and humidity jumps across the inversion layer. The availability of aircraft observations and satellite retrievals allows for a detailed verification of model results.

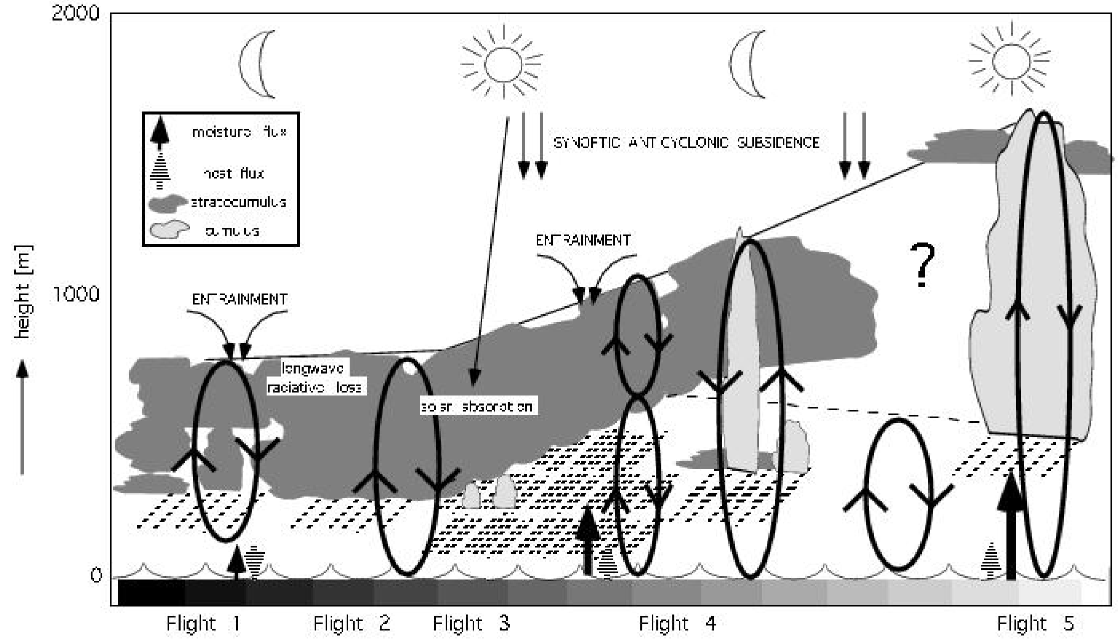

Figure 41. *Schematic of the stratocumulus to cumulus transitions as observed during the First Lagrangian of ASTEX. Five aircraft flights were performed between 12-14 June 1992.*

The set up description of the GPCI steady state cases can be found in Blossey et al. 2012, the set up description ASTEX langrangian case is reported in van der Dussen et al 2013 and the composite transition cases are published in Sandu and Stevens 2010). On the EUCLIPSE website (www.euclipse.eu), PDF versions of all these papers can be found.

3. Storage of instantaneous 3D LES fields and key statistical variables in a public archive.

Deliverable 3.2

Five LES models and twelve SCMs (see Tables 5 and 6 for a list of participating models) have submitted the results of the Lagrangian transitions.

Investigator	*Affiliation*	*Model*	*ASTEX*	*Composite cases*
Johan van der Dussen	**TUD**	**DALES**	✓	✓
Irina Sandu Thijs Heus	**MPI**	**UCLA**	✓	✓
Adrian Lock	**UK Met Office**	**MOLEM**	✓	✓
Marcin Kurowski	**U Warsaw**	**EULAG**	*v*	*x*
Peter Blossey	U Washington	SAM	✓	×
Andy Ackerman	NASA	DHARMA	✓	✓

Table 5. *Summary of participating LES models in the Lagrangian transition intercomparison cases. The participating EUCLIPSE models are written with bold face letters. The '✓' symbol indicates that the simulation results have been submitted.*

Investigator	*Affiliation*	*Model*	*ASTEX*	*Composite cases*
Eric Basile	**Meteo France**	**AROME**	✓	✓
		ARPEGE-NWP	✓	✓
Isabelle Beau	**Meteo France**	**ARPEGE-CLIMAT**	✓	✓
Sara dal Gesso **Roel Neggers**	**KNMI**	**EC-Earth**	✓	✓
		RACMO	✓	✓
Suvarchal Kumar	**MPI**	**ECHAM6**	*v*	*v*
Ian Boutle	**UK Met Office**	**UKMO**	✓	✓
Irina Sandu Martin Köhler	**ECMWF** DWD	**ECMWF**	**v**	✓
Vincent Larson	UWM	CLUBB	✓	×
Hideaki Kawai	JMA	JMA	✓	✓
Anning Cheng	NASA LaRC	LaRC	✓	✓
Heng Xiao	UCLA	UCLA-AGCM	✓	✓

Table 6. *Summary of participating SCMs in the Lagrangian transition intercomparison cases. The participating EUCLIPSE models are written with bold face letters. The '✓' symbol indicates that the simulation results have been submitted.*

The model results are stored and can be viewed at the KNMI Parameterization Testbed (KPT) web site (http://www.knmi.nl/samenw/rico/RICO) The purpose of the test bed project is to comprehensively evaluate existing and new parameterizations for general circulation models (GCMs) against atmospheric measurements from various permanent meteorological "supersites" on a continuous, daily basis. In addition, the site also hosts a suite of model intercomparison cases, including ASTEX and the three composite Lagrangian cases.

The user-friendly test-bed web interface allows for an easy visualization of any arbitrary variable that has been requested for data submission. Figure 42 displays an example of a plot produced from the test-bed web interface, and shows the cloud cover for the ASTEX First Lagrangian as obtained from the LES and SCM output. If available, results from aircraft measurements may also be added to the plots.

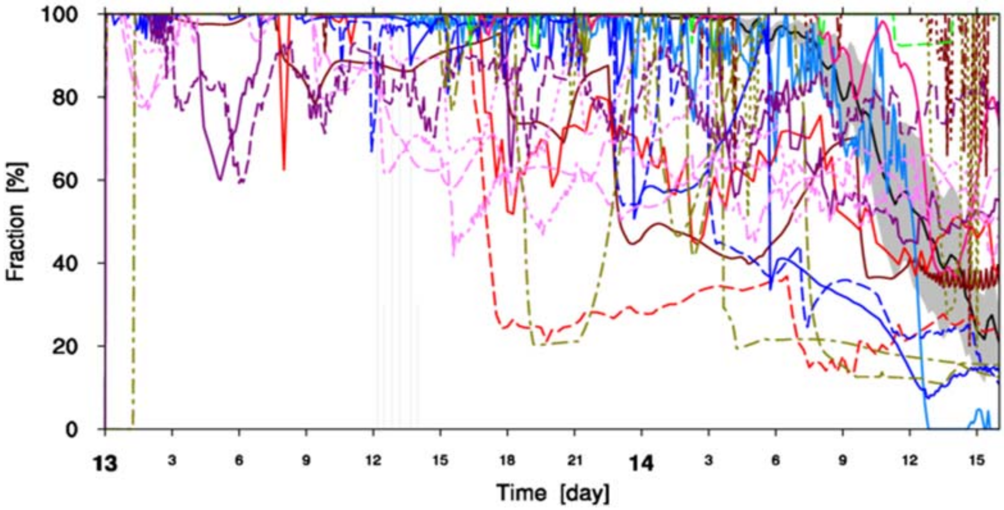

Figure 42. *Cloud cover results of twenty-four SCM simulations of the ASTEX Lagrangian. The grey band show the LES results, where the width of the band the standard deviation from the mean. The lines represent different models, and also display results obtained with modified set-ups of the model in order to test the effects of vertical resolution and changes in the parameterization scheme.*

The data of the instantaneous 3D LES fields are put in a public archive and can be found assessed through www.euclipse.nl/wp3/LES_DATA/ASTEX/Dales. The precise description of the data can be found in the Deliverable D3.2 that is posted at http://www.euclipse.eu/products.html.

4. Detailed analyses of the LES and SCM results the three GPCI columns for present and future climate.

Deliverable 3.3 and 3.9

i) Control (Present Day) Climate

The differences among all models can be seen in the time-averaged cloud profiles in Figure 43, from S6 in the top row to S12 in the bottom row. SCMs results are in the left column; LES models in the middle column; observations from C3M in the right column for the summers of 2006 to 2009. Note that the observations may have categorized drizzles as clouds, therefore having a different definition of clouds from that in the models. The blue lines denote the ensemble averages or multi-year averages; the red lines denote the 25 and 75 percentiles.

Despite large differences among the models, the intended shallow cumulus, stratocumulus, and coastal stratus are generally simulated. The values of the ensemble average of the SCMs and the LES models, and the cloud-top altitudes lie close to the range of the observations, even though the models used constant large-scale forcing. The spread in the LES models is much smaller than that in the SCMs, but they tend to overestimate the cloud peak height at S11 and S12 relative to observations. This is at least partially due to the idealized setup in which the large scale subsidence does not respond to clouds and the forcing is constant. The use of the same forcing for all models may have exaggerated the inter-model differences in the SCMs, especially in the depth of the capping inversion, since in GCMs the large scale circulation can respond to local differences in the inversion height to partially compensate them (Blossey et al. 2009).

In conclusion the realistic representation of the LES results and their small intermodal spread especially when compared with the intermodel spread between the SCM's justifies the approach to use the steady state LES results as a constraint to evaluate the SCM results and to use LES as a tool to assess how these cloud regimes will change in a future climate.

ii) LES results for cloud feedback in a Perturbed Climate

In order to mimic future climate conditions the three control cases vave been perturbed by an increase of the SST by 2K, the free troposphere is assumed to respond moist-adiabatically, the relative humidity is assumed to remain constant and the subsidence is weakened as indicated in Figure 40. The effect of clouds on the radiative budget is usually measure in terms of the cloud radiative effect (CRE) which is defined as

$$CRE = F_{clr} - F_{obs} \qquad (3)$$

where F_{clr} is the top of the atmosphere (TOA) outgoing radiation in the absence of clouds while F_{obs} denotes the TOA observed outgoing radiation. For the present case of boundary layer clouds CRE is negative, dominated by shortwave effects and roughly proportional to the cloud fraction and the liquid water path (LWP). Less clouds and/or a lower LWP will make the CRE less negative. Therefore a positive change in CRE ($\Delta CRE > 0$) corresponds to a positive cloud feedback. Fig. 6 displays ΔCRE for S12, S11 and S6.

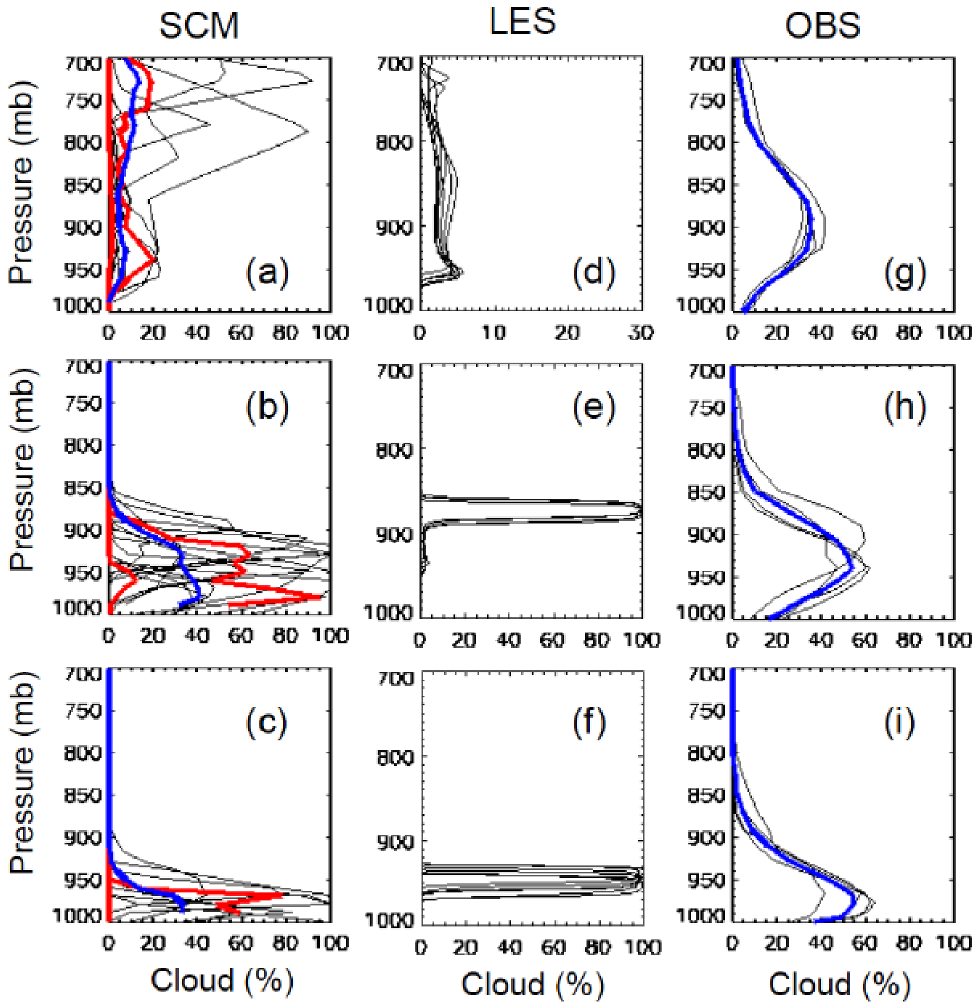

Figure 43: *(a)-(c) are the averaged profiles of cloud amount (%) by SCMs for S6, S11 and S12 respectively (from top to bottom panels). (d)-(f) are the same as (a)-(c) but by the LES models. (g)-(i) are from the C3M satellite measurements. The blue lines are ensemble averages; the red lines are the 25% and 75% percentiles.*

For the coastal Scu case S12, all the LES results, except DALES, remain overcasted in the perturbed climate with a thickening of the LWP resulting in a negative change in CRE. DALES gives a slight decrease of LWP. This might be due to the fact that DALES is the only model that does not employ a monotone advection scheme, which might result in artificial drying due to entrainment. The general consensus is therefore that for this well-mixed Scu case a warming SST and a weakened subsidence perturbation results in a *negative* cloud feedback. There is no consensus on the strength of the feedback which varies between marginal negative up to ~-10W/m^2. The LES results for cumulus under Stratocumulus case S11, show a neutral to positive cloud feedback feedback mainly due to a small decrease in LWP. A similar neutral to positive cloud feedback response is also found for the Cumulus case S6, mainly due to a small decrease in cloud fraction.

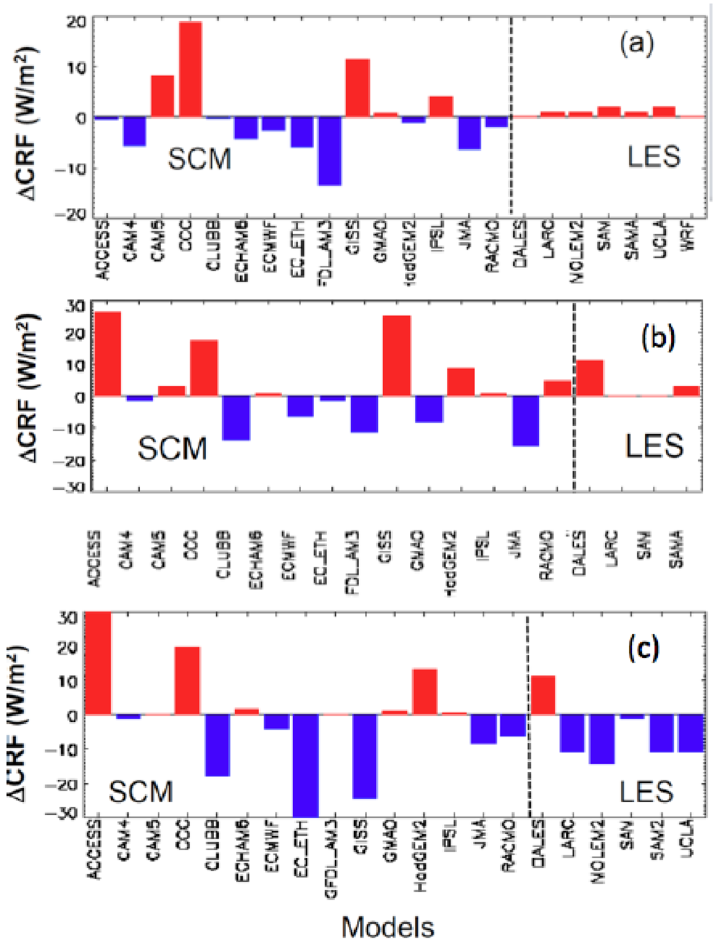

Figure 44. *Cloud feedback ΔCRF at S6 (a), S11 (b), and S12 (c), from Zhang et al. (2012a).*

<u>*iii) Interpretion of the LES results*</u>

The imposed climate change that of the LES runs consist of a simultaneous warming of the SST and a reduction of the subsidence (P2S). In order to gain a further insight on how these perturbation influence the mean state, an additional test has been made, which includes the thermodynamic (SST) warming but not the subsidence weakening (P2S). This is roughly analogous to the partitioning of tropics-wide cloud feedbacks into thermodynamic and dynamic components proposed by Bony et al. (2004). Cloud changes from the CTL to P2 simulations represent a sensitivity to thermodynamic changes, while cloud changes between the P2 and P2S simulations reflect a sensitivity to dynamic (subsidence) changes.

Figure 46 shows time-height cross-sections of cloud fraction from the CTL, P2 and P2S simulations from DALES; these are broadly representative of the evolution of all the models. The thermodynamic (SST) warming (P2) has a thinning effect on the Scu deck while the additional dynamical subsidence reduction (P2S) allows to cloud deck to grow deeper, resulting in a thicker cloud deck. The thermodynamical (P2) and the additional dynamical (P2S) for all LES codes are displayed in terms of change in short wave CRE and inversion height. These results show that the thermodynamic SST warming gives a rather strong weakening of the CRE (positive feedback) while the additional subsidence weakening results in a higher inversion height and a strengthening of the CRE (negative feedback).

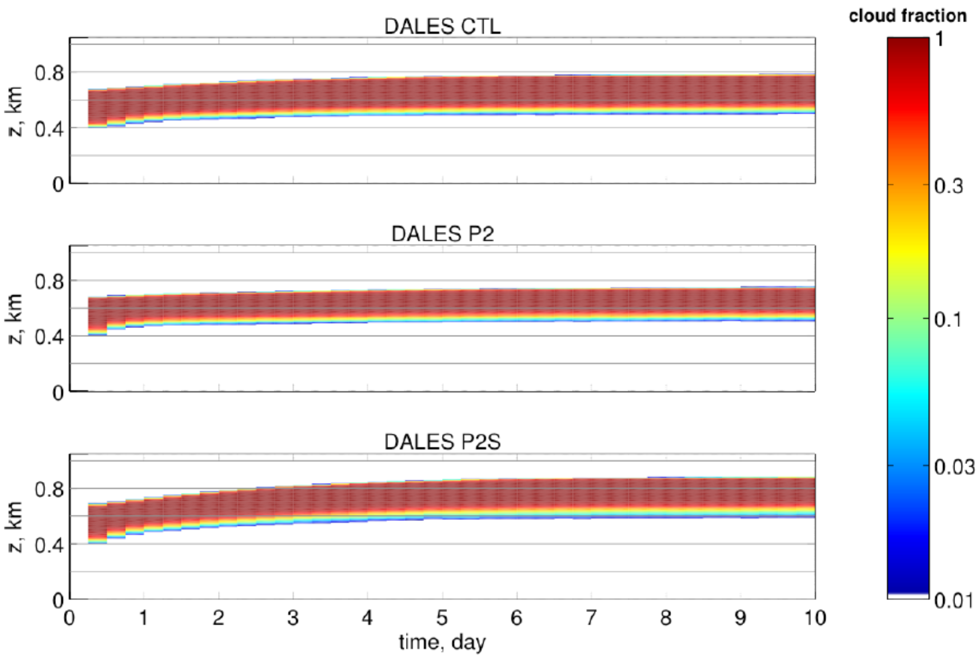

Figure 45. *Time-height profiles of cloud fraction for the S12 control, P2 and P2S simulations from DALES.*

This shows that the net cloud feedback is a result of two strong opposing effects and the net effect is subtle: For most models the negative cloud feedback effect of the weakening subsidence is stronger than the positive cloud feedback effect due to the thermodynamic SST warming. As mentioned before, the only exception is DALES, mainly due to the fact that this model has a stronger thinning of the cloud deck due to the SST warming than the other LES codes. As we will (see Section 7) many of the findings for especially S11 and S12 can be further understood and modelled by simple mixed layer models

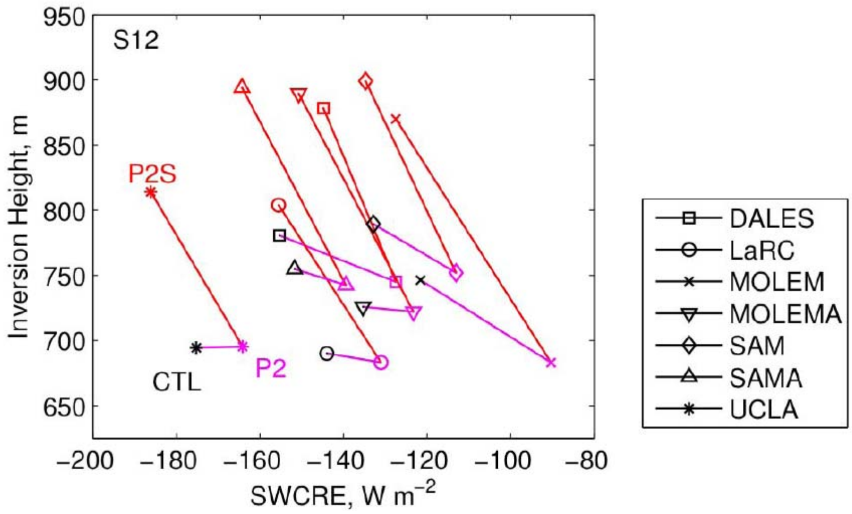

Figure 46. *Scatter plot of inversion height and shortwave cloud radiative effect from the CTL, P2 and P2S simulations for each of the CGILS models at S12. Lines connect the CTL, P2 and P2S simulations from each model.*

iv) SCM results of the cloud feedback in the perturbed climate

The responses of 15 SCM's to the perturbed climate in terms of change in CRE are displayed in Fig 47. For all three cases the cloud feedback response of the SCM's vary strongly in sign and magnitude. It is difficult to draw general conclusions since the various SCM's all have different parameterization packages that treat the turbulent mixing and the cloud formation processes. One commonality is that all SCM's do give enhanced surface latent heat fluxes (see Figure 47). This is due to the fact that due to the Clausius Clayperon relation the difference between the sea surface humidity and the near surface atmospheric humidity is increasing, provided that the relative humidity in the atmosphere is not changing too much. Since the surface latent heat flux is directly proportional to the humidity difference between the sea surface and the atmosphere, this explains the increase of the surface evaporation.

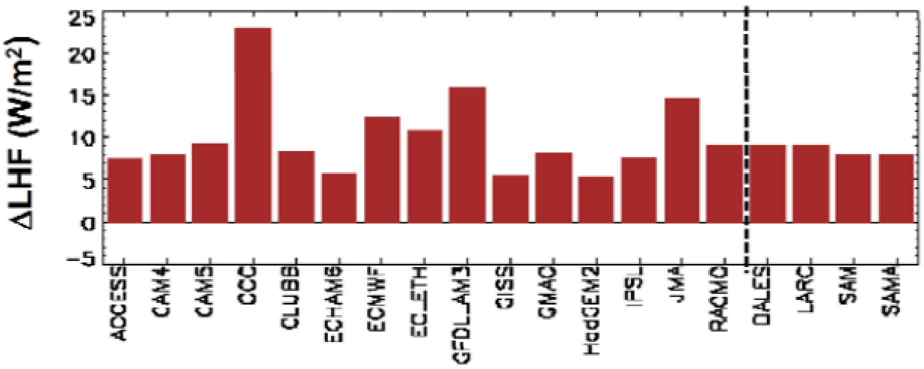

Figure 47. *Change in the latent heat flux ΔLHF at S11 , from Zhang et al. (2012a).*

However the resulting new cloud amount that determines the cloud feedback depends on many other processes. For the stratocumulus cases (S12 and S11) the entrainment of dry warm air from the free troposphere into the boundary layer is key to find the new equilibrium humidity and temperature in the mixed layer. As the various SCM's use different entrainment formulations that also depend strongly on the vertical resolution and hence on the numerical discretization, this is a prime source for uncertainty of the cloud feedback for these two cases. Additional sources are i) how well the turbulent mixing schemes are capable of mixing heat and humidity within the boundary layer, ii) how much precipitation is produced by the SCM's and iii) to what extend the SCM's are prone to grid locking which might prevent the SCM's to grow in response to the weakened subsidence. For the cumulus case (S6) the used convection and cloud schemes in the SCM's are an additional source of uncertainty. Dependent on how the convective entrainment is parameterized the mass flux can either decrease or increase in a warmer climate. The detrainment rates in the convection schemes are in many cloud scheme an important source for the cloud amount. The details of how the detrainment rates are vertically distributed determine largely the cloud fraction and thereby the CRE.

5. Detailed analyses of the LES and SCM results for the breakup of Scu observed during ASTEX

Deliverable 3.3

i) LES Results of the ASTEX case

Van der Dussen et al. (2012) compare LES results of a transition from a relatively well-mixed to a thin, decoupled stratocumulus layer with cumulus cloud penetration from below with aircraft observations collected during the Atlantic Stratocumulus Transition Experiment (ASTEX). Figure 48 shows the lowest cloud base heights that are indicative of the lifting condensation level of the cumuli, in addition to the mean stratocumulus cloud base and cloud top heights. It can be seen that as the simulation progresses, the mean stratocumulus cloud base height keeps increasing, whereas the minimum cloud base height is approximately constant. The large separation between these heights in the second half of the simulation is indicative of the decoupling of the boundary layer and the development of saturated updrafts below the stratocumulus layer. The general picture of the transition is consistent in the models and in a close agreement with the observations which showed that after the second night the stratocumulus gradually broke up. The LES model results furthermore show that differences in the minimum cloud base height, which is indicative of lowest height where shallow cumulus clouds are present, are negligible small.

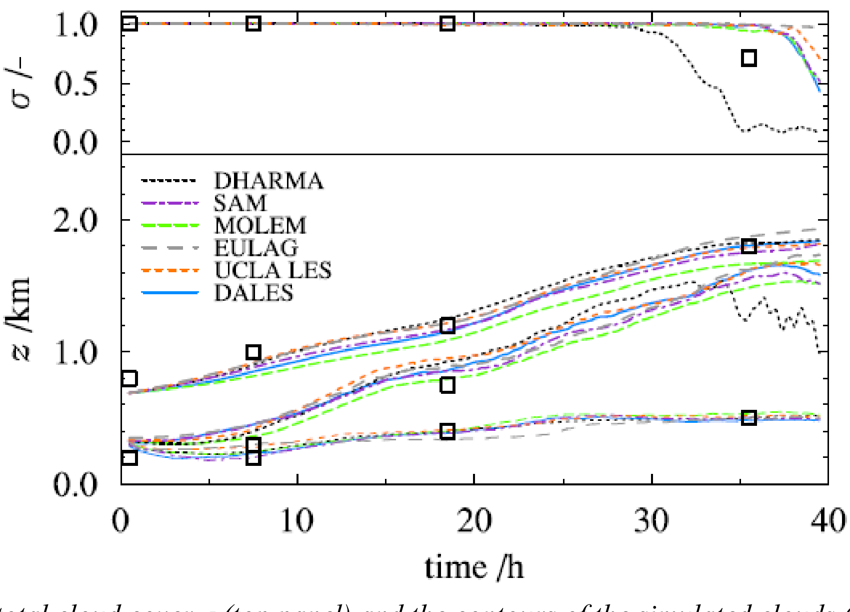

Figure 48. *The total cloud cover σ (top panel) and the contours of the simulated clouds (bottom panel) composed of the inversion height (as an indication of the mean stratocumulus cloud top), the minimum cloud base height and the mean cloud base height, for each of the models shown in the legend. The squares denote similar quantities, estimated from the profiles of the observed liquid water content.*

A plot of the entrainment rate we as a function of time is shown in Figure 49a, including estimates made on the basis of observations (De Roode and Duynkerke, 1997). The diurnal cycle is clearly visible in this plot, with significantly more entrainment during the night compared to daytime. The smaller entrainment rates during the day can be explained from the absorption of solar radiation in the cloud layer, which acts to stably stratify the cloud layer with respect to the underlying subcloud layer. Figure 49b shows the liquid water path

(LWP). Estimates derived from the measured average liquid water specific humidity profiles are indicated by squares. During the night, the models show an increasing trend in the LWP. During early daytime, approximately 8 h after the start of the simulation, the LWP starts to decrease, to a local minimum approximately 2-3 hours after local noon. Even though the models agree on the bulk features of the transition, the spread in the LWP and the entrainment rate during the first 12 hours of the simulation is large. However, during daytime this spread is reduced significantly which can be explained by the fact that thicker clouds tend to absorb more solar radiation.

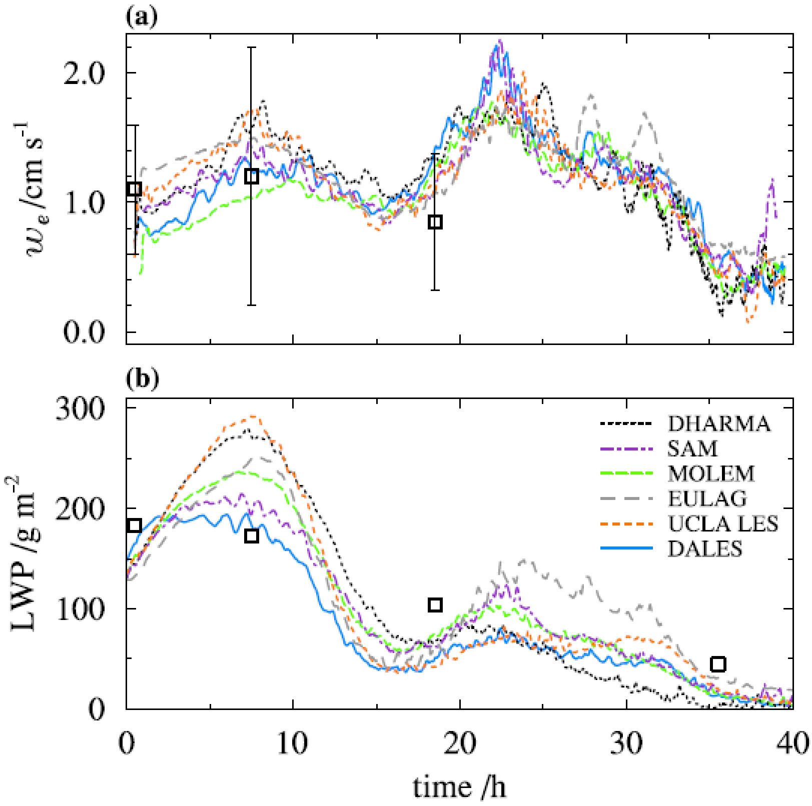

Figure 49. *The entrainment rate we (a) and the liquid water path LWP (b) as a function of time for the models indicated in the legend. Estimates based on observations of we, including uncertainties were obtained from De Roode and Duynkerke (1997), while the values of the LWP where obtained by integrating the mean liquid water content profiles. A running averaging filter with a width of 1 h has been applied on the entrainment rates from the simulations.*

Figure 50a shows the LWP as a function of the precipitation rate at the stratocumulus cloud base. Both quantities are averaged over the first 12 hours of the transition. The top axis of the figure shows the LWP tendency due to precipitation. In addition to the reference case set-up, additional simulations were performed with DALES, using three different values of the cloud droplet concentration, namely 60, 100 (reference) and 200 cm^{-3}. In addition to the scheme by Khairoutdinov and Kogan (2000), which was used for the reference simulation, the simulations were also performed using the scheme of Seifert and Beheng (2001). The results strongly suggest that differences in the precipitation rates at cloud base explain the spread in the LWP, such as found in Figure 49b. Based on the LWP tendencies presented at the top x-axis of the figure, the expected LWP difference between for instance the UCLA LES and DALES results over the 12 hour period is approximately 250 gm^{-2}. Because the actual difference in the LWP at t=12 hr between these models is much smaller than this tendency suggests, some negative feedback mechanism must be present. Figure 50b clearly demonstrates
that the entrainment rate decreases if the precipitation rate is higher. For the ASTEX case a smaller entrainment rate acts to reduce the drying at the top of the cloud, thereby counteracting the enhanced depletion of cloud water by precipitation (Ackerman et al., 2004). We also identify warming by solar radiation during daytime as an important feedback mechanism to reduce intermodel differences in the

stratocumulus cloud thickness. Because thicker clouds absorb more solar radiation causing a larger thinning tendency, the LWP spread diminishes rapidly during the day.
Although the differences in the precipitation rates have a significant impact on the LWP during the night, the fact that during daytime the LWP values tend to converge suggests that for the ASTEX case the details of the microphysics parameterization are of little importance to the timing of the stratocumulus cloud breakup.

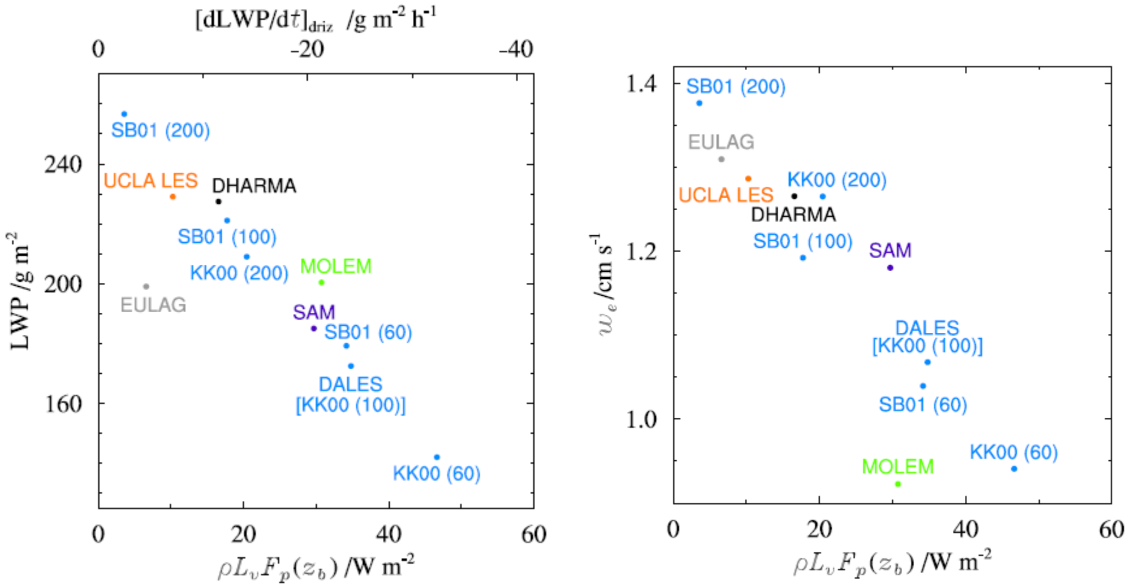

Figure 50. *Scatter plots of the time averaged (left panel) LWP and entrainment rate (right panel) as a function of time averaged precipitation rate at stratocumulus cloud base. Each quantity is averaged over the first 12 hours of the simulation. The top axis shows the precipitation rate in terms of a LWP tendency in gm^{-2} h^{-1}. The labels indicate the model or the microphysics scheme (in DALES) used, while the numbers between the parentheses indicate the cloud droplet number density in cm^{-3}.*

The manuscript by Van der Dussen et al. (2012) presents a detailed analysis of the contribution of turbulent fluxes, radiation and precipitation to the LWP budget. Van der Dussen et al. (2012) discuss sensitivity experiments with DALES, and show that smaller subsidence rates tend to cause deeper stratocumulus cloud layers and a longer persistence of the cloud layer.

ii) Broadening the phase space: Composite Lagrangian Cases

Sandu and Stevens (2011) present the setup of the 'Reference case', which is based on a composite of the large-scale conditions encountered along a set of individual trajectories performed for the northeastern Pacific during the summer months of 2006 and 2007. Both the initial profiles and the large-scale conditions represent the medians of the distributions of these various properties obtained from the European Centre for Medium-Range Weather Forecasts (ECMWF) Interim Re-Analysis (ERA-Interim) for the analyzed set of trajectories. For the study presented in this paper an additional ’Slow’ and ’Fast’ composite case are proposed, each of which has a slightly different initial thermodynamic state. The initial vertical profiles of the liquid water potential temperature and total water specific humidity for the four different stratocumulus to shallow cumulus experiments are shown in Figure 51.

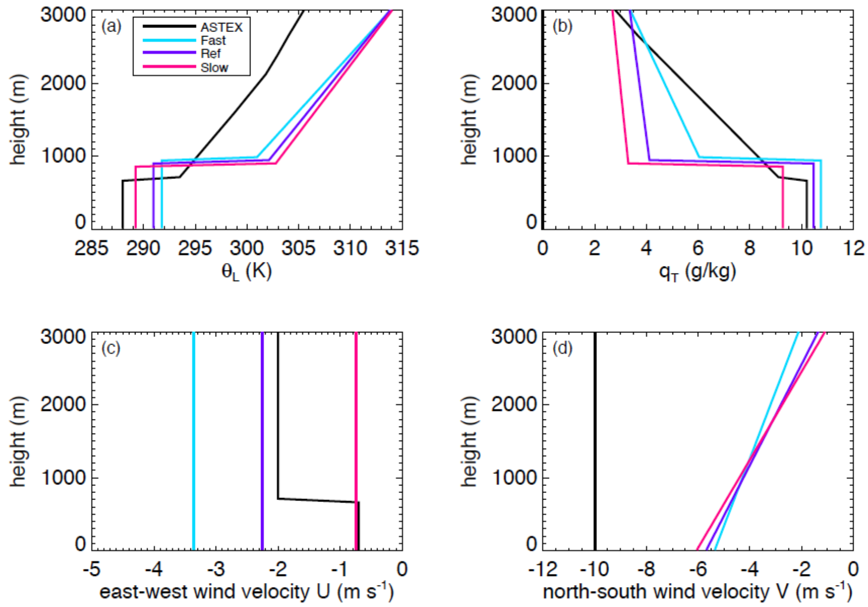

***Figure 51**: Vertical profiles of the initial liquid water potential temperature θL, total water content qT , and the horizontal wind velocity components U and V for the ASTEX, Fast, Reference and Slow cases. The line styles are according to the legend*

The ASTEX case has the smallest value for the initial inversion jump in the liquid water potential temperature, which gradually increases in magnitude for the Fast, Reference and Slow cases, respectively. The inversion jumps in the total specific humidities are also different for each case, with the Slow case having the driest free atmosphere.

Figure 52 shows that the sea surface temperature (SST) increases with time for each case, which reflects the equatorwards lagrangian advection of the simulated air mass. For theASTEX case the large-scale divergence gradually decreases with time, whereas a weakening of the wind velocities is taken into account by a time-varying geostrophic forcing. For the composite cases both the large-scale divergence and the geostrophic forcing are constant in time. Because the lower tropospheric stability is key for the evolution of the StCu to ShCu transition, a realistic tendency of the temperature is needed in particular as the simulations were performed for a period of two or three days. Therefore, for a faithful representation of the radiative transfer in a cloudy atmosphere all models applied a full radiation code. The simulations lasted 72 hours, except for ASTEX which was simulated for 40 hours.

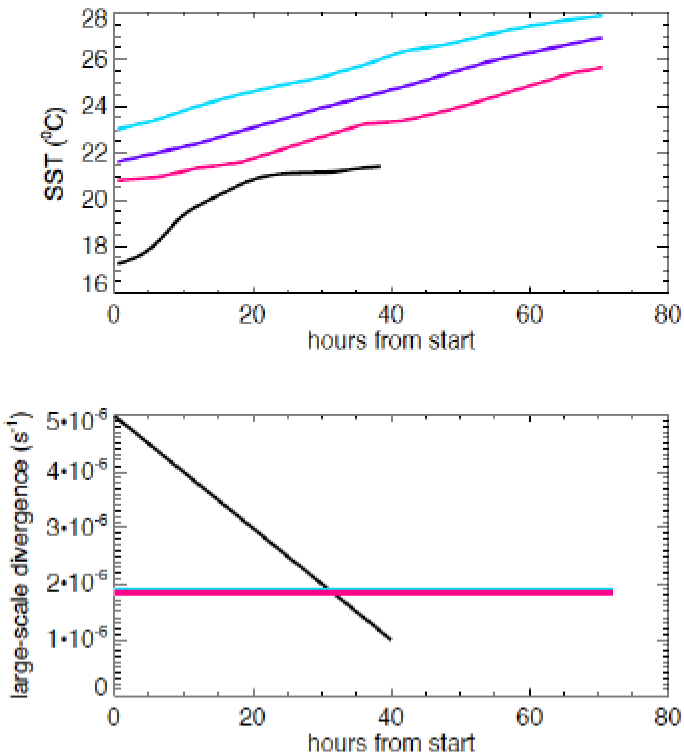

Figure 52: *Prescribed sea surface temperature and large-scale divergence as a function of time for the four stratocumulus to shallow cumulus transition cases. The linestyles are the same as in Figure 51.*

Figure 53a shows that for the three composite cases the LES models are rather well consistent in predicting the break-up and recovery of the stratocumulus. It appears that the LTS controls the dip in the cloud cover during daytime, with the 'Fast' case exhibiting the largest decrease. However, well before sunset the stratocumulus cloud deck recuperates with the cloud cover getting back to near unity values. Figure 8b shows that for the three composite cases the LWP increases the most during the night in the same models that showed a similar behavior as for the ASTEX case. As a measure of the degree of decoupling De Roode et al. (2012) analyse the thermodynamic states of the subcloud and cloud layer for the liquid water potential temperature and the total water content. They find that for both quantities the difference between the two layer becomes larger for deeper boundary layers which is in agreement with observations reported by Wood and Bretherton (2004).

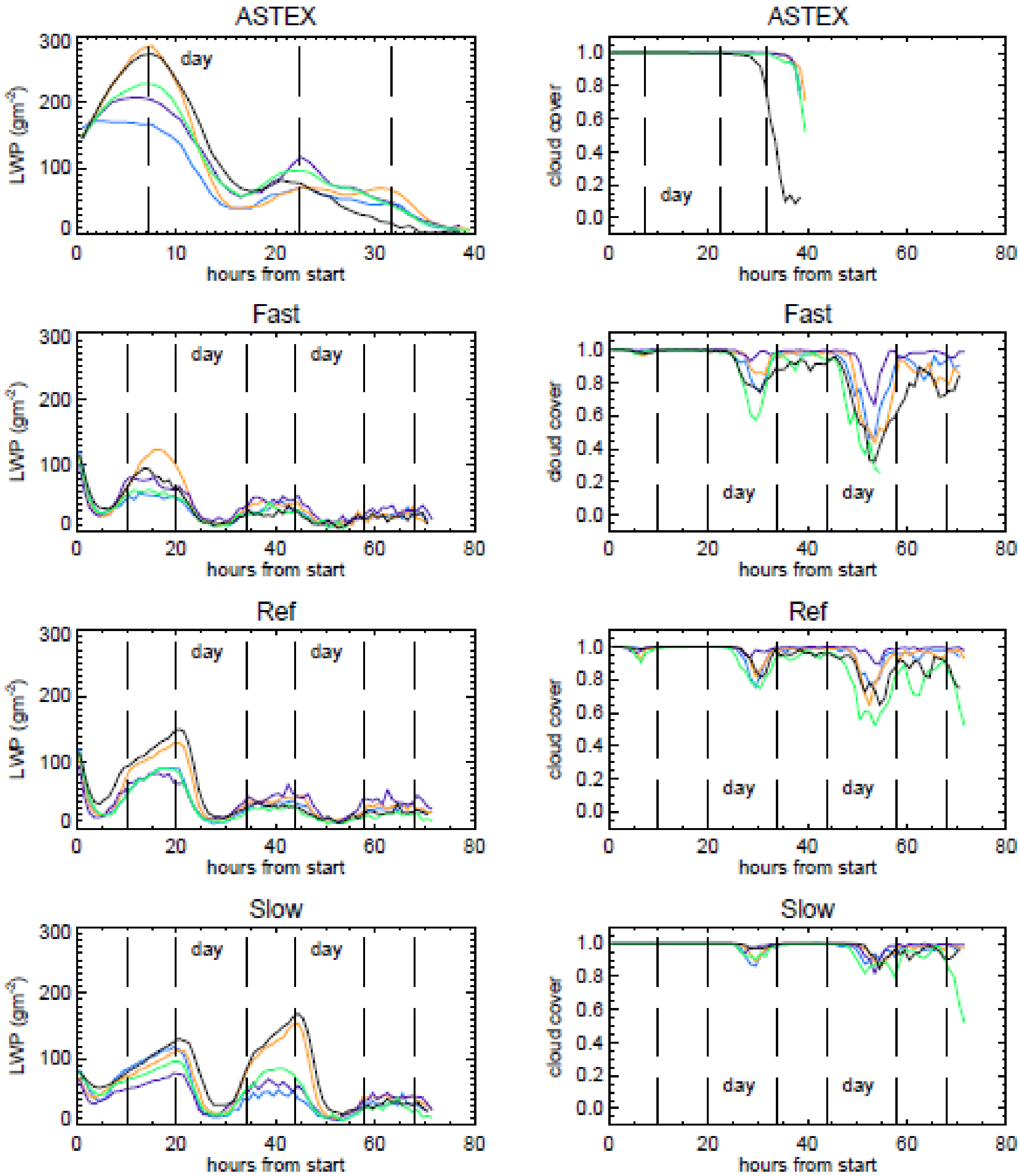

***Figure 53**: LES results of the cloud cover (left) and the liquid water path (LWP, right) for the ASTEX, Fast, Reference and Slow cases. The line colors are as in Figure 1.*

<u>*iii) SCM Results of the ASTEX Lagrangian*</u>

Figure 54 evaluates the SCM results against LES for three cloud variables. The participating models are summarized in Table 6. For both LES and SCM the ensemble of models is plotted as a probability density function. A motivation for such ensemble-plotting is to clarify visualization, which gets complicated when the model ensemble contains a large number of codes. But perhaps the most important benefit of ensemble plotting is that it conveys how well the ensemble performs as a collective; it answers the question if common errors exist in the mean bias and time-development of the cloud transition.

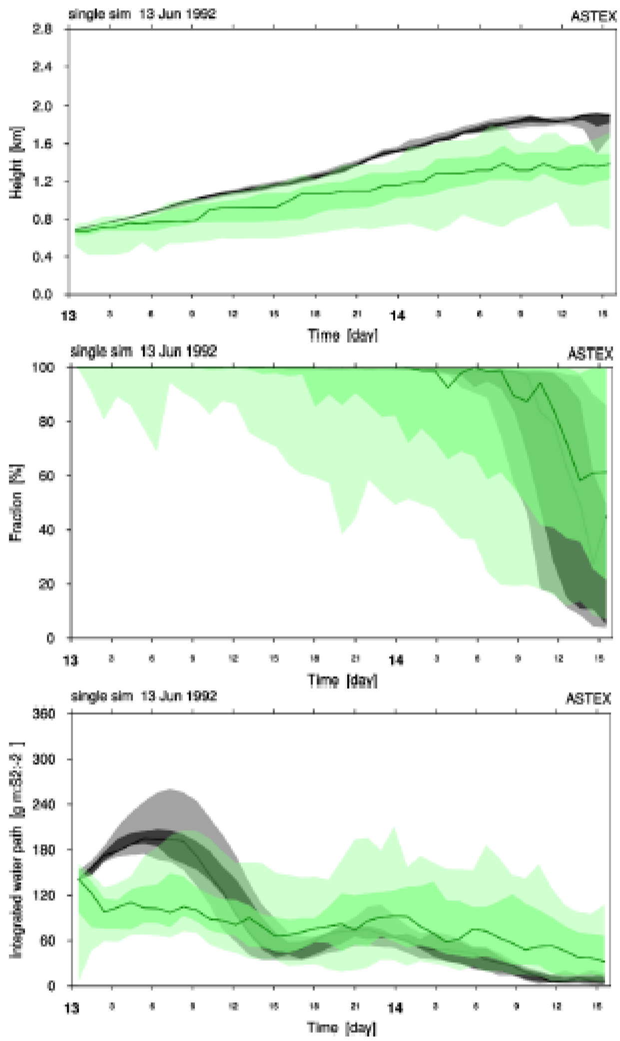

Figure 54. *Time-series of the liquid water path during the cloud transition in the ASTEX case. The ensemble of LES models is shown in grey, while the SCM ensemble is shown in green. In both distributions the 50 percentiles (the median) is indicated by the solid line. The areas of different shading correspond to various percentiles of the distribution; the part of the PDF between the 5-95 percentile is lightly shaded, while that between the 25-75 percentiles in densely shaded.*

We find that in general the SCMs underestimate the rate of deepening of the boundary layer during the transition. What is also apparent is that considerable scatter still exists among the SCMs concerning the timing of the cloud break-up, a behaviour already established in the first intercomparison by Bretherton et al. (1999). In that sense not much improvement has been achieved since then. Finally, the variation in amplitude in the liquid water path during the transition is not well captured by the SCM ensemble, which fails to capture the transition from high values to low values as displayed by the LES ensemble. As will be discussed in the last part of this section, an individual assessment of the model skill to capture the transition suggests that relatively new or updated schemes tend to perform better. A model may perform well in representing one aspect of the cloud transition, but less well for another. It is therefore interesting to search for an appropriate method to assess the overall performance of a model in representing the stratocumulus-to-cumulus transition. This may help in establishing which general approach in parameterization development is the most promising. To this purpose model performance is assessed for a chosen set of variables that reflect key aspects of the stratocumulus-to-cumulus transitions that we require the models to represent correctly.

Variable	Acronym	Units	Description
Total Cloud Cover	TCC	%	Vertically projected area covered by clouds
Liquid water path	LWP	g m^{-2}	Vertically integrated liquid water
Cloud top height	z_{top}	km	
Cloud base height	z_{base}	km	
Height of 1st maximum in cloud fraction	z_{max}^{1st}	km	
Height of 2nd maximum in cloud fraction	z_{max}^{2nd}	km	
Depth of capping cloud layer	Δz_{cap}	km	
Decoupling parameter	α	-	The difference In total specific humidity between the mixed=layer and cloud layer, normalized by the mixed layer humidity (Wood and Bretherton, 2004)
Cloud top entrainment instability parameter	κ	-	Ratio of the temperature jump to the humidity jump across the boundary-layer inversion (Kuo and Schubert, 1988)

Table 7. *The set of nine variables used for evaluation of the SCMs*

The set of nine state variables is listed in Table 3, including both vertically integrated properties as well as vertical structure. While most variables concern cloud state, some reflect the thermodynamic state of the boundary layer and its inversion. The cumulative score for the set of nine variables is shown in Fig. 55, and is calculated as follows. The contribution for each variable can vary between 0 and 1, and is a linear function of the rank of each code as sorted on the distance between its position in bias-CRMS space and the origin (see Neggers, 2012). The best performing code (with the smallest distance) has the smallest contribution in the cumulative score. The summation of the contributions for all variables yields a single value that expresses the overall performance of the model relative to the other members of the ensemble for this particular set of variables. An interesting result that can be interpreted from Fig. 55 is that the models making up the top third of the list are generally those codes that are either i) entirely newly conceived concepts or are ii) existing schemes have seen significant renovation of their internal structure in recent years. What this suggests is that boundary-layer parameterization schemes that have some form of internal consistency between their individual components (such as thermodynamic transport, cloud macrophysics and microphysics) generally tend to do better for this type of cloud transition. An important reason could be that these type of internally consistent codes tend not to have a discretized configuration in which each cloud-regime has a different setting, but are formulated to be more generally and uniformly applicable to all regimes, including any transitions between them. The schemes thus respond smoothly to a smooth variation in the applied forcings, as is the case in the StCu to ShCu cloud transition.

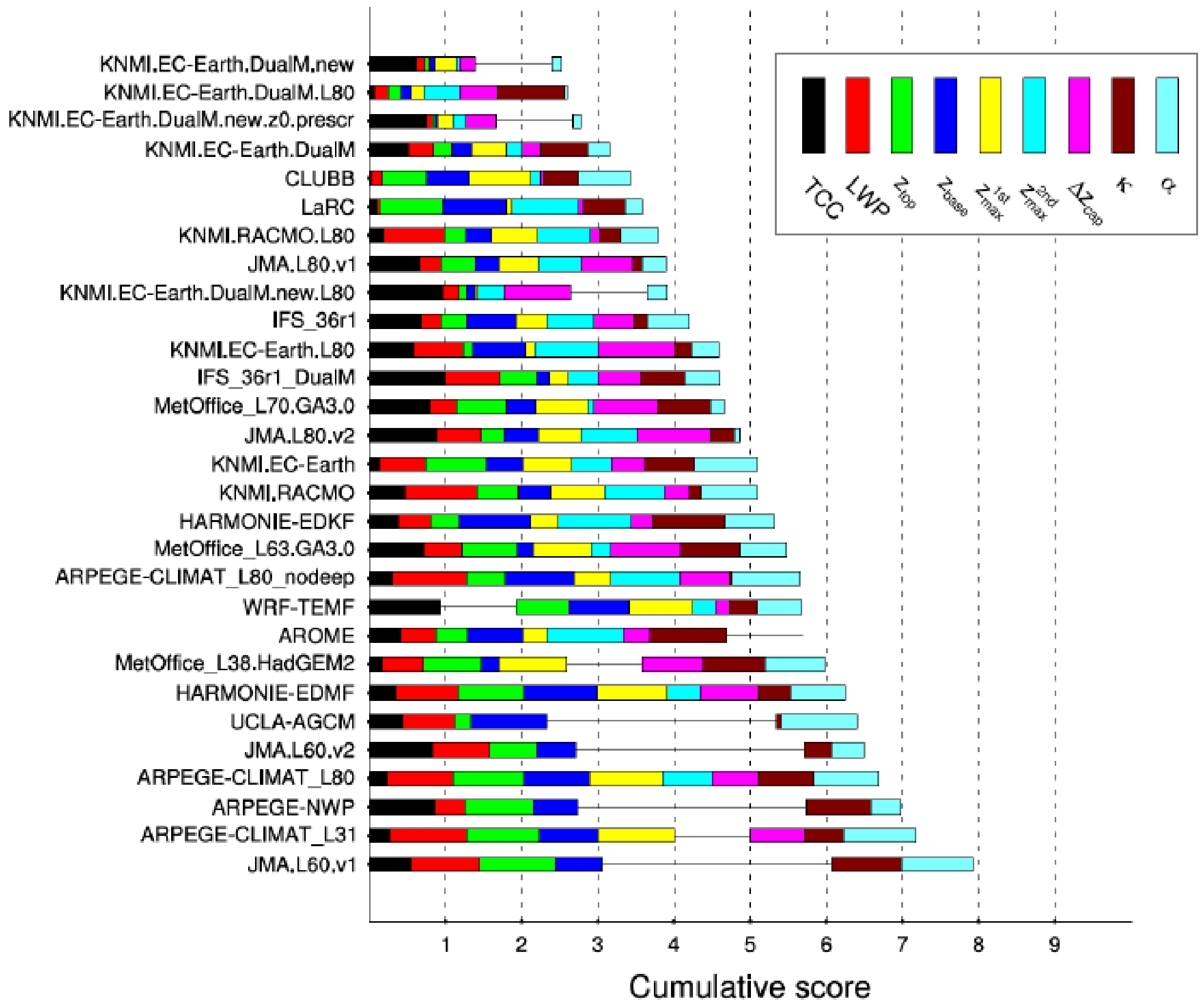

Figure 55*. Bar-chart showing cumulative model performance estimated over nine variables according to Table 3 reflecting key aspects of the cloud transition. The colors indicate the contribution to the cumulative score by individual variables, as explained in the legend. The models on the vertical axis are sorted on their cumulative scores, with the best performing model (lowest cumulative score) positioned at the top. In case the model output on a certain variable is unavailable, the contribution is assumed equal to 1 and is shown as a solid horizontal line.*

6. Identification and comparison of the key quantities used in ESM parameterization schemes with LES results and observations

Deliverable 3.4

i) Background, motivation and aim

The analysis of the ASTEX results of the cloud cover show that the ASTEX SCM results exhibit a large scatter (see Figure **). By contrast, the LES results show a much better consistency among the models as is clear from the solid cloud deck that is maintained during the first full day of the simulation.

Lock (2009) investigated the relation between the cloud cover and a factor κ that is related to the inversion stratification according to,

$$\kappa = \frac{\Delta\theta_e}{(L_v/c_p)\Delta q_T} = 1 + \frac{\Delta\theta_L}{(L_v/c_p)\Delta q_T} \qquad (4)$$

with θ_e and θ_L the equivalent and liquid water potential temperature respectively, q_T the total specific humidity, L_v the latent heat of vaporization, c_p the specific heat of dry air. The symbol Δ indicates the jump across the inversion layer (see Fig. 2 for a schematic representation).

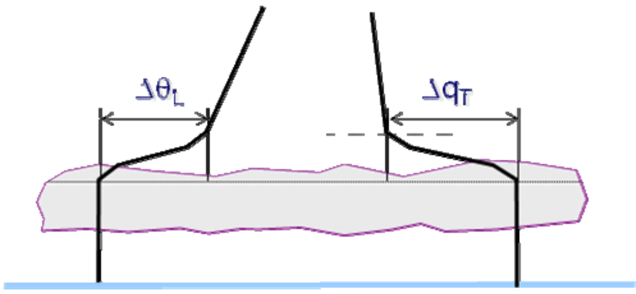

Figure 56*: Schematic representation of the vertical profiles of* θ_L *and* q_T*. The thin horizontal grey lines near the cloud top indicate the bottom and top of the inversion layer, across which the inversion jumps* $\Delta\,\theta_L$ *and* $\Delta\,q_T$ *are determined.*

Lock showed that the cloud cover rapidly decreases for κ-values that are approximately larger than 0.2 (see Fig. 56). To assess whether there are systematic differences in the cloud cover and the inversion strength diagnosed the relation between the κ-factor and the cloud fraction for the LES models and the SCMs is diagnosed. In addition, Van der Dussen et al. (2012) investigate the budget equation for the liquid water path in order to quantify the contribution of processes like entrainment warming and drying to the LWP change. The relevance of this work to the κ-factor analysis is that if it is assumed that the entrainment velocity is proportional to the reciprocal of the liquid water potential temperature jump across the inversion, then the budget equation predicts a rapid thinning of the stratocumulus cloud deck for κ larger than about 0.2.

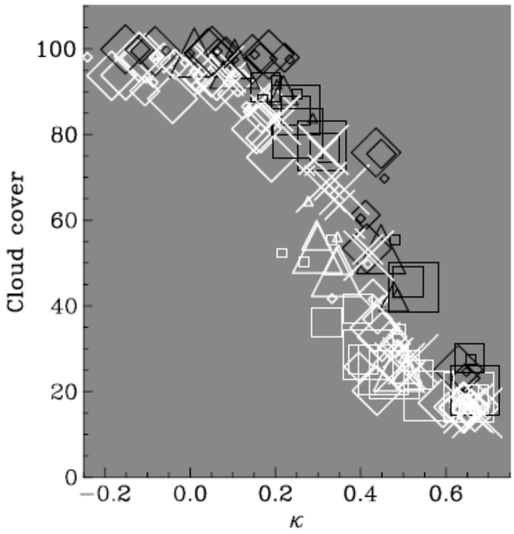

Figure 57: Relation between cloud cover and the inversion stability factor κ (from Lock 2009).

ii) Results

We diagnosed the relation between the κ factor and the cloud cover for the ASTEX case, in addition to three "composite" cases proposed by Irina Sandu and Bjorn Stevens. The three composite transitions are based on the observational study of the transitions in boundary layer cloudiness described in Sandu et al. (2010). While ASTEX offers the opportunity to evaluate models against in situ data, this set of composite transitions represents a more idealized framework for model evaluation, which offers the possibility of comparing the models for a variety of transition cases, which differ for example in terms of amplitude or timescale of the transition. The composite reference case, and two of its variations corresponding to a faster, and respectively a slower transition in cloud fraction. A key difference in the ASTEX and three composite cases is the inversion stratification.

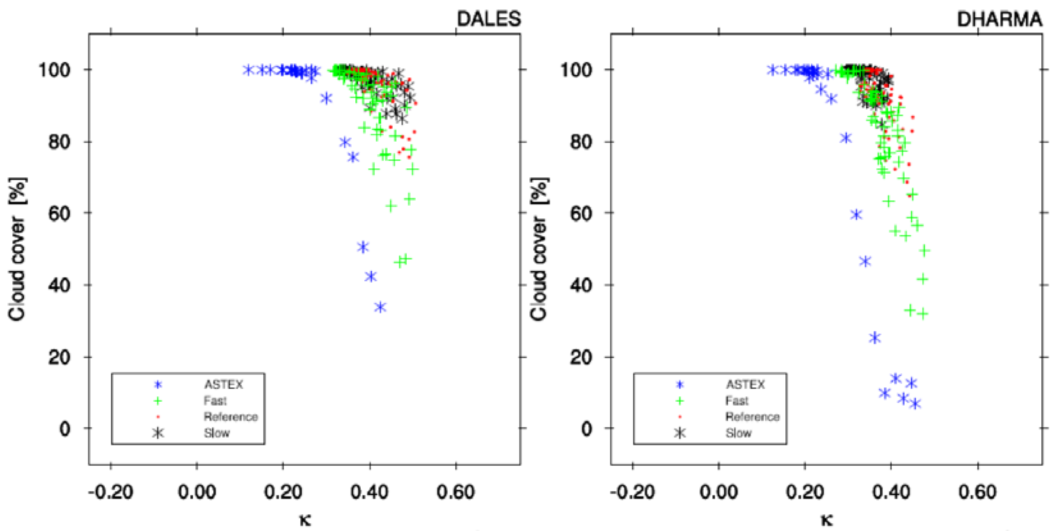

***Figure 58**: Relation between cloud cover and the inversion stability factor κ from two different LES models (DALES and DHARMA) for the ASTEX and three composite transition cases.*

The LES model results presented in Figure 58 show a qualitative similar picture as Lock (2009) in the sense that for κ values larger than 0.2 the cloud fraction tends to diminish quickly. In a manuscript that is currently in preparation, the timing of the break-up will be explained from the budget equation for the LWP which is presented in Van der Dussen et al. (2012). It can be shown that the surface evaporation flux is a key component of this budget. The larger its value, the longer the stratocumulus case will be maintained. Except for the LaRC model all the SCMs exhibit a different relation between κ and the cloud cover. The analysis proposed by Lock (2009) seems to be an effective tool for characterizing and inter-comparing the behavior of fast parameterized physics across a hierarchy of simulations. In deliverable 3.6 it will be discussed that these diagrams for the SCM results of the transition cases are representative for the GCM behavior.

Van der Dussen et al. (2012) present an analytical equation for the tendency of the liquid water path (LWP). By substituting the definition of κ according to Eq. (4), and assuming that the entrainment rate is inversely proportional to the liquid water potential temperature jump across the inversion, they calculated the tendency of the LWP due to entrainment only. Figure 60 shows that the LWP tendency due to entrainment is strongly dependent on the value of κ. For $\kappa > 0.23$ LWP tendencies due to other processes than entrainment are typically much smaller which strongly suggests that the cloud layer is likely to thin due to the strong entrainment tendency. It is important to note that this effect is not due to a built-in buoyancy reversal process, since a very simple entrainment parameterization that only depends on the radiative divergence over the cloud layer and the inversion jump of θ_L is used. This notion seems to be corroborated by the LES results, while the SCM results suggest that the entrainment process is not adequately represented in these models.

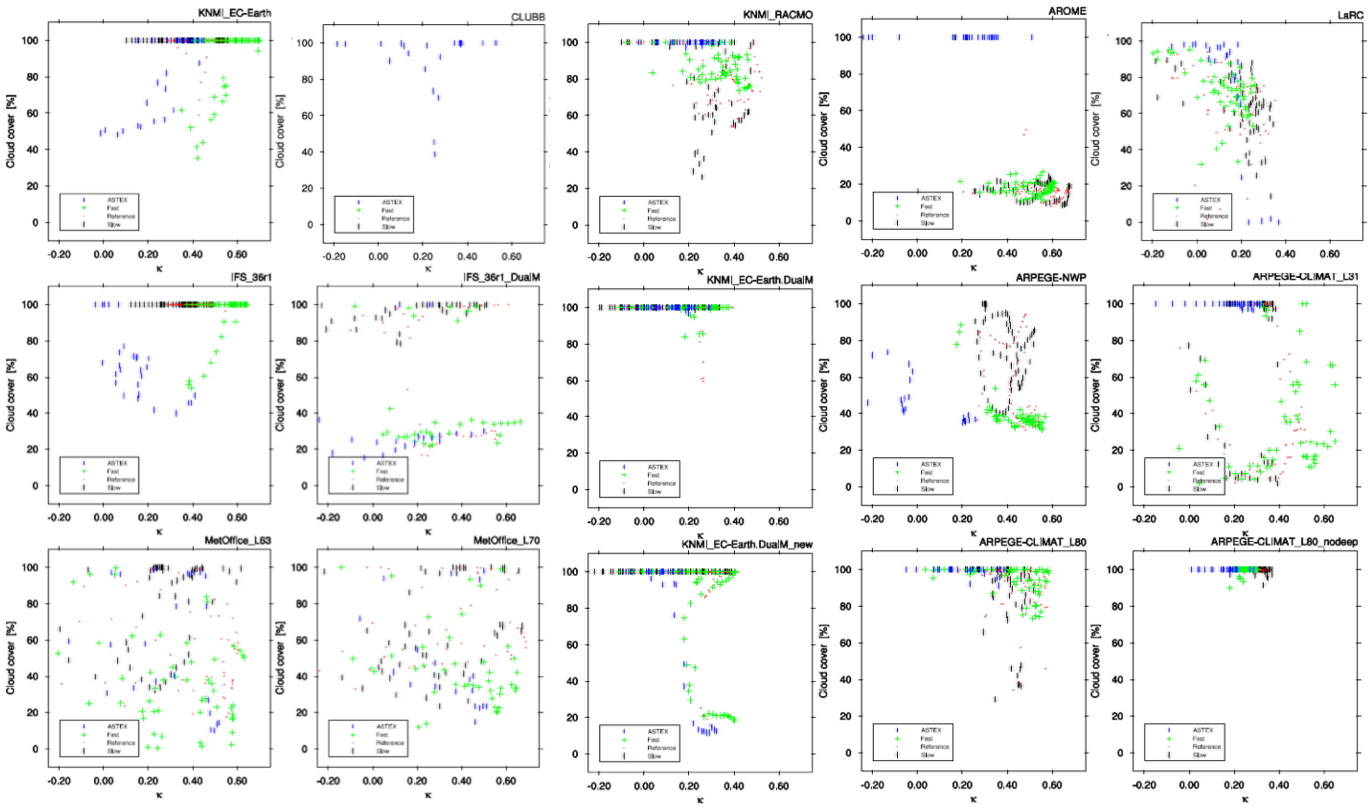

Figure 59*: Relation between cloud cover and the inversion stability factor κ from different SCMs for the ASTEX and three composite transition cases.*

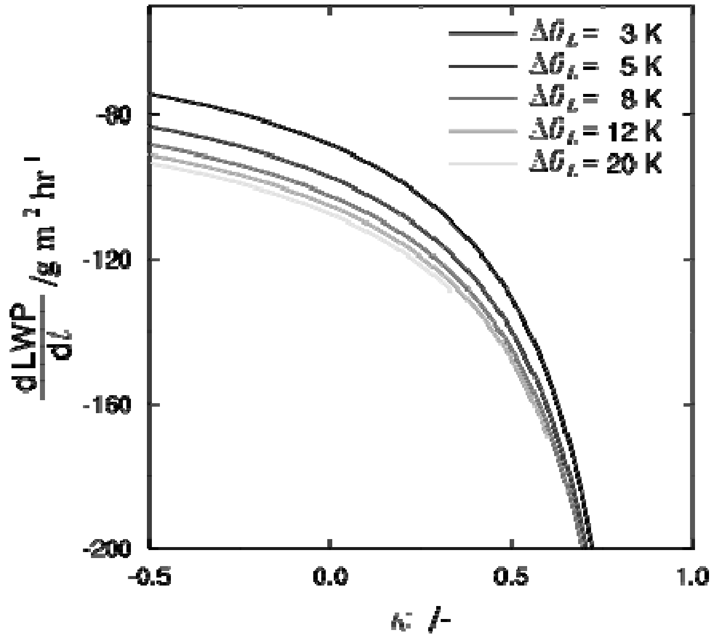

Figure 60: *The LWP tendency as a function of the factor κ. and for different values of the liquid water potential temperature jump across the inversion The result has been computed analytically from the budget equation for the LWP.*

Last, we discuss the vertical stratification of the cloud-topped boundary layer. Wood and Bretherton (2004) used aircraft observations collected in cloudy boundary layers to calculate the difference in θ_L and q_T between the cloud and subcloud layer. To quantify this difference they introduced a decoupling factor α_q,

$$\alpha_q = \frac{q_{T,cld} - q_{T,sub}}{q_{T,z_i^+} - q_{T,sub}} \tag{5}$$

with the subscripts 'cld', 'sub' and 'z_i^+' indicating the value of q_T in the cloud layer, subcloud layer and just above the inversion, respectively. An analogous factor α_θ was defined for θ_L. The factors are equal to zero if the boundary layer is vertically perfectly mixed. Wood and Bretherton found that the value for the decoupling parameter increased for deeper boundary layers. As can be seen from Figure 61, the LES models roughly follow the same trend with somewhat larger values for the decoupling factor for the total specific humidity than for the liquid water potential temperature. This difference might be explained from the fact that there are the surface moistening and entrainment drying will tend to enhance the vertical moisture gradient, whereas for heat both processes act to warm. It should be stressed that any models must be well capable of representing the decoupling factor, as deviations will result in an error in the liquid water content. For example, models have a too weak decoupling will tend to overestimate the liquid water content, and vice versa.

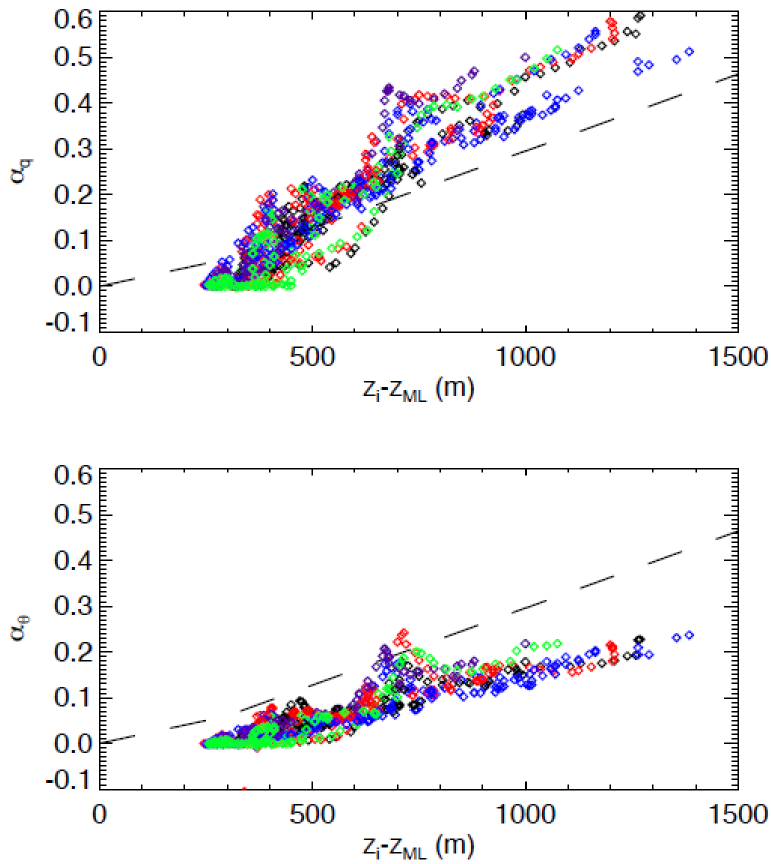

Figure 61:. *Decoupling parameters* α_q *and* $\alpha\theta$. *The dashed lines indicate a fit using the aircraft observations of* α_q *presented in Figure 59 of Wood and Bretherton (2004). The colors of the data points represent results from the different LES models.*

iii) Conclusions

The cloud cover during four Lagrangian transition cases was analyzed. The LES results do all show a consistent reduction of the cloud cover for $\kappa>0.2$. In general a wide scatter in the cloud cover behaviour is found in the SCM results. The analysis procedure is found to be useful for a assessing in under which inversion conditions SCMs tend to predict either a solid stratocumulus cloud deck or a broken shallow cloud cumulus field.

7. Equilibrium solutions of SCMs

Deliverable 3.5

i) Background, motivation and aim

The main purpose is to understand how low clouds respond to a change in the sea surface temperature and perturbed large-scale forces in a future climate. To this end we have followed three pathways. Stratocumulus clouds are studied with a mixed-layer model, and shallow cumulus clouds with a large-eddy simulation model. In each case the models are run to a steady-state. The results are analyzed with aid of the governing budget equations for heat and moisture, which demonstrates the key role cloud-top entrainment is playing. The response of the stratocumulus cloud amount is studied for a wide range of external conditions defined by the large-scale divergence, horizontal wind speed, the sea surface temperature and the thermodynamic state of the free troposphere. As a last step, a similar approach is followed to study the stratocumulus response with SCMs.

ii) Stratocumulus clouds

De Roode et al. (2012) use a mixed-layer model to study the response of stratocumulus to changes in cloud controlling factors. The mixed-layer model assumes a vertically well-mixed boundary layer, and includes the relevant physical processes acting in stratocumulus clouds such as a net radiative cooling at the top of the cloud and turbulent fluxes of heat and moisture (see Figure 62 for a schematic representation). The surface fluxes are calculated from a bulk formula including a drag coeffient, the horizontal wind speed, and the difference between the mixed-layer and surface value of the quantity considered. To close the model the entrainment parameterization proposed by Nicholls and Turton (1986) was used.

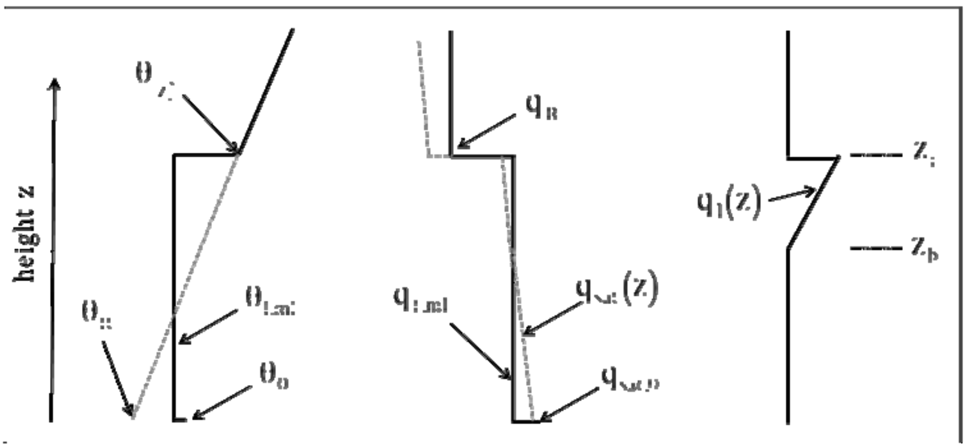

Figure 62: Schematic of the vertical profiles of the liquid water potential temperature, total specific humidity and liquid water specific humidity in the mixed layer model.

In the reference case, equilibrium state solutions were computed for a wide range of values for the low tropospheric stability (LTS) and total specific humidity values in the free troposphere q_{ft}. The radiative forcing was set to a constant value. Figure 63a shows that for low LTS values, relatively high LWP equilibrium values are found. This can be understood from the fact that the entrainment rate will become large if the buoyancy jump across the inversion becomes relatively small which is the case for low LTS values, such that for this regime the highest entrainment rates and consequently the deepest mixed layers are found. Figures 63b and c also show that the effect of q_{ft} on the entrainment rate is subtle, with maximum values for the entrainment rate w_e roughly at about q_{ft} = 5 g/kg. Although q_{ft} has only a weak effect on the entrainment rate, Figures 63d, e and f show that it has a distinct influence on the thermodynamic structure of the boundary layer as quantified by the liquid water potential temperature and total specific humidity in the boundary layer, $\theta_{l,ml}$ and $q_{t,ml}$, respectively, and on the cloud base height z_b.

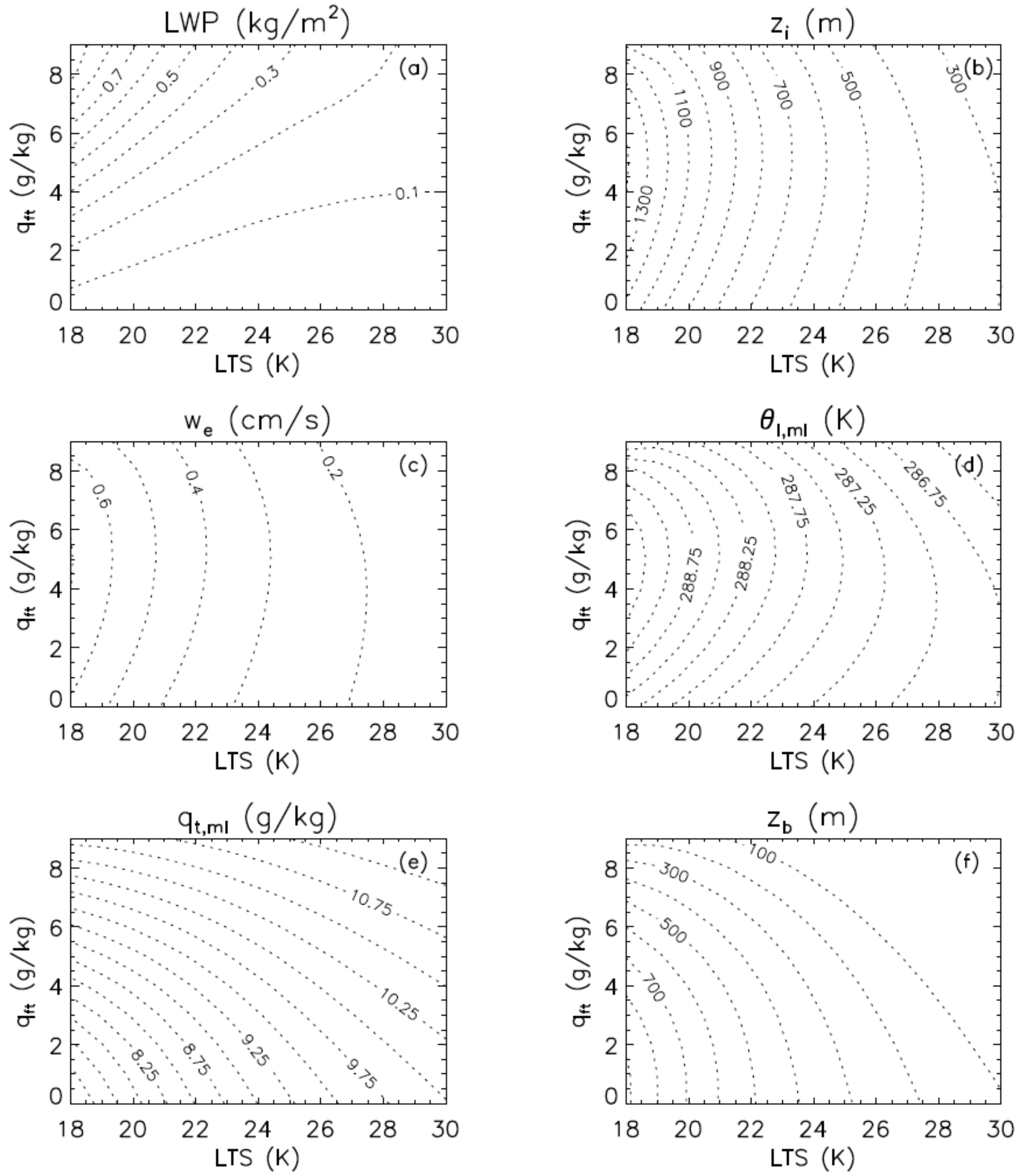

Figure 63: Steady-state solutions as a function of the lower tropospheric stability (LTS) and the free tropospheric specific humidity (q_{ft}) for (a) the liquid water path LWP, (b) the inversion height z_i, (c) the entrainment rate w_e, (d) the liquid water potential temperature $\theta_{l,ml}$ and (e) total water specific humidity in the mixed layer $q_{t,ml}$, respectively, and (f) the cloud base height z_b.

As a next step, De Roode et al. perturb cloud controlling factors one by one in order to assess the influence of single changes on the stratocumulus cloud amount. Figure 64 shows the LWP response to changes in the potential sea surface temperature θ_0, the free tropospheric potential temperature θ_{ft} and the specific humidity q_{ft}, respectively, the horizontal wind speed U, and the large-scale divergence D. In the lower right corner of the phase space in Figure 64a, that is for a relatively warm and dry free troposphere, the total response of the LWP is negative for an increase in θ_0. In this regime the rise of the cloud base height is larger than that of the cloud top, leaving a thinner cloud layer and a lower LWP. Furthermore, a moistening of the free troposphere, or an increase of the wind speed will yield a thicker stratocumulus cloud deck. The possibility that the large-scale divergence will also change in a future climate has an important consequence for the stratocumulus liquid water path, as an increase will cause a cloud thinning.

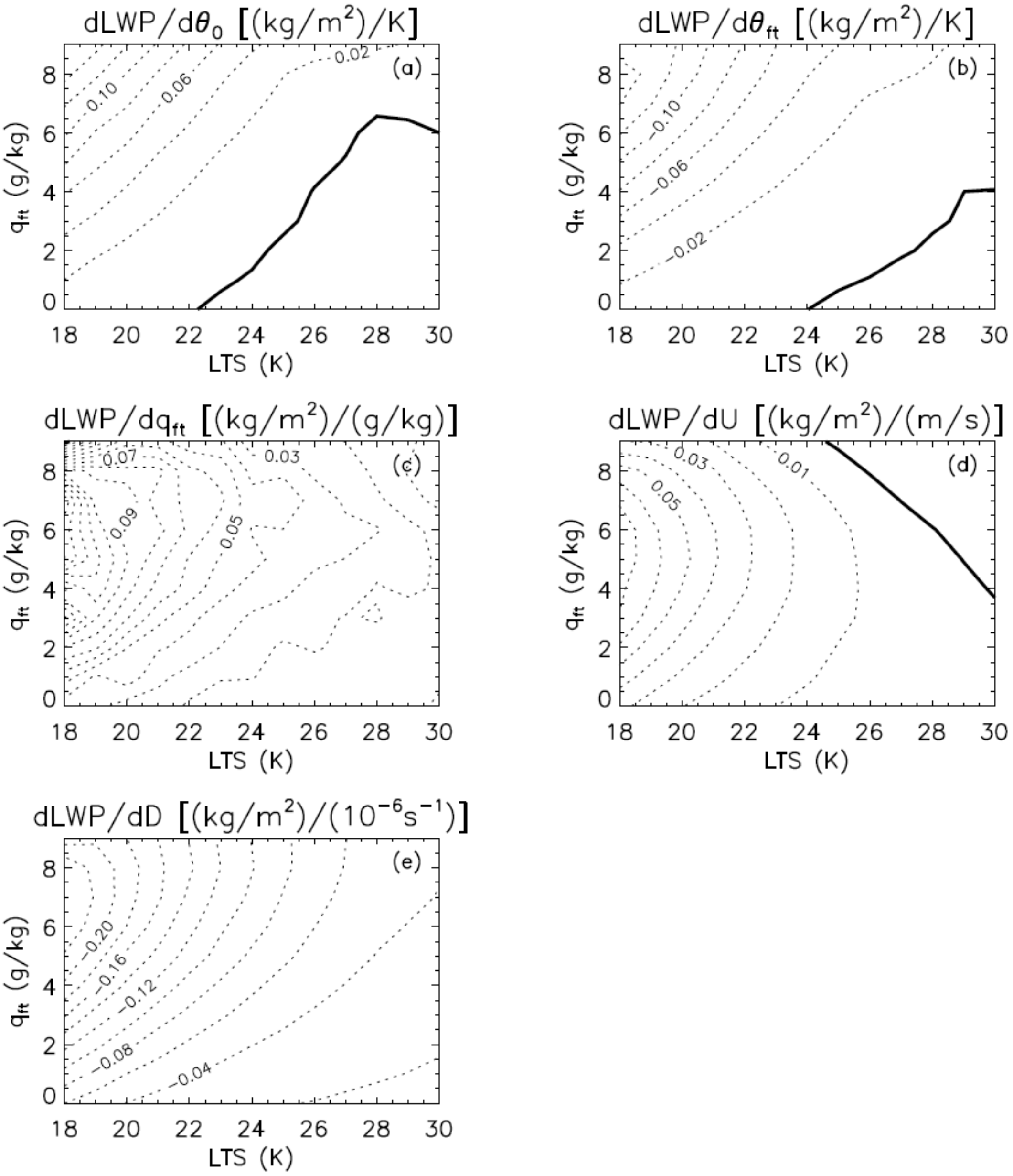

Figure 64: The total response of the liquid water path to changes in (a) the potential sea surface temperature θ_0, (b) the free tropospheric potential temperature θ_{ft} and (c) the specific humidity q_{ft}, respectively, (d) the horizontal wind speed U, and (e) the large-scale divergence D. A thick solid line indicates the zero isoline.

Zhang et al. (2012) explain that the amount of simulated low clouds in the SCMs is largely the result of moistening from the PBL turbulence schemes, radiative cooling at the cloud tops and dilution which is controlled by the shallow convection and cloud top entrainment schemes. These schemes differ greatly among the models, leading to very different cloud fields. Motivated by these findings, De Roode et al. also quantified the changes in the LWP provided that the entrainment rate would not change for perturbations in the cloud controling factors. In this way they are able to show that in a part of the phase space the sign of the LWP response can change. For example, if the entrainment is fixed for a change in the sea surface temperature the LWP tends to increase in the entire part phase space shown in Figure 64.

Figure 65 explains how the LWP will change as a result of a change in the entrainment rate. Apparently, an increase in the entrainment rate will yield a cloud thinning if the free troposphere is sufficiently dry or warm, and vice versa. This finding suggests that the differences in the LWP responses in the CGILS SCM experiments may be due to either a weak or strong response to perturbations in the cloud controlling factors.

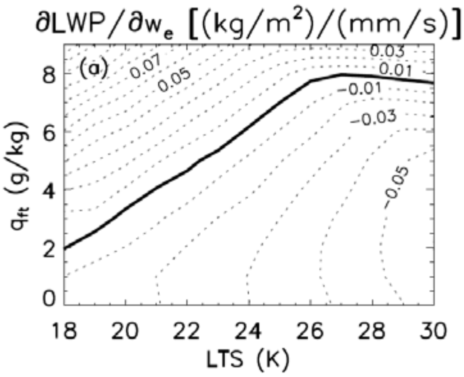

***Figure 65**: The partial derivatives with respect to the entrainment rate for the liquid water path LWP.*

<u>*iii) Shallow cumulus clouds*</u>

Schalkwijk et al. (2012) present a bulk model for shallow cumulus to study equilibrium solutions for somewhat idealized large-scale conditions. The analytical results are verified with a large-eddy simulation model. The phase space they explore includes the sea surface temperature and the large-scale divergence (D). A key finding of their study is the relation found between the cloud layer thickness and these two quantities (see Figure 66). It can be seen that if a critical value for the large-scale divergence is exceeded, the atmosphere remains free of clouds. By contrast, if D decreases, or if the sea surface temperature increases, the cloud layer depth increases. For the purpose to solve the cumulus cloud system equation analytically, this study uses a radiative forcing profile which is strongly idealized. However, this study identifies and isolates some of the processes through which a cumulus layer influences the boundary layer system in response to external forcings, which may be worthwhile to study in a single-column model framework.

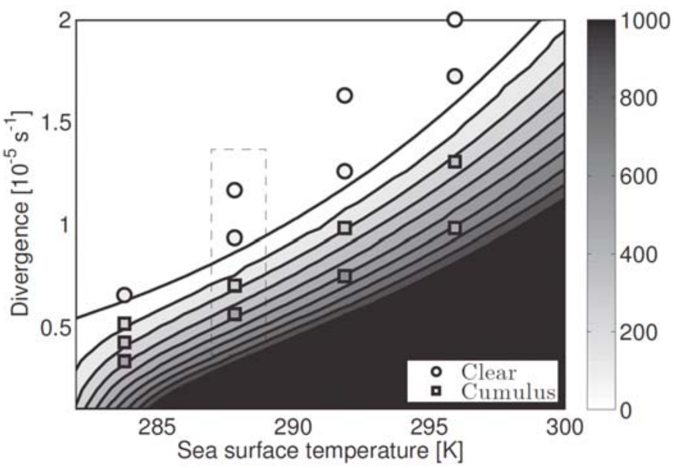

***Figure 66**: The cumulus cloud layer depth as a function of the sea surface temperature and large-scale divergence. The shaded contours depict the model predictions for cloud layer depth, the uppermost line thus depicting the transition from a clear to a cloudy boundary layer. The overlaid symbols each depict the state of a LES simulation after 200 hours of simulated time. Circles are clear cases, squares cumulus cases, and the symbol's fill-color represents the cloud layer depth in the LES case.*

iv) Conclusions

As a first step to explore the cloud response to a future climate change in a phase space consisting of cloud controlling factors we have applied simple conceptual bulk models like the mixed-layer model to study equilibrium solutions for stratocumulus and shallow cumulus clouds. Rather than applying multiple changes in the cloud controlling factors, in the spirit of partial derivatives De Roode et al. (2012) have perturbed them one by one to assess the change in the cloud liquid water path. An increase in the cloud layer thickness is found if the sea surface temperature is increased except for the situation where the free troposphere is sufficiently dry and warm. However, if the free troposphere is also warming, this will cause a thinning of the cloud layer. The moistening of the free troposphere, or an increase in the horizontal wind velocity each cause a cloud thickening, which may be partly counteracted by an increase in the large-scale divergence. In principle, single perturbations may also be applied in SCM runs towards equilibrium states which may help to identify whether the change in the LWP is dominated by the change in the cloud controlling factor or by a subsequent change in the entrainment velocity. Schalkwijk et al. (2012) studied analytical solutions of the shallow cumulus cloud top height in a phase space determined by the sea surface temperature and large-scale divergence and are able to find the conditions necessary for the formation and maintenance of shallow cumulus clouds.

Development and application of methods to exploit high frequency data for understanding of cloud feedbacks

Deliverable 3.8

i) Introduction

Cloud feedbacks continue to make the largest contribution to inter-model differences in climate sensitivity (Randall et al, 2007, Dufresne and Bony 2008), even when cloud adjustments (Gregory and Webb, 2008, Andrews and Forster 2008) are allowed for (Webb et al 2012, Andrews et al 2012). Understanding the underlying causes of these differences remains a priority. However, the high frequency variability of clouds means that time averaged model output gives a fairly limited picture of the physical mechanisms underlying cloud simulations. High frequency, instantaneous diagnostics are potentially able to give more insight into the physical processes operating and the interactions between them, for example convective intermittency and convective/boundary layer interactions (Zhang and Bretherton, 2008). They also support the diagnosis of any unphysical behaviour related to numerical noise and vertical discretisation effects.

The US Climate Process Team (CPT) on low latitude cloud feedbacks was amongst the first to save high frequency output of this type from GCMs at selected points, and found for example that models could show very different cloud simulations in stratocumulus regions in spite of similar values of net cloud forcing (Bretherton et al 2006). Mapes et al (2009) used these data to relate cloud radiative effects to convective precipitation events, revealing substantial differences in the behaviour of the models' convection schemes. The WGNE-GCSS Pacific Cross Section Intercomparison Project (GPCI, Teixeira et al 2011) saved high frequency data from more than twenty NWP and climate models along a section sampling the stratocumulus regime off the coast of California, the shallow cumulus to the south west and the deep convection in the ITCZ (as well as the transitions between them). They found that the systematic underestimate in cloud fraction in the stratocumulus regimes was in part due to a stratocumulus-to-cumulus transition that occurs too early along the trade wind Lagrangian trajectory, and also noted that some models exhibit a quasi-bimodal structure with cloud cover being either very large or very small, while other models show a more continuous transition.

As part of the second phase of the Cloud Feedback Model Intercomparison Project (CFMIP-2), new cloud feedback experiments were added to the CMIP5 experimental design (Taylor et al 2011), which included additional process diagnostics designed to support investigation of the physical mechanisms underlying cloud feedbacks and adjustments (Bony et al, 2011). These included time-step frequency outputs at 120 locations around the globe, including those analysed by the CPT and GPCI projects, but extended to additionally include various observational sites, and locations with large inter-model differences in cloud feedback (Figure 67). For a detailed list of the location we refer to the full report of Deliverable 3.8 (http://www.euclipse.eu/products.html/). These are included in AMIP experiments forced with observed SSTs which form the basis for +4K global mean SST perturbation experiments. These include one where AMIP SSTs are increased uniformly by 4K (amip4K) and another where a patterned SST perturbation with a global mean of +4K is applied, based on a composite SST response from coupled models in CMIP3 (amipFuture). High frequency outputs are also included in a CO2 quadrupling experiment with fixed AMIP SSTs designed for the analysis of cloud adjustments (amip4xCO2). These data are now available from several models for each experiment type (Table 8).

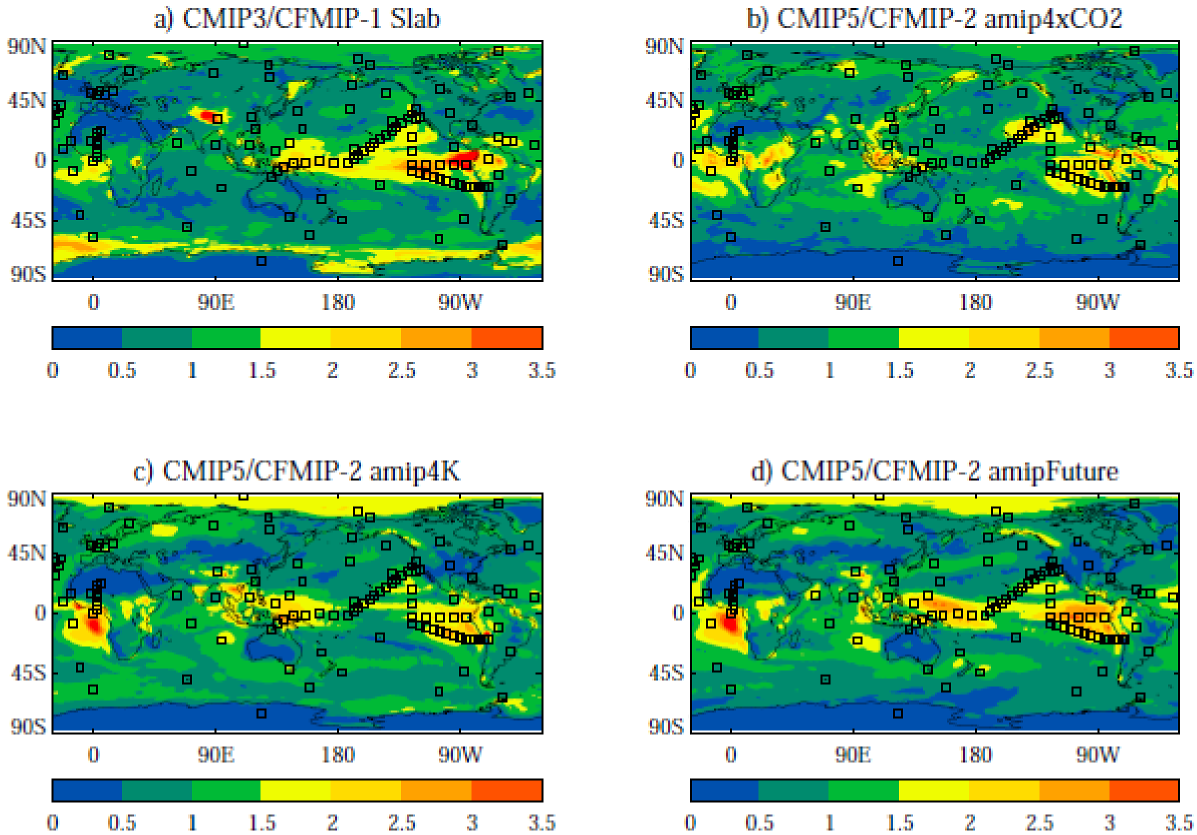

Figure 67. CFMIP time series output locations. *The maps show the relative contributions of difference parts of the globe to inter model spread in (a) cloud feedbacks from CFMIP-1, (b) cloud adjustments in CFMIP-2 and (c,d) cloud feedbacks in CFMIP-2. The maps show local standard deviations across each ensemble, normalised to the same global mean. The squares show the locations of the CFMIP-2 high frequency outputs*

Here we present an analysis of the diurnal cycle of cloud feedback in the CFMIP-2 uniform +4K experiments. The primary aims of this analysis are to establish which times of day show the strongest cloud feedbacks, which times of day contribute most to inter-model spread in cloud feedback, and what impact (if any) changes in the diurnal cycle of cloud have on cloud feedback.

AGCM	AMIP	AMIP4xCO2	AmipFuture	Amip4K
CNRM-CM5	✓		✓	✓
CanAM4	✓		✓	✓
HadGEM2-A	✓	✓	✓	✓
IPSL-CM5A-LR	✓	✓		✓
EC-EARTH	✓		✓	✓
MPI-ESM-LR	✓	✓		✓
MRI-CGCM3	✓	✓	✓	✓
BCC-CSM-1	✓			
Number of models	8	4	5	7

Table 8: *CMIP5/CFMIP-2 GCM experiments with time series data available.*

ii) Results and Discussion

Relevance of CFMIP locations

To give an indication of the extent to which the CFMIP locations sample the regions which contribute the most to inter-model spread in cloud feedbacks and adjustments, Figure 67 shows maps of ensemble standard deviations of the local cloud feedbacks in the CFMIP-1, CFMIP-2 amip4K and CFMIP-2 amipFuture ensembles, and the cloud adjustments in the CFMIP-2 amip4xCO2 ensemble. The feedbacks and cloud adjustments are diagnosed using the change in the Cloud Radiative Effect (CRE), which quantifies the net radiative impact of cloud changes and the climatological effect of cloud masking on the non-cloud responses (Soden et al, 2004). These are normalised to have global means equal to unity, to support a relative comparison of cloud adjustments and cloud feedbacks. They show that the CFMIP points sample all of the major regimes contributing to inter-model spread in cloud feedback and cloud adjustment, including the subtropical stratocumulus and trade cumulus regions.

Calculation of diurnally resolved quantities

Figure 68 shows diurnally resolved changes in the shortwave and longwave CRE between the AMIP and AMIP+4K experiments averaged over the CFMIP-2 ocean locations (see Table 8). The change in CRE can in this case be considered a measure of the cloud feedback for comparison purposes because all of the models are subject to the same SST increase. For each of the 119 locations available from all six models, we calculated the 30 year climatological annual mean changes for each time of day (UTC). We then rotated the time coordinates for each location to align the times of the maximum solar insolation, placing these at 12 noon (mean solar time) before averaging across locations. Radiative fluxes are only available every three hours from CNRM-CM5, which means that the diurnal cycle is less well resolved, and the time of the maximum insolation is less accurately diagnosed. Shortwave radiative fluxes are not yet available from EC-EARTH which precludes this model from our current analysis, although it will be included in the future.

Time of largest shortwave CRE response

Figure 68(a) shows that the models show a range of shortwave CRE responses varying from weakly negative to positive, as seen in many previous studies. If there was no change in the diurnal cycle of the cloud properties (i.e. cloud properties changed by the same amount at all times of day) then we would expect the shortwave CRE responses to be symmetric about a maximum at solar noon, with a diurnal cycle following the solar insolation but with different magnitudes depending on the size of the diurnal mean change in cloud properties. The majority of models show only modest deviations from this situation, suggesting that changes in the diurnal cycle of cloud properties are generally small compared to changes in diurnal mean quantities.

Figure 69(a, b) confirms that this is generally the case for low cloud fraction and cloud liquid water path. CanAM4 is the exception to this however. Although its shortwave CRE response peaks with a positive value in the morning, a negative local minimum is present in the afternoon which is unusual compared to the other models (Figure 68(a)). We attribute this behaviour to the fact that CanAM4 has an unusually large change in the diurnal cycle of its low cloud fraction relative to the size of the change in its diurnal mean (Figure 69(a)).

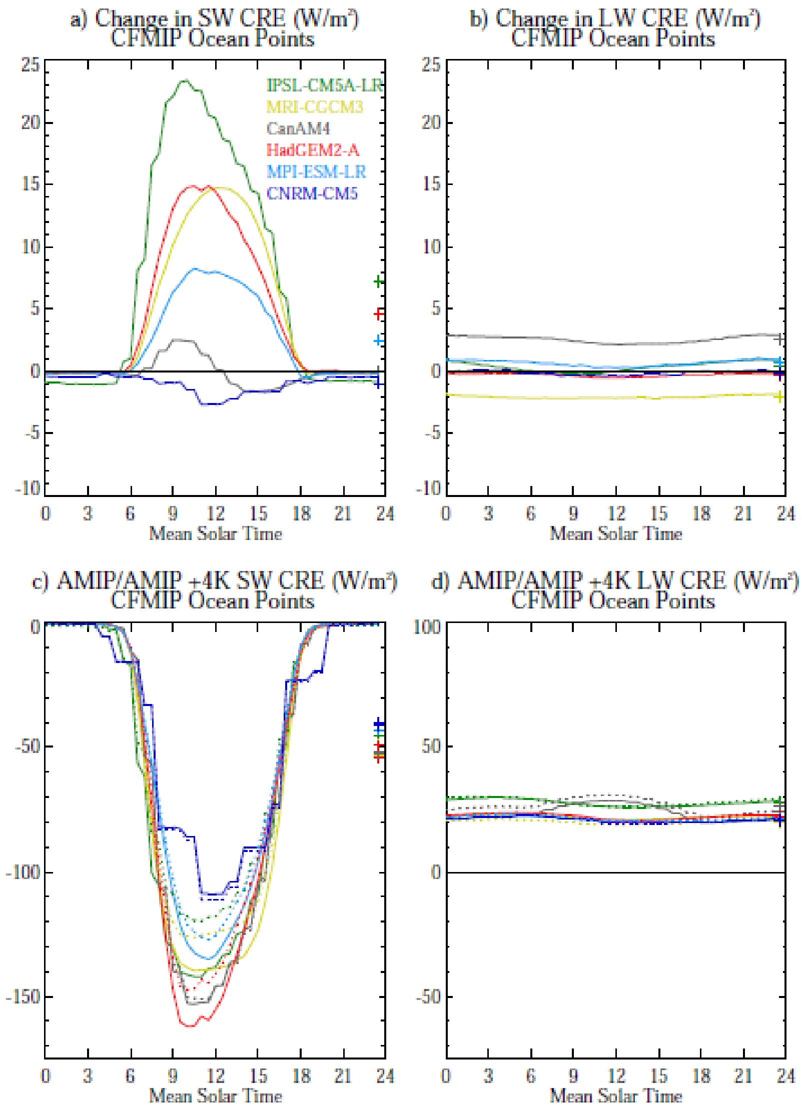

Figure 68. *Diurnal cycle of the Cloud Radiative Effect (CRE) averaged over CFMIP-2 ocean locations in CFMIP-2/CMIP5 AMIP and uniform +4K perturbation experiments.* ***a)*** *and b) show responses in the shortwave and longwave CRE respectively to the uniform +4K SST perturbation. c) and d) show the shortwave and longwave values in the AMIP (solid) and AMIP + 4K (dashed) experiments. + symbols indicate the diurnal mean values.*

Most of the models show the largest shortwave CRE response in the morning (Figure 68(a)), which means that cloud properties must be changing more at that time than at midday. Low level cloud fraction reduces in all of the models at all times of day over the oceans (Figure 69(a)), and the models which have stronger shortwave CRE responses in the morning show larger decreases in low cloud fraction at that time than at midday. MRI-CGCM3 is the exception, with the largest positive changes in shortwave CRE around and soon after noon, and the largest decreases in low cloud fraction in the afternoon. The tendency for the models to show the largest shortwave CRE response in the morning results in the inter-model spread also being largest at that time.

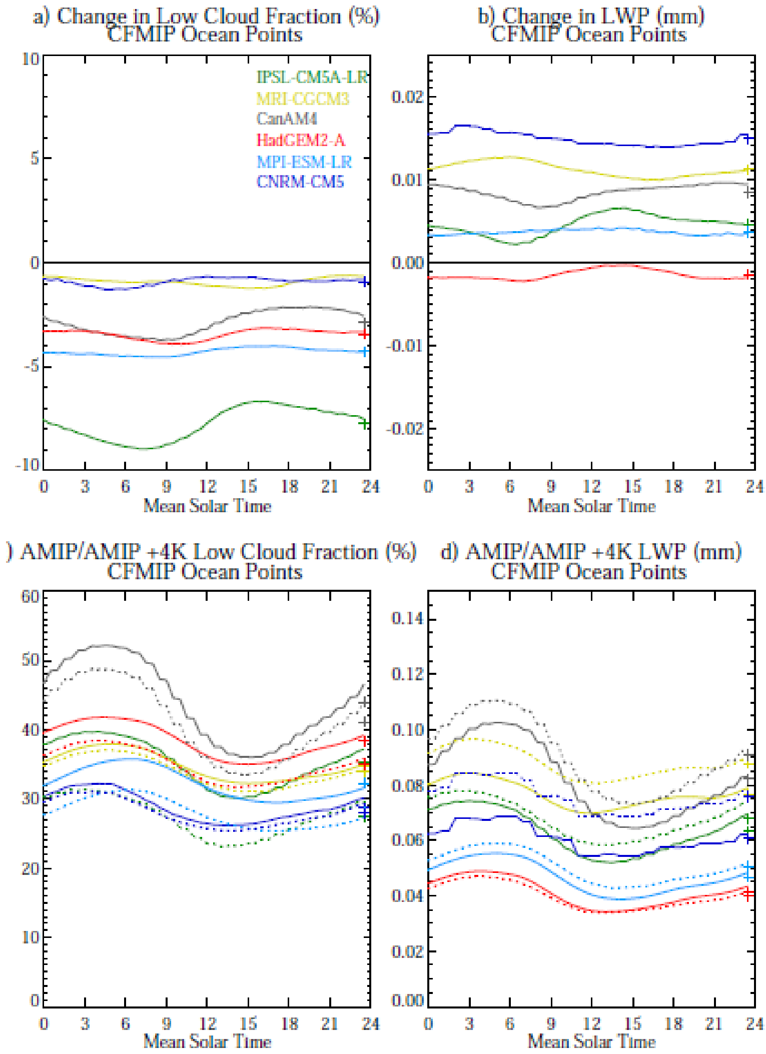

Figure 69*: As Figure 2, but for low cloud fraction and liquid water path***. *The low cloud fraction is calculated by taking the maximum cloud fraction below 640hPa.*

Relative impact of low cloud fraction and liquid water path changes

The liquid water path increases in most of the models, the exception being HadGEM2-A, which shows a small decrease (Figure 69(b)). This slightly unusual behaviour in HadGEM2-A may be related to the nature of its PDF based cloud scheme which has a strong coupling between cloud fraction and cloud water content. The increases in the majority of models would on their own result in a negative shortwave CRE response, but in most cases they are not large enough to overcome the positive response due to the reductions seen in the low cloud amounts. For example, IPSL-CM5-LR shows a 23% reduction in diurnal mean low cloud fraction relative to its control value, while its liquid water path increases by just 7% (Figure 69(c,d)). These results are consistent with the findings of Zelinka et al (2013), who show that cloud optical depth does generally increase in the warmer climate in models, but that the effect of this on the shortwave cloud CRE response is more than compensated for by reductions in cloud fraction. CNRM-CM5 is an exception to this however; it has the largest increase in cloud liquid water and one of the smallest reductions in low cloud fraction, which presumably explains its weakly negative shortwave CRE response. The diurnal variations of the present-day values of liquid water path about the mean tend to be in phase with those of the low cloud fraction (Figure 69(c, d)), which is consistent with observations (Wood et al, 2002). The diurnal variations of the low cloud and liquid water path responses also tend to be in phase in most models, but CNRM-CM5 is an exception to this, with the largest liquid water path increase occurring in the morning rather than the afternoon (Figure 69(a ,b)).

Present-day diurnal cycle in marine low cloud properties

Why do the models generally show the largest changes in marine low-cloud properties in the mornings? Observations show that oceanic stratocumulus clouds tend to form overnight and then break up through the day as the cloud layer is heated by solar absorption. For example, Wood et al (2002) showed that cloud liquid water paths retrieved from the Tropical Rainfall Measuring Mission Microwave Imager over the tropical and subtropical oceans tend to peak in the early morning. If the models capture this behaviour, it is conceivable that smaller cloud amounts later in the day mean that there is less cloud to break up, resulting in a weaker cloud feedback. Figure 69(c, d) shows that the models do a remarkably good job of capturing the observed phase in the diurnal cycle; all have a maximum low cloud fraction and liquid water path in the morning and a minimum at or after solar noon, and this is reflected in present-day values of the shortwave CRE which are most negative before 12 noon (Figure 68(c)). Wood et al (2002) find that diurnal amplitudes in liquid water path are observed which are considerable fractions of the mean, reaching as much as 15-35% in coastal stratocumulus regions. There are however large differences in amplitude between the models; CanAM4 has the largest diurnal amplitude in liquid water path, and its amplitude is 43% the size of its diurnal mean, somewhat larger than observed. MRI-CGCM3 has the smallest, at 13%.

Diurnal cycle in longwave CRE over the oceans

Figure 68 shows that over the oceans the diurnal cycle in the longwave CRE and its response to a +4K perturbation is much smaller than that in the shortwave. The models mostly show minima in the longwave CRE response around or before noon (Figure 68(b)), generally coinciding with minima in the high cloud response (Figure 70(a)). This is consistent with the expectation that deep convection over the oceans is slightly suppressed during the daytime because of atmospheric stabilisation due to enhanced shortwave heating. CanAM4 is an exception in that it shows a minimum longwave CRE response centred near early afternoon, which is at a time when both the high cloud and ice water path responses are weakening. There is no obvious relationship across the models between the changes in the diurnal cycle of these quantities and their present-day diurnal cycles. However, it is perhaps worth noting that the models with the strongest diurnal cycles in their high-cloud responses (MPIESM- LR and CNRM-CM5) are also those that have the most high cloud in the present day (Figure 70(a,c)). Also the model with the smallest present-day high cloud fraction (HadGEM2-A), has the smallest diurnal cycle in the high cloud response. CanAM4 is slightly unusual compared to the other models in that is has a local maximum in longwave CRE over the ocean points in its present-day simulation. We attribute this effect to the inclusion of near-infrared solar radiation with wavelengths above 4 microns in the longwave radiation diagnosed from CanAM4 (Li et al, 2010). The diurnally varying components of the longwave CRE responses discussed above are small compared to the inter-model differences present in the diurnal meaned responses (Figure 68(b)). MRI-CGCM3 shows a reduction in longwave CRE, with relatively neutral changes in ice water path and high cloud fraction (Figure 70(a,b)), which would be consistent with the reduction in longwave CRE in this model mainly being a cloud masking effect. CanAM4 has the largest increase in high cloud fraction and one of the largest increases in ice water path, consistent with it having the strongest longwave CRE increase. These upper level cloud changes in CanAM4 would also be expected to make the shortwave CRE response less negative, and this might explain the relatively small diurnally meaned shortwave CRE response in this model given its somewhat typical changes in diurnal mean low cloud properties. The other models show diurnally meaned changes in high cloud fraction and/or ice water path consistent with more neutral longwave CRE responses.

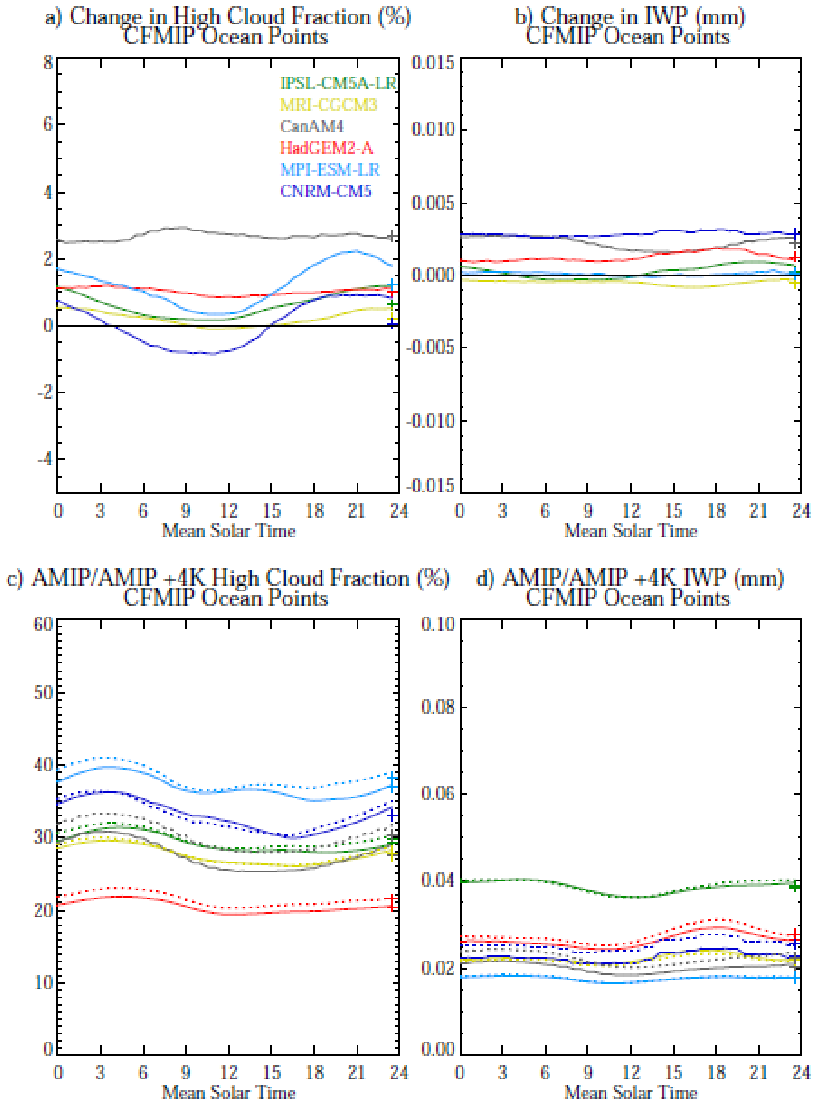

Figure 70. *As Figure 2, but for high cloud fraction and ice water path. The high cloud fraction is calculated by taking the maximum cloud fraction above 440hPa.*

Diurnal cycle over land points

Figure 71(c) shows that the diurnal cycle in present-day shortwave CRE over land points is generally more symmetric than that seen over the ocean points (cf Figure 68(c)); this can be explained by present-day diurnal cycles in low and high cloud fraction which are generally smaller over land than ocean (see Figure 72(c) cf Figure 69(c) and Figure 73(c) cf Figure 70(c)). Although smaller in amplitude, the majority of the models show a quite similar diurnal cycle in low cloud properties over the land compared to the ocean, with maxima in the morning and minima in the afternoon (Figure 72(c) cf Figure 69(c)). HadGEM2-A and CNRM-CM5 are exceptions however, with local maxima in low cloud amount and liquid water path later in the day, presumably related to deep convective activity.

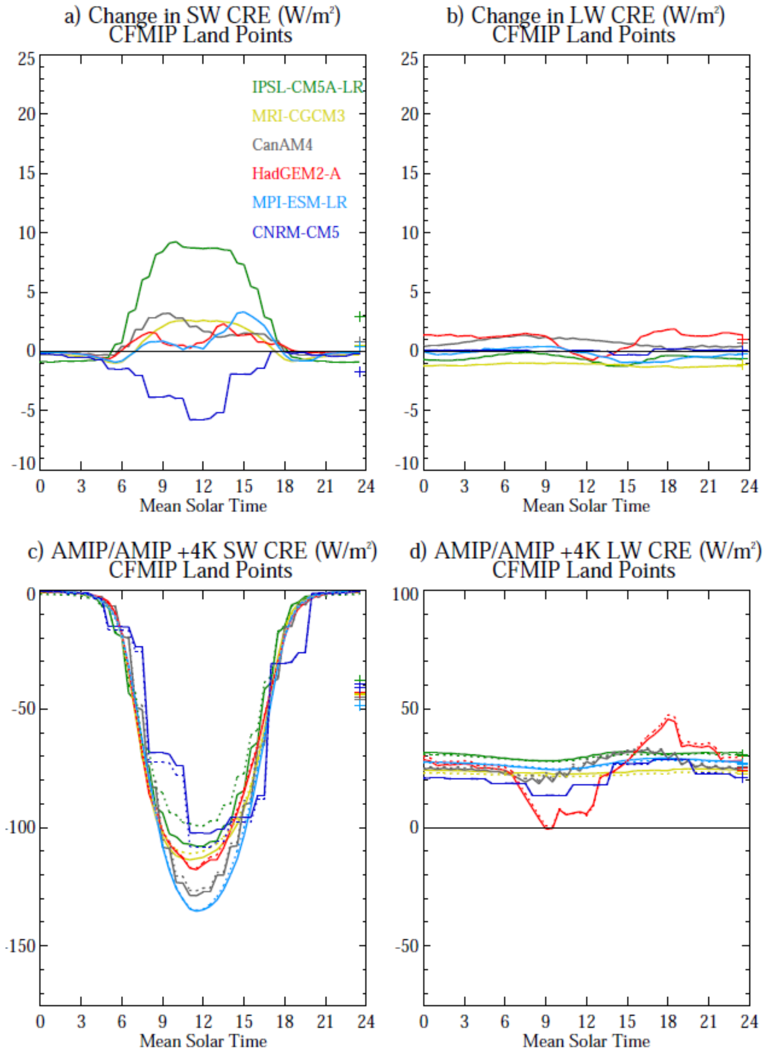

Figure 71: *As Figure 2, but for land points.*

We would expect the diurnal cycle of high cloud to be quite different over land compared to ocean, the result of deep convection building up through the day in response to increasing land surface temperatures. The models tend to show a minimum in present-day longwave CRE in the mornings and a maximum around midafternoon, which is consistent with this expectation (Figure 71(d)). High cloud fraction and ice water path values tend to be smallest in the morning, rising to their maximum values in the afternoon (Figure 73(c,d)). The amplitudes of the diurnal variations in the longwave CRE are mostly small compared to the diurnal mean. CNRM-CM5 shows a diurnal cycle in present-day longwave CRE which is slightly stronger than the majority of the models (Figure 71(d)); we attribute this to a slightly stronger diurnal cycle in high cloud fraction and ice water path (Figure 73(c,d)). HadGEM2-A however has an unusually large diurnal cycle in longwave CRE which is not apparent in the high cloud fraction or ice water path. We attribute this behaviour to an adjustment which is made to the outgoing longwave radiation in HadGEM2-A to improve the diurnal cycle of surface temperature. In HadGEM2-A and earlier versions of the Met Office model, the radiation code is called every three hours. This limits the ability of the land surface to emit more longwave radiation with increasing temperatures between radiation time steps, resulting in an unrealistically

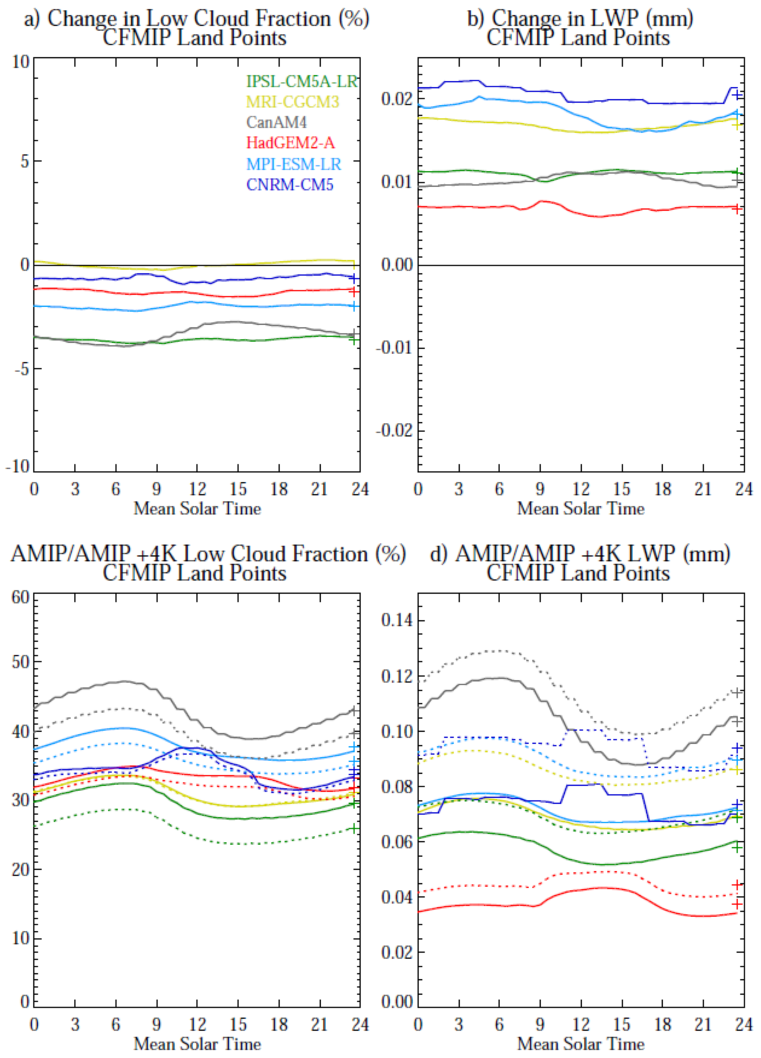

Figure 72: *As Figure 3, but for land points.*

large diurnal cycle in surface temperature. For this reason the additional surface emission due to changes in surface temperature between radiation time steps is estimated and radiated to space via an adjustment to the outgoing longwave radiation. This adjustment is not applied to the clear-sky outgoing longwave radiation however, resulting in an exaggerated diurnal cycle in the diagnosed longwave CRE. This could be corrected for in future by using all-sky and clear-sky longwave fluxes which are adjusted consistently. The shortwave CRE response to the +4K SST perturbation is much smaller over land than ocean in the majority of models (Figure 71(a) cf Figure 68(a)). CNRMCM5 is an exception to this, with a strong negative shortwave CRE response over land, which we attribute to a strong increase in cloud liquid water path combined with a relatively small decrease in low cloud fraction (Figure 72(a,b)). The strongest shortwave CRE responses are in the morning in IPSL-CM5-LR and CanAM4, and in the afternoon in HadGEM2-A and MPI-ESM-LR. The responses in MRI-CGCM3 and CNRM-CM5 are largest around noon. The times of the maximum longwave CRE response are equally diverse (Figure 71(b)). This is a less coherent picture than that seen over the ocean which may reflect the diversity of deep convection schemes used in climate models. This also suggests that the behaviour of deep convection schemes in the present day is not a good guide to how they will respond in the warming climate.

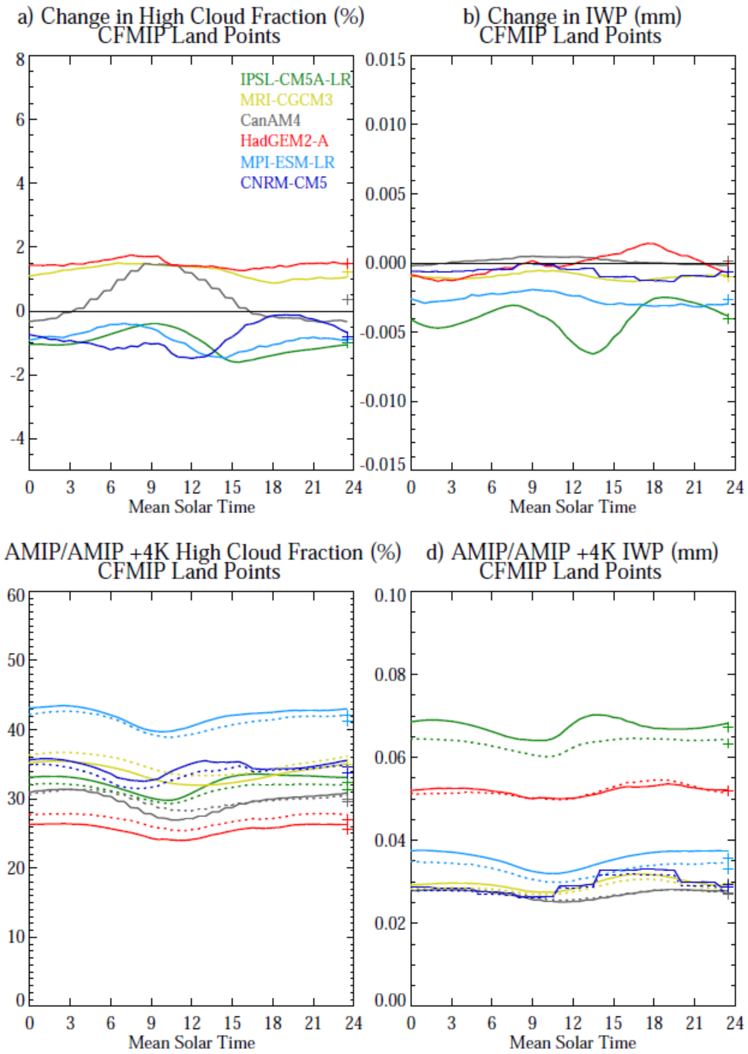

***Figure 73**: As Figure 4, but for land points*

iii) Conclusions and Future Work

Here we have examined the diurnal cycle of clouds and cloud feedbacks using high frequency outputs from six CFMIP models. The models capture the observed phase of the diurnal cycle in low cloud properties over the oceans, although the amplitude of this variation varies and is in some cases larger relative to the diurnal mean than is the case in observations. The fact that the models all capture this suggests that the mechanism is likely to be quite simple; one possibility is that increased solar absorption by clouds during the day heats the cloud layer, reducing relative humidity and hence cloud fraction. The models tend to show larger changes in low cloud properties in the warmer climate in the morning when more low cloud is present in the control. This results in shortwave cloud feedbacks being strongest and having the largest inter-model spread at this time of day. This suggests that careful comparisons with observations might help to constrain future model predictions of changes in the diurnal cycle of low clouds. However, this is unlikely to have a large impact of inter-model spread in cloud feedback, which is mainly explained by differing responses in diurnally meaned cloud properties, rather than changes in the diurnal cycle. A number of unusual behaviours have been noted in individual models. We would like to analyse these in more detail in future work, to establish which models are representing key processes unusually well or unusually badly. We consider an improved understanding of such behaviours in models to be a necessary pre-requisite for reducing uncertainty in future model predictions. An obvious next step is to extend this analysis to additional models as they become available, and also to apply it to the other CFMIP-2 experiments, for example in the context of cloud adjustments and in idealised aquaplanet configurations. Examination of the diurnal cycle is but one

application of these high frequency model outputs. Many other questions remain which can be investigated using these data.
They can be used to refine large scale forcings used to run LES models in cloud feedback studies such as CGILS (The CFMIP-GCSS Intercomparison of LES and SCMs, Zhang et al (2013)). They can be used to separate cloud feedback into contributions from times when convection is dominant from those when turbulent boundary layer processes are dominant. More generally, relationships between clouds and other model variables such as surface fluxes, temperature and humidity profiles and their tendency terms can be investigated. One advantage of these outputs is that the order of events can potentially be used to determine causality in a way that is not possible with time meaned outputs. Moreover these model outputs constitute a rich database of model behaviour against which physical hypotheses on cloud feedback mechanisms can be tested.

WP4 : Sensitivity Experiments and Hypothesis Testing

1. Introduction

In this WP we will integrate results from other work-packages to develop numerical experiments designed to both test our developing understanding and identify observables that can help further constrain cloud feedbacks.

2. A developing database and protocol for parameter and structural (numerical) sensitivity studies.

Deliverable 4.1

Cloud-radiative effects are expected to control many aspects of the current and future climates, ranging from the large-scale circulation of the atmosphere and intra-seasonal variability to climate sensitivity and precipitation projections. However, investigations so far have been carried out using individual models and various methodologies. To identify robust effects and facilitate physical understanding, the role of clouds in climate and climate change needs to be investigated in a more coordinated way and through a wider range of model configurations and complexity. The Clouds On Off Klima Intercomparison Experiment (COOKIE) proposes a simple set of atmosphere only experiments designed to better understand the impacts of clouds on climate and climate change. Groups who wish to participate in the COOKIE are requested to perform an additional six experiments with fixed sea-surface temperatures, totaling 105 years of simulation time. In addition to the base COOKIE an number of other COOKIES and an extension called CREAM expands the project into a tiered set of experiments designed to better isolate the effects of clouds, convection, and eventually aerosols on equilibrium climate sensitivity. The ultimate idea behind COOKIEs and CREAM is to control the representation of cloud radiative ffects (clouds on-off) in a hierarchy of models so as to better identify large-scale constraints that might be controlling the basic factors through which changes in temperature, and radiative uxes associated with different distributions of greenhouse gases or aerosols, influence cloudiness. A detailed prescription of the COOKIE and CREAM experiments can be find at the EUCLIPSE website http://www.euclipse.eu/wp4/wp4.html .

EUCLIPSE PUBLICATIONS

Bellenger, H., E. Guilyardi, J. Leloup, M. Lengaigne, and J. Vialard (2012): ENSO representation in climate models: from CMIP3 to CMIP5. Submitted for publication in Climate Dynamics.

Blossey, P. N., C.S. Bretherton, M. Zhang, A. Cheng, S. Endo, T. Heus, Y. Liu, A. Lock, S.R. de Roode and K.-M. Xu, (2012): Marine low cloud sensitivity to an idealized climate change: The CGILS LES Intercomparison. Accepted in *J. Adv. Model. Earth Syst*. pending minor revisions.

Bodas-Salcedo, A., M.J. Webb, S. Bony, H. Chepfer, J.-L. Dufresne, S.A. Klein, Y. Zhang, R. Marchand, J.M. Haynes, R. Pincus, and V.O. John, (2011): COSP: satellite simulation software for model assessment. *Bull. Amer. Meteor. Soc*., **92**, 1023-1043, doi: 10.1175/2011BAMS2856.1

Bony S., G. Bellon, D. Klocke, S. Sherwood, S. Fermepin and S. Denvil, (2013): Direct effect of carbon dioxide on future tropical atmospheric circulation and regional precipitation. Submitted for publication in *Nature Geoscience* (in revision).

Brient, F. and S. Bony, (2012): Interpretation of the positive low-cloud feedback predicted by a climate model under global warming. Accepted for publication in *Climate Dynamics*, DOI 10.1007/s00382-011-1279-7.

Brient, F. and S. Bony, (2012): How may low-cloud radiative properties simulated in the current climate influence low-cloud feedbacks under global warming. Published in *Geophys. Res. Lett*., **39**, L20807, doi:10.1029/2012GL053265.

Cattiaux, J., H. Douville, and Y. Peings, (2012): European temperatures in CMIP5 origins of present-day biases and future uncertainties. Submitted for publication in *Climate Dynamics*.

Cattiaux, J.,H. Douville, A. Ribes, F. Chauvin, and C. Plante, (2012): Towards a better understanding of changes in wintertime cold extremes over Europe: A pilot study with CNRM-CM5 and IPSL-CM5 atmospheric models. *Climate Dynamics*, published online. doi:10.1007/s00382-012-1436-7.

Cheruy, F., A. Campoy, J.-C. Dupont, A. Ducharne, F. Hourdin, M. Haeffelin, M. Chiriaco, A. Idelkadi, (2012): Combined influence of atmospheric physics and soil hydrology on the simulated meteorology at the SIRTA atmospheric observatory. Submitted for publication in *Climate Dynamics*.

Crueger, T., C. Hohenegger, W. May, (2012): Tropical precipitation and convection changes in the MPI-ESM in response to CO2 forcing. Submitted for publication in the *J. Adv. Model. Earth Syst*.

Crueger, T. and B. Stevens, (2012): The Madden-Julian Oscillation in ECHAM6 and the Introduction of an Objective MJO Metric. Submitted for publication in the *J. of Climate*.

Dussen, J.J. van der, S.R. de Roode, A.S. Ackerman, P.N. Blossey, C.S. Bretherton, M.J. Kurowski, A.P. Lock, R.A.J. Neggers, I. Sandu, and A.P. Siebema, (2012): The GASS/EUCLIPSE Model Intercomparison of the Stratocumulus Transition as Observed During ASTEX: LES results. Submitted for publication in the *J. Adv. Model. Earth Syst*.

Koenigk T., L. Brodeau, R.G. Graversen, J. Karlsson, G. Svensson, M. Tjernström, U. Willén and K. Wyser, (2012): Arctic climate change in 21st century CMIP5 simulations with EC-Earth. Published in *Climate Dynamics*, DOI 10.1007/s00382-012-1645-0.

Lacagnina, C., F. Selten, (2013): Changes in the cloud properties in response to El Niño: a bivariate approach. Published on line in *Climate Dynamics*, DOI: 10.1175/JCLI-D-11-00178.1 .

Lloyd, J., E. Guilyardi and H. Weller, (2012): The role of atmosphere feedbacks during ENSO in the CMIP3 models. Part III: the shortwave flux feedback Published in J. Climate, **25**, 4275-4293, DOI: 10.1175/JCLI-D-11-00178.1 .

Mauritsen, T., et al., (2012): Tuning the Climate of a global model. Submitted for publication in the *J. Adv. Model. Earth Syst*.

Moebis, B. and B. Stevens, (2012): Factors influencing ITCZ placement on an aquaplanet. Submitted for publication in the *J. Adv. Model. Earth Syst*.

Nam, C. , S. Bony, J.-L. Dufresne and H. Chepfer, (2012): The 'too few, too bright' tropical low-cloud problem in CMIP5 models. Published in *Geophysical Research Letters* , vol. **39** , issue 21. doi.org/10.1029/2012GL053421 .

Neggers, R.A.J. and A.P. Siebesma, (2012): Constraining a system of interacting parameterizations through multiple-parameter evaluation: Tracing a compensating error between cloud vertical structure and cloud overlap. Submitted for publication in the *J. of Climate*.

Neggers, R.A.J., A.P. Siebesma and T. Heus, (2012): Continuous single-columnmodel evaluation at a permanent meteorological supersite. Published in *Bull. Am. Meteorol. Soc.*, **93**, 1389-1400, DOI:10.1175/BAMS-D-11-00162.1.

Oueslati, B. and G. Bellon, (2012): Tropical precipitation regimes and mechanisms of regime transitions: contrasting two aquaplanet general circulation models. Published in *Climate Dynamics*, DOI 10.1007/s00382-012-1344-x.

Oueslati, B. and G. Bellon, (2013): Convective entrainment and large-scale organization of tropical precipitation: sensitivity of the CNRM-CM5 hierarchy of models. In press *Journal of Climate*.

Popke, D., B. Stevens, A. Voigt, (2012): Investigation of climate change using a radiative convective equilibrium configuration of ECHAM6. Submitted for publication in the *J. Adv. Model. Earth Syst*.

Roode, S.R. de, A.P. Siebesma, S. Dal Gesso, H.J.J. Jonker, J. Schalkwijk, and J. Sival, (2012): The stratocumulus response to a single perturbation in cloud controlling factors. Submitted for publication in the *J. of Climate*.

Schalkwijk, J., H.J.J. Jonker and A.P. Siebesma, (2012): Simple Solutions to Steady-state Cumulus Regimes in the Convective Boundary Layer. Submitted for publication in the *J. Atm. Sci*.

Schubert, J.J., B. Stevens , T. Crueger, (2012): The Madden-Julian Oscillation as Simulated by the MPI Earth System Model: Over the Last and Into the Next Millennium. Submitted for publication in the *J. Adv. Model. Earth Syst*.

Stevens, B., et al., (2012): The Atmospheric Component of the MPI-ESM: ECHAM6 Submitted for publication in the *J. Adv. Model. Earth Syst*.

Tselioudis, G., W. Rossow, Y. Zhang and D. Konsta, (2012): Global Weather States and their Properties from Passive and Active Satellite Cloud Retrievals. Submitted for publication in the *J. of Climate*.

Tsushima, Y., M.A. Ringer, M.J. Webb and K.D. Williams, (2012): Quantitative Evaluation of the Seasonal Variations in Climate Model Cloud Regimes. Published in *Climate Dynamics*, DOI 10.1007/s00382-012-1609-4

Vial, J., J.-L. Dufresne and S. Bony, (2013): On the interpretation of inter-model spread in CMIP5 climate sensitivity estimates. Submitted for publication in Climate Dynamics

Webb, M.J. and A.P. Lock, (2012): Coupling between subtropical cloud feedback and the local hydrological cycle in a climate model. Published in *Climate Dynamics*, DOI 10.1007/s00382-012-1608-5

Zelinka, M.D., S.A. Klein, K.E. Taylor, T. Andrews, M.J. Webb, J.M. Gregory, and P.M. Forster, (2013): Contributions of Different Cloud Types to Feedbacks and Rapid Adjustments in CMIP5. In press, *J. Climate*. doi: 10.1175/JCLID-12-00555.1.

Zhang, M., C.S. Bretherton, P.N. Blossey, P.A. Austin, J.T. Bacmeister, S. Bony, F. Brient, A. Cheng, S.R. De Roode, S. Endo, A.D. Del Genio, C.N. Franklin, J.-C. Golaz, C. Hannay, T. Heus, F.A. Isotta, J.-L. Dufresne, I.-S. Kang, H. Kawai, M. Koehler, S. Kumar, V.E. Larson, Y. Liu, A.P. Lock, U. Lohman, M.F. Khairoutdinov, A.M. Molod, R.A.J. Neggers, P. Rasch, I. Sandu, R. Senkbeil, A.P. Siebesma, C. Siegenthaler-Le Drian, B. Stevens, M.J. Suarez, K.-M. Xu, K. von Salzen, M.J. Webb, A. Wolf, M. Zhao, (2012): CGILS First results from an International Project to Understand the Physcial Mechanisms of Low Cloud Feedbacks in General Circulations Models. Submitted for publication in the *Bull. Am. Meteorol. Soc.*

Zhang, M., C.S. Bretherton, P.N. Blossey, S. Bony, F. Brient and J.-C. Golaz, (2012): The CGILS experimental design to investigate low cloud feedbacks in general circulation models by using single-column and large-eddy simulation models. Submitted to the *J. Adv. Model. Earth Syst*.

REFERENCES

Ackerman, A.S., M.P. Kirkpatrick, D. E. Stevens, and O. B. Toon, (2004): The impact of humidity above stratiform clouds on indirect aerosol climate forcing, *Nature*, **432**,1014–1017.

Andrews, T., and P.M. Forster (2008): CO2 forcing induces semi-direct effects with consequences for climate feedback interpretations. *Geophys. Res. Lett*., **35**, L04802, doi:10.1029/2007GL032273.

Andrews, T., Gregory, J.M., Webb, M.J., and K.E. Taylor, (2012): Forcing, feedbacks and climate sensitivity in CMIP5 coupled atmosphere-ocean climate models. Geophys. Res. Lett., **39**, L09712, doi:10.1029/2012GL051607.

Andrews, T., J.M. Gregory, M J. Webb, and K.E. Taylor (2012): Forcing, feedbacks and climate sensitivity in CMIP5 coupled atmosphere-ocean climate models, *Geophys. Res. Lett*., **39**, L09712, doi:10.1029/2012GL051607.

Bauer, M., and A.D. Del Genio, (2006): Composite analysis of winter cyclones in a GCM: Influence on climatological humidity, *J. Climate*, **19**, 1652–1672, doi:10.1175/JCLI3690.1.

Bellucci, A., S. Gualdi, A. Navarra (2010): The Double-ITCZ Syndrome in Coupled General Circulation Models: The Role of Large-Scale Vertical Circulation Regimes. *J. Climate*, **23**, 1127-1145.

Blossey, P. N., C.S. Bretherton, and M.C. Wyant, (2009): Understanding subtropical low cloud 552 response to a warmer climate in a superparameterized climate model. Part II: Column 553 modeling with a cloud-resolving model. *Journal of Advancing Modeling Earth Systems*, **1**, 14 pp., doi:10.3894/JAMES.2009.1.8 .

Bodas-Salcedo, A., et al., (2011): COSP: satellite simulation software for model assessment, *Bull. Am. Meteorol. Soc.*, *92*(8), 1023–1043, doi:10.1175/2011BAMS2856.1.

Bodas-Salcedo, A., K.D. Williams, P.R. Field, and A.P. Lock, (2012): The surface downwelling solar 13 radiation surplus over the Southern Ocean in the Met Office model: the role of midlatitude cyclone clouds, *J. Climate*, doi:10.1175/JCLI-D-11-00702.1, in press.

Boer, G.J. and B. Yu (2003): Dynamical aspects of climate sensitivity. *Geophys. Res. Lett*., **30**(3), 1135.

Bony, S. and J.-L. Dufresne. Marine boundary layer clouds at the heart of tropical cloud feedback uncertainties in climate models, *Geophys. Res. Lett*., **32**, No. 20, L20806, doi:10.1029/2005GL023851, 2005.

Bony, S., et al. (2011): CFMIP: Towards a better evaluation and understanding of clouds and cloud feedbacks in CMIP5 models. *Clivar Exchanges*, **56**, 16, 2.

Bony, S., J.-L. Dufresne, H.L. Treut, J.-J. Morcrette, and C.A. Senior (2004): On dynamic and thermodynamic components of cloud changes, *Clim. Dyn*., **22** (2-3), 71–86, doi:10.1007/s00382-003-0369-6.

Boucher, O., (2012): The aerosol effect: An essential pursuit, *Nature*, **490**, 40-41.

Bretherton C.S. (2006): The climate process team on low-latitude cloud feedbacks on climate sensitivity. US *Clivar Variations* **4**:7–12.

Bretherton, C.S. , S.K. Krueger, M.C. Wyant, P. Bechtold , E. Van Meijgaard, B. Stevens, and J. Teixeira J, (1999): A GCSS boundary-layer cloud model intercomparison study of the first ASTEX Lagrangian experiment. *Bound.-Layer Meteor*., **93**, 341–380.

Cassou, C. (2008): Intraseasonal interaction between the Madden-Julian Oscillation and the North Atlantic Oscillation, *Nature,* **455** (7212), pp. 523-527. doi: 10.1038/nature07286.

Cassou, C., L. Terray, and A.S. Phillips (2005): Tropical Atlantic Influence on European Heat Waves, *J. Climate*, **18** (15), pp. 2805-2811.

Cattiaux, J., P. Yiou, and R. Vautard (2011): Dynamics of future seasonal temperature trends and extremes in Europe: a multi-model analysis from CMIP3, *Climate Dynamics*, published online. doi:10.1007/s00382-011-1211-1.

Cess, R.D, and Coauthors, (1990): Intercomparison and interpretation of cloud-climate feedback processes in nineteen atmospheric general circulation models. *J. Geophys. Res.,* **95**, 16 601–16 615.

Chepfer, H., S. Bony, D. Winker, G. Cesana, J.-L. Dufresne, P. Minnis, C. J. Stubenrauch, and S. Zeng, (2010): The GCM Oriented Calipso Cloud Product (CALIPSO-GOCCP), *J. Geophys. Res.*, ***115***, D00H16, doi:10.1029/2009JD012251.

Chepfer, H., S. Bony, D. Winker, M. Chiriaco, J.-L. Dufresne, and G. Sèze, (2008): Use of CALIPSO lidar observations to evaluate the cloudiness simulated by a climate model., *Geophys. Res. Lett.*, **35,** L15,704, doi:10.1029/2008GL034207.

Collins, W.J., et al., (2011): Development and evaluation of an earth-system model - hadgem2, *Geosci. Model Devel.*, **4**, 1051–1075, doi:10.5194/gmd-4-1051-2011.

Dai, A. (2006): Precipitation Characteristics in Eighteen Coupled Climate Models. J. Climate, 19, 4605-4630.

De Roode, S. R., and P.G. Duynkerke, (1997): Observed Lagrangian transition of stratocumulus into cumulus during ASTEX: Mean state and turbulence structure, *J. Atmos. Sci.,* **54**, 2157–2173.

de Szoeke, Simon P., Shang-Ping Xie (2008): The Tropical Eastern Pacific Seasonal Cycle: Assessment of Errors and Mechanisms in IPCC AR4 Coupled Ocean-Atmosphere General Circulation Models. *J. Climate*, **21**, 257-2590.

Dee, D. P., et al., (2011): The ERA-Interim reanalysis: configuration and performance of the data assimilation system, *Q. J. R. Meteorol. Soc.*, **137**(656), 553–597, doi:10.1002/qj.828.

Dong, Buwen, Jonathan M. Gregory, Rowan T. Sutton, (2009): Understanding Land-Sea Warming Contrast in Response to Increasing Greenhouse Gases. Part I: Transient Adjustment. *J. Climate*, **22**, 3079–3097.

Dufresne, Jean-Louis, Sandrine Bony (2008): An Assessment of the Primary Sources of Spread of Global Warming Estimates from Coupled Atmosphere-Ocean Models. *J. Climate*, **21**, 5135–5144, 2008.

Field, P.R., and R. Wood, (2007): Precipitation and cloud structure in midlatitude cyclones, *J. Climate*, ***20***(2), 233–254, doi:10.1175/JCLI3998.1.

Govekar, P.D., C. Jakob, M.J. Reeder, and J. Haynes, (2011): The three-dimensional distribution of clouds around Southern Hemisphere extratropical cyclones, *Geophys. Res. Lett.*, ***38***, L21,805, doi:10.1029/2011GL049091, 2011.

Gregory, J.M., W.J. Ingram, M.A. Palmer, G.S. Jones, P.A. Stott, R.B. Thorpe, J.A. Lowe, T.C. Johns, and K.D. Williams (2004): A new method for diagnosing radiative forcing and climate sensitivity, *Geophys. Res. Lett.*, **31**, L03205, doi:10.1029/2003GL018747.

Gregory, J.M. and M.J. Webb (2008): Tropospheric adjustment induces a cloud component in CO2 forcing. J.Climate, **21**, 58-71, doi:10.1175/2007JCLI1834.1.

Guilyardi E. and A. Wittenberg (2010): ENSO and tropical Pacific metrics for CMIP5. IPCC Expert meeting on Assessing and Combining Multi Model Climate Projections, Boulder, USA, January 2010

Guilyardi E., P. Braconnot, F.-F. Jin, S.T. Kim, M. Kolasinski, T. Li and I. Musat (2009): Atmosphere feedbacks during ENSO in a coupled GCM with a modified atmospheric convection scheme. *J. Climate*, **22,** 5698-5718.

Hansen, J., et al. (2005): Efficacy of climate forcings. *J. Geophys. Res*., **110**, D18104, doi:10.1029/2005JD005776.

Haylock, M.R. et al. (2008): A European daily high-resolution gridded data set of surface temperature and precipitation for 1950-2006, *J. Geophys. Res*., **113**, pp. 20119. doi: 10.1029/2008JD10201.

Haynes, J.M., C. Jakob, W.B. Rossow, G. Tselioudis, and J. Brown, (2011): Major characteristics of Southern Ocean cloud regimes and their effects on the energy budget, *J. Climate*, **24**, 5061–5080, doi:10.1175/2011JCLI4052.1.

Held, I.M. and B.J. Soden, (2006): Robust responses of the hydrological cycle to global warming. *J. Clim*. **19**, 5686-5699, DOI:10.1175/JCLI3990.1.

Hourdin, F., et al., Impact of the LMDZ atmospheric grid configuration on the climate and sensitivity of the IPSL-CM5A coupled model, *Clim. Dyn.*, in press

Hourdin, F., et al., LMDZ5B: the atmospheric component of the IPSL climate model with revisited parameterizations for clouds and convection, *Clim. Dyn.*, in press.

Kanamitsu, M. et al. (2002): NCEP-DOE AMIP-II Reanalysis (R-2), *Bull. Amer. Meteorol. Soc***., 83** (11), pp. 1631-1643.

Karlsson, J., and G. Svensson, (2011): The simulation of Arctic clouds and their influence on the winter surface temperature in present-day climate in the CMIP3 multi-model dataset, *Clim. Dyn.*, **36**, 623–635, doi:10.1007/s00382-010-0758-6.

Khairoutdinov, M., and Y. Kogan, (2000): A new cloud physics parameterization in a large-eddy simulation model of marine stratocumulus, *Mon. Wea. Rev*., **128**, 229–243.

Klein, S.A. and Jakob, C. (1999): Validation and sensitivities of frontal clouds simulated by the ECMWF model. *Mon. Weather Rev*., **10**, 2514-2531

Klein, S.A., and C. Jakob, (1999): Validation and sensitivities of frontal clouds simulated by the ECMWF model., *Mon. Weather Rev.*, **127**(10), 2514–2531.

Klein, S.A., and D.L. Hartmann, (1993): The seasonal cycle of low stratiform clouds, *J. Climate*, **6**(8), 1587–1606.

Klein, S.A., and D.L. Hartmann, (1993): The seasonal cycle of low stratiform clouds. *J. Climate*, **6**, 1587–1606.

Klocke, D., R. Pincus and J. Quaas, (2011): On Constraining Estimates of Climate Sensitivity with Present-Day Observations through Model Weighting. *J. Climate*, **24** (23), 6092-6099.

Konsta, D., J.L. Dufresne, H. Chepfer, A. Idelkali, and G. Cesana, Evaluation of clouds simulated by the LMDZ5 GCM using A-train satellite observations (CALIPSO-PARASOL-CERES), *Clim. Dyn.*, submitted.

Li, J., Curry, C. L., Sun, Z. and Zhang, F. (2010): Overlap of Solar and Infrared Spectra and the Shortwave Radiative Effect of Methane. *Journal of the Atmospheric Sciences*, 2010, **67**, 2372-2389.

Lin, Jia-Lin (2007): The Double-ITCZ Problem in IPCC AR4 Coupled GCMs: Ocean-Atmosphere Feedback Analysis. *J. Climate*, **20**, 4497-4525.

Lin, Jia-Lin, and Coauthors (2006): Tropical Intraseasonal Variability in 14 IPCC AR4 Climate Models. Part I: Convective Signals*. J. Climate*, **19**, 2665-2690.

Lloyd, J.,E. Guilyardi and H. Weller (2011): The role of atmosphere feedbacks during ENSO in the CMIP3 models, Part II: using AMIP runs to understand the heat flux feedback mechanisms, *Clim. Dynamics*, **37**, 1271-1292, DOI: 10.1007/s00382-010-0895

Lock, A.P., (2009): Factors influencing cloud area at the capping inversion for shallow cumulus clouds. *Q.J.R. Meteorol. Soc*., **135**, 941–952.

Loeb, N. G., B.A. Wielicki, D R. Doelling, S. Kato, T. Wong, G.L. Smith, D.F. Keyes, and N. Manalo-Smith, (2009): Toward optimal closure of the Earth's top-of-atmosphere radiation budget, *J. Climate*, **22**(3), 748–766, doi:10.1175/2008JCLI2637.1.

Mapes BE, Bacmeister J, Khairoutdinov M, Hannay C, Zhao M (2009): Virtual field campaigns on deep tropical convection in climate models. *J. Climate,* **22,**244–257. doi:10.1175/2008JCLI2203.1

Martin, G.M., D. W. Johnson, D.P. Rogers, P.R. Jonas, P. Minnis, D.A. Hegg, (1995): Observations of the interaction between cumulus clouds and warm stratocumulus clouds in the marine boundary layer during ASTEX. *J. Atmos. Sci.*, **52**, 2902–2922.

Martin, G.M., N. Bellouin, W.J. Collins, I.D. Culverwell, P.R. Halloran, S.C. Hardiman, T.J. Hinton, and C.D. Jones, (2011): The HadGEM2 family of Met Office Unified Model climate configurations., *Geosci. Model Devel.*, **4**, 723–757, doi:10.5194/gmd-4-723-2011.

Medeiros, B., and S. Stevens, (2011): Revealing differences in GCM representations of low clouds., *Clim. Dyn.*, **36**(1-2), 385–399, doi:10.1007/s00382-009-0694-5.

Mizuta, R., et al., (2012): Climate simulations using MRI-AGCM3.2 with 20-km grid, *J. Meteorol. Soc. Jpn*, **90A**, 233–258, doi:10.2151/jmsj.2012-A12.

Nicholls, S. and J.D. Turton, (1986): An observational study of the structure of stratiform cloud sheets: Part II. Entrainment. *Quart. J. Roy. Meteorol. Soc.*, **112**, 461–480.

Norris, J.R., (1998): Low cloud type over the ocean from surface observations. Part II: Geographical and seasonal variations. *J. Climate*, **11**, 383-403.

Prenni, A.J., J.Y. Harrington, M. Tjernström, P.J. Demott, A. Avramov, C.N. Long, S.M. Kreidenweis, P.Q. Olsson, and J. Verlinde, (2007): Can Ice-Nucleating Aerosols Affect Arctic Seasonal Climate?, *Bull. Am. Meteorol. Soc.*, **88,** 541, doi:10.1175/BAMS-88-4-541.

Quaas, J., Y. Ming, S. Menon, T. Takemura, M. Wang, J. Penner, A. Gettelman, U. Lohmann, N. Bellouin, O. Boucher, A.M. Sayer, G.E. Thomas, A. McComiskey, G. Feingold, C. Hoose, J.E. Kristjánsson, X. Liu, Y. Balkanski, L.J. Donner, P.A. Ginoux, P. Stier, B. Grandey, J. Feichter, I. Sednev, S.E. Bauer, D. Koch, R.G. Grainger, A. Kirkevåg, T. Iversen, Ø. Seland, R. Easter, S.J. Ghan, P J. Rasch, H. Morrison, J.-F. Lamarque, M.J. Iacono, S. Kinne, and M. Schulz, (2008): Aerosol indirect effects - general circulation model intercomparison and evaluation with satellite data, Atmos. Chem. Phys., **9**, 8697-8717, 2009.

Ramanathan, V., R.D. Cess, E.F. Harrison, P. Minnis, B.R. Barkstrom, E. Ahmad, and D. Hartmann, (1989(: Cloud radiative forcing and climate: Results from the Earth Radiation Budget Experiment, *Science*, **243**, 57–63.

Randall, D.A., Harshvardhan, D.A. Dazlich and T.G. Corsette, (1989): Interactions among Radiation, Convection and Large-Scale Dyamics in a General Circulation Model. *J. Atmos. Sci*., **46** (13), 1943-1970.

Randall DA, R.A. Wood, S. Bony, R. Colman, T. Fichefet, J. Fyfe, V. Kattsov, A. Pitman, J. Shukla, J. Srinivasan, R.J. Stouffer, A. Sumi, K.E. Taylor, (2007): Climate models and their evaluation. In: Solomon S, Qin D, Manning M, Chen Z, Marquis MC, Avery KB, Tignor M, Miller HL (eds) Climate Change 2007: The physical science basis. Contribution of Working Group I to the fourth assessment report of the intergovernmental panel on climate change, 589–662, Cambridge University Press.

Randall, D.A., et al. Climate models and their evaluation, in Climate Change (2007): The Physical Science Basis. Contribution of Working Group I to the Fourth Assessment Report of the Intergovernmental Panel on Climate Change, edited by S. Solomon et al., pp. 591-662, Cambridge Univ. Press, Cambridge, U. K..

Rieck, M., L. Nuijens and B. Stevens, (2012): Marine boundary-layer cloud feedbacks in a constant relative humidity atmosphere. *J. Atmos Sci*., in press.

Ringer, M.A., et al. (2006): Global mean cloud feedbacks in idealized climate change experiments, *Geophys. Res. Lett.*, **33**, L07718, doi:10.1029/2005GL025370.

Rossow, W.B., and R.A. Schiffer, (1999): Advances in understanding clouds from ISCCP, *Bull. Am. Meteorol. Soc.*, **80**, 2261–2287.

Rotstayn, L.D., M.A. Collier, M.R. Dix, Y. Feng, H.B. Gordon, S.P. O'Farrell, I.N. Smith, and J. Syktus, (2010): Improved simulation of Australian climate and ENSO-related rainfall variability in a global climate model with an interactive aerosol treatment, *Int. J. Climatol.*, **30**, 1067–1088, doi:10.1002/joc.1952.

Sandu, I. and B. Stevens, (2011): On the factors modulating the stratocumulus to cumulus transitions. *J. Atmos. Sci.,* **68**, 1865–1881.

Sandu, I., B. Stevens and R. Pincus, (2010): On the transitions in marine boundary layer cloudiness, *Atmos.Chem. Phys*.,**10**, 2377-2391.

Schwartz, S. E., Uncertainty in climate sensitivity: Causes, consequences, challenges. Energy Environ Sci, **1**:430–453.

Seifert, A., and K.D. Beheng, (2001): A double-moment parameterization for simulating autoconversion, accretion and selfcollection, *Atmos. Res*., **59-60**, 265–281.

Shupe, M. D., S.Y. Matrosov, and T. Uttal, (2006): Arctic Mixed-Phase Cloud Properties Derived from Surface-Based Sensors at SHEBA, *J. Atmos. Sci.*, **63**, 697–711.

Slingo, A. and J.M. Slingo, (1988): The response of a general circulation model to cloud longwave radiative forcing. I: Introduction and initial experiments. *Quart. J. Roy. Meteor. Soc*., **114** (482), 1027-1062.

Slingo, J.M. and A. Slingo, (1991): The response of a general circulation model to cloud longwave radiative forcing. II: Further studies. *Quart. J. Roy. Meteor. Soc*., **117** (498), 333-364.

Soden, B.J. and I.M. Held. (2006): An assessment of climate feedbacks in coupled ocean atmosphere models. *J. Climate*, **19** (14), 3354-3360, doi:10.1175/JCLI3799.1.

Soden, B. J., A.J. Broccoli, and R.S. Hemler, (2004): On the use of cloud forcing to estimate cloud feedback. *J.Climate*, **17**, 36613665.

Soden, B.J., and G.A. Vecchi, (2011): The vertical distribution of cloud feedback in coupled ocean-atmosphere models, Geophys. Res. Lett., 38, L12704, doi:10.1029/2011GL047632.

Soden, B.J., et al. (2008): Quantifying climate feedbacks using radiative kernels, *J. Climate*, **21**, 3504-3520, doi:10.1175/2007JCLI2110.1.

Soden, B.J., I.M. Held (2006): An Assessment of Climate Feedbacks in Coupled Ocean Atmosphere Models. *J.Climate*, **19**, 33543360.

Stevens, B., (2012): The aerosol effect: Grains of salt, *Nature*, **490**, 40-41.

Svensson, G., and J. Karlsson, (2011): On the Arctic wintertime climate in global climate models, *J. Climate*, doi:10.1175/2011JCLI4012.1.

Taylor, K. E., R. J. Stouffer, and G. A. Meehl, (2009): A Summary of the CMIP5 Experiment Design, available at http://cmip-pcmdi.llnl.gov/cmip5/docs/Taylor_CMIP5_design.pdf.

Taylor, K.E., R.J. Stouffer, and G.A. Meehl, (2012): An overview of CMIP5 and the experiment design, *Bull. Am. Meteorol. Soc.*, **93**, 485–498, doi:10.1175/BAMS-D-11-00094.1.

Teixeira, J., and Coauthors, (2011): Tropical and Subtropical Cloud Transitions in Weather and Climate Prediction Models: The GCSS/WGNE Pacific Cross-Section Intercomparison (GPCI). *J. Climate*, **24**, 5223–5256. doi: http://dx.doi.org/10.1175/2011JCLI3672.1

Tjernström, M., J. Sedlar, and M.D. Shupe, (2008): How Well Do Regional Climate Models Reproduce Radiation and Clouds in the Arctic? An Evaluation of ARCMIP Simulations, *J. Appl. Meteorol. Clim.*, **47**, 2405–+, doi:10.1175/2008JAMC1845.1.

Trenberth, K.E., and J.T. Fasullo, (2010): Simulation of present-day and twenty-first-century energy budgets of the southern oceans, *J. Climate*, **23**(2), 440–454, doi:10.1175/2009JCLI3152.1.

Vecchi, G.A., and B.J. Soden (2007): GlobalWarming and theWeakening of the Tropical Circulation. *J. Climate*, **20**, 4316-4340.

Verlinde, J., et al., (2007): The Mixed-Phase Arctic Cloud Experiment, *Bull. Am. Meteorol. Soc.*, **88**, 205, doi:10.1175/BAMS-88-2-205.

Voldoire, A., et al., (2012): The CNRM-CM5.1 global climate model: description and basic evaluation, *Clim. Dyn.*, doi:10.1007/s00382-011-1259-y.

Volodin, E. M., N.A. Dianskii, and A.V. Gusev, (2010): Simulating present-day climate with the INMCM4.0 coupled model of the atmospheric and oceanic general circulations, *Isvestiya*, **46**, 414–431, doi:10.1134/S000143381004002X.

Wang, Q., D.H. Lenschow, (1995): An observational study of the role of penetrating cumulus in a marine stratocumulus-topped boundary layer. *J. Atmos. Sci*., **52**, 2778–2787.

Watanabe, M., et al., (2010): Improved climate simulation by MIROC5: Mean states, variability, and climate sensitivity, *J. Climate*, **23**, 6312–6335, doi:10.1175/2010JCLI3679.1.

Webb, M.J.. and C. Senior and S. Bony and J.J. Morcrette, (2001): Combining ERBE and ISCCP data to assess clouds in the Hadley Centre, ECMWF and LMD atmospheric climate models. Clim. Dyn. **17,** 905-922.

Webb, M.J. and F.H. Lambert and J.M. Gregory (2013): Origins of differences in climate sensitivity, forcing and feedback in climate models, (2012) *Clim. Dyn*., **40**, Issue 3-4, pp 677-707, 10.1007/s00382-012-1336-x

Webb, M.J., et al. (2006): On the contribution of local feedback mechanisms to the range of climate sensitivity in two GCM ensembles, *Clim*. Dyn., **27**, 17-38, doi:10.1007/s00382-006-0111-2.

Webb, M.J. and A. Lock, (2012): Cloupling between subtropical cloud feedback and the local hydrological cycle in a climate model. Accepted Clim. Dyn. DOI 10.1007/s00382-012-1608-5.

Wheeler, Matthew, George N. Kiladis (1999): Convectively Coupled Equatorial Waves: Analysis of Clouds and Temperature in the Wavenumber-Frequency Domain. J. Atmos. Sci., **56**, 374-399.

Wielicki, B., and Coauthors, (1996): Clouds and the Earth’s Radiant Energy System (CERES): an earth observing system experiment, *Bull. Am. Meteorol. Soc.*, **77**(5), 853–868.

Williams, K. D., and M.J. Webb, (2009): A quantitative performance assessment of cloud regimes in climate models, *Clim. Dyn.*, **33**(1), 141–157, doi:10.1007/s00382-008-0443-1.

Williams, K.D., et al., (2012): The transpose-amip ii experiment and its application to the understanding of southern ocean cloud biases in climate models, *J. Climate*, submitted.

Wood, R., and C. Bretherton, (2004): Boundary layer depth, entrainment, and decoupling in the cloud-capped subtropical and tropical marine boundary layer. *J. Climate*, **17**, 3576-3588.

Wood, R., Bretherton, C.S. and Hartmann, D. L. (2002): Diurnal cycle of liquid cloud water path over the subtropical and tropical oceans. Geophysical Research Letters, **29**, 2092-2095.

Yukimoto, S., et al., (2011): Meteorological Research Institute-Earth System Model Version 1 (MRIESM1): Model description, *Tech. Rep.* **64**, Meteorological Research Institute, Japan.

Zelinka, M.D., S.A. Klein, and D.L. Hartmann, (2012): Computing and Partitioning Cloud Feedbacks Using Cloud Property Histograms. Part II: Attribution to Changes in Cloud Amount, Altitude, and Optical Depth. *J. Climate,* **25**, 37363754. doi:10.1175/JCLI-D-11-00249.1.1

Zhang, Y., W.B. Rossow, A.A. Lacis, V. Oinas, and M.I. Mishchenko, (2004): Calculation of radiative fluxes from the surface to top of atmosphere based on ISCCP and other global data sets: Refinements of the radiative transfer model and input data, *J. Geophys. Res.*, **109**(D19,105), doi:10.1029/2003JD004457.

Zhang M., C.S. Bretherton, (2008): Mechanisms of low cloud climate feedback in idealized single-column simulations with the community atmospheric model (CAM3). *J. Climate*, **21**,4859–4878. doi:10.1175/2008JCLI2237.1

M. Zhang, C.S. Bretherton, P.N. Blossey, S. Bony, F. Brient and J.-C. Golaz, (2013): The CGILS Experimental Design to Investigate Low Cloud Feedbacks in General Circulation Models by Using Single-Column and Large-Eddy Simulation Models. In press, *J. Adv. Model. Earth Syst*., doi:10.1029/2012MS000182

Presentations at Conferences, Symposia and Workshops

2010

Roode, S.R. de, and J. van der Dussen 2010: Large-Eddy Simulation of a stratocumulus top cumulus cloud transition as observed during ASTEX *19th Symposium on Boundary Layers and Turbulence*, 1-6 August 2010, Keystone, CO., USA.

2012

Dussen, J. van der, S.R. de Roode and A.P. Siebesma, 2012: LES sensitivity experiments of the EUCLIPSE stratocumulus to cumulus transition based on ASTEX. *20th Symposium on Boundary Layers and Turbulence*, 9-13 July 2012, Boston, MA, USA.

Roode, S.R. de, I. Sandu, J. van der Dussen, A.S. Ackerman, P.N. Blossey, A. Lock, A.P. Siebesma and B Stevens, 2012: LES results of the EUCLIPSE Lagrangian stratocumulus to shallow cumulus transition cases. 20th Symposium on Boundary Layers and Turbulence, 9-13 July 2012, Boston, MA, USA.

Kurowski, M., D. Jarecka, H. Pawlowska, and W.W. Grabowski: Extended abstract presented at 16th International Conference on Clouds and Precipitation in Leipzig Germany, 29 July - 3 August 2012: Large-Eddy Simulations of Stratocumulus to Cumulus transitions.

3.2.3 Project management during the period

- *Consortium management tasks and achievements;*

i) set up of the management consortium

The agreed management structure for the project such as proposed in the DOW has been implemented. *The Project Office*: the coordinator (Pier Siebesma, KNMI) responsible for the overall coordination of the project, a project assistant manager (Karin van der Schaft, KNMI) assisting the coordinator with the external and internal communication of the project, a financial officer (Jeroen Sassen, KNMI), responsible for the financial administration of the project
The Work Package Leaders: (Sandrine Bony, Bjorn Stevens, George Tselioudis, Stephan de Roode) are together with the coordinator responsible for the efficient running and the progress of the WPs and oversee the collaborations between the WPs.
The Management Board: consists of the WP leaders and representatives of all partners and is chaired by the coordinator.
The General Assembly: consists of all representatives of all institutions such as presented in the DOW and which has been enhanced through additional contractors that have entered the project.

i) Website (Deliverable D0.1, D0.4)

A project public website can be found at http:/www.euclipse.eu where all information of the project can be found. It includes news on the project, information on the deliverables, the data sets, software products, outreach activities, information on the meetings, including agenda, minutes and presentations. As there was no real need for an internal website these deliverables have been merged.

ii) International Summer School on the achievements of EUCLIPSE (Deliverable D0.9, Month 40)

A location has been found in the Les Houches Physics School in France (http://houches.ujf-grenoble.fr/) .
An application to organise a EUCLIPSE summer school at this prestigious location has been approved and a reservation has been made for the period June 24th -July 5th 2013. We have received more than 130 applications and selected 55 excellent candidates . For more information on the Summerschool, invited speakers, programme. Participants we refer to the EUCLIPSE website:
http://www.euclipse.eu/summerschool/About_the_course.html

iii) Edited book with lectures from the summer school (Deliverable D0.10, Month 48)

The possibility of an edited book was discussed during the general assembly in June in Exeter (UK). The general feeling was that there is a need for a comprehensive textbook on the topic “Clouds & Climate”. As EUCLIPSE consists of an excellent group of experts on this theme we feel that this is a unique opportunity to write a standard text book. The expected audience will be advanced graduate students, PhD candidates with a background in one of the disciplinary areas the book will cover. A breakdown in 13 chapters has been made. Each chapter will be written by 2 authors from the EUCLIPSE consortium. A preliminary version of the book is expected to be ready during the Summer school in 2013 and the final release date is expected in early 2014. A proposal for the book has been send and accepted by Cambridge University Press who will be the editor of the book.

- *Problems which have occurred and how they were solved or envisaged solutions;*

Due to administrative reasons that were beyond control of the EUCLIPSE project office the final contracts and the money transfer was only arranged in May 2010. As a result numerous partners could start advertising for personal only after this date. There have been discussions with the EU officer whether EUCLIPSE should postpone the starting date. It was advised to keep the starting date fixed and to consider an extension of the project if this appears to be necessary. The effects of this have been minor the only mild delay of a few months in the delivery of the output of the ESM simulations (deliverable D1.4). This deliverable has been submitted now. However since various partime employers which are hired for a 4 time period started to work on the Project a few months after the start of the project they will be employed beyond the enddate of the project. We therefore think it would be desirable to extend the period for a period of 4 Months and propose that the end data will be changed into July 1st 2014.

- *Changes in the consortium, if any;*

The consortium is unchanged with respect to the start of the project.

- *List of project meetings, dates and venues;*

An up-to-date list of project meetings (including meeting agendas, presentations and reports) is maintained on the project website (www.euclipse.eu). It therefore suffices here to give a list with the EUCLIPSE project meetings:

a. Technical Meeting on the construction of a EUCLIPSE observational database for European Atmospheric Profiling Stations, October 24, 2011, IPSL, Paris France.
b. Planning Meeting on cross-links between the EUCLIPSE Work Packages, October 6-7,2011, Cologne, Germany.
c. WP3 meeting on the various intercomparison cases jointly with the GEWEX Atmospheric System Studies (GASS), April 6-7, 2012, Toulouse, France.
d. 3nd EUCLIPSE General Assembly (combined with CFMIP and GASS), May 29-June 1 , 2012, Paris, France.
e. Planning Meeting on cross-links between the EUCLIPSE Work Packages, February, 20-21, De Bilt, The Netherlands.

Besides the EUCLIPSE project meetings EUCLIPSE partners have been invited to various meetings to inform other international projects on the progress and content of the EUCLIPSE project:

i) 6th EU-Japan Workshop on Climate Change Research, October, 10-11 2011, , Brussels, Belgium.
ii) Coordination Meeting, Climate Modeling and Services, June, 7-8, 2012, Brussels, Belgium
iii) 1st PAN-GASS meeting "Advances in the modelling of atmospheric physical processes", September 10-14, 2012, Denver, USA.
iv) WGNE/WCRP/WWRP Workshop on "The Physics of Weather and Climate Models", March 20-23, Pasadena, USA
v) US/European Workshop on Aerosol-Cloud-Precipitation Processes, Washington DC, USA, November 6-8, 2012.
vi) "Towards an integrated atmospheric observing system in Europe" December 3-4, 2012.

- *Project planning and status*

Del. no.	Deliverable name	WP	Lead Benef.	Del Date

D0.6	Year 2 report	0	KNMI	26
D0.8	Brochure	0	KNMI	36
D1.6	Reprocessed version of EUCLIPSE model data products for long-term archiving within WDCC beyond the runtime of the project	1	DKRZ	36
D2.1.	Evaluation of clouds, radiation and precipitation in ESMs using COSP, clustering and compositing techniques.	2	METO	30
D2.2	Report on the evaluation of cloud-aerosols-radiation interactions in ESMs	2	MPG	30
D2.3	Design and application of a set of metrics that synthesises the ability of climate and weather prediction models to simulate clouds, precipitation and radiation	2	METO	36
D2.4	ESM evaluation of the ITCZ, the intra-seasonal and inter-annual variability of the tropical atmosphere, and temperature extremes over Europe	2	MF-CNRM	24
D2.6	Diagnostic of the climate feedbacks, including global and regional spreads, produced ESMs and of cloud and precipitation responses to climate change for CMIP5 runs; comparisons with estimates from the CMIP3 models	2	CNRS-IPSL	24
D2.7	Identification of the processes or cloud types most responsible for the spread in climate change cloud feedbacks and precipitation responses	2	CNRS-IPSL	36
D3.2	Storage of instantaneous 3D LES fields and key statistical variables in a public archive	3	TUD	24
D3.3	Detailed analyses of the LES and SCM results for ASTEX and the two GPCI columns	3	TUD	30
D3.4	Identification and comparison of the key quantities used in ESM parameterization schemes with LES results and observations	3	TUD	30
D3.5	SCM equilibrium states in the Hadley circulation	3	TUD	30
D3.6	Results at selected grid points (GCPI/CloudNet/ ARM/AMMA)	3	KNMI	18
D3.7	Comparison of the hydrological and energy balance and the cloud amount as computed by ESMs	3	MF-CNRM	36
D3.8	Development and application of methods to exploit high frequency for understanding cloud feedbacks	3	METO	36
D3.9	Quantification of the cloud-climate feedback and its uncertainty for prescribed large-scale conditions	3	MPG	36
D4.1	A developing database and protocol for parameter and structural (numerical) sensitivity studies	4	MPG	24
D4.2	Comparison study of the model sensitivity to the numerical structure of the computations (grid and time step) with the parameter sensitivity of the model.	4	MPG	36
D4.3	Report on a study identifying the utility of NWP based methods for identifying and narrowing sources of divergent behaviour in cloud-climate feedbacks in ESMs	4	ECMWF	36

- *Impact of possible deviations from the planned milestones and deliverables, if any;*

None

- *Any changes to the legal status of any of the beneficiaries, in particular non-profit public bodies, secondary and higher education establishments, research organisations and SMEs;*

None

- *Development of the Project website, if applicable;*

See http://www.euclipse.eu

- *short comments and information on co-ordination activities during the period in question, such as communication between beneficiaries, possible co-operation with other projects/programmes etc.*

EUCLIPSE has provided useful input for various international programs and initiatives. We provide a list here

- EUCLIPSE is closely collaborating with WCRP's Cloud Feedback Model Intercomparison Project (CFMIP). Through this collaboration many of the analyses of climate models in WP2 have been extended to climate model output provided by climate model institutes outside Europe. Exactly for this reason the annual meetings of EUCLIPSE are organized together with CFMIP.

- For the same reason EUCLIPSE is closely collaborating with the WCRP's GEWEX Atmospheric System Studies (GASS). Through this collaboration many of the initiatives of WP3 on cloud process studies are done in close collaboration with institutes outside Europe. Also for this reason the many members from GASS have been invited to the EUCLIPSE annual meetings and many institutes outside the EUCLIPSE consortium have been participating in the process intercomparison studies that are designed by EUCLIPSE.

- Participants of EUCLIPSE (Sandrine Bony and Bjorn Stevens) have been working on formulating a white paper of one of WCRP's grand challenges: "Clouds, Circulation and Climate Sensitivity".

- Participants of EUCLIPSE have been actively working on the upcoming next IPCC report and especially on the role of cloud processes. Many of the results and published papers from EUCLIPSE will be explicitly used for the upcoming IPCC report.

- EUCLIPSE is collaborating with IS-ENES to come up with a community radiation code and with EMBRACE intercomparison studies on deep convection.

- **List of acronyms**

- AA - Academy of Athens (http://www.academyofathens.gr)
- AMMA – African Monsoon Multi-disciplinary analyses (http://www.amma-international.org/)
- AMIP – Atmosphere Model Intercomparison Project (http://www-pcmdi.llnl.gov/projects/amip)
- AMS – American Meteorological Society
- AOGCM – Atmosphere Ocean General Circulation Model
- AR4 – Fourth Assessment Report (http://www.ipcc.ch/ipccreports/assessments-reports.htm)
- ARCMIP – Arctic Regional Climate Model Intercomparison (http://curry.eas.gatech.edu/ARCMIP/)
- ARM – Atmospheric Radiation Measurement program (http://www.arm.gov/)
- AROME – Applications of Research to Operations at MEsocale (the Meteo-France mesoscale model)
- ARPEGE - Action de Recherche Petite Echelle Grande Echelle (the MF-CNRM
- atmospheric GCM)
- ASTEX - Atlantic Stratocumulus Transition Experiment (http://kiwi.atmos.colostate.edu/scm/astex.html)
- CALIPSO - Cloud-Aerosol Lidar and Infrared Pathfinder Satellite Observations (http://www-calipso.larc.nasa.gov/)
- CERES – Clouds and the Earth's Radiant Energy System (http://science.larc.nasa.gov/ceres/index.html)
- CFMIP – Cloud Feedback Model Intercomparison Project (http://www.cfmip.net)
- CGILS - CFMIP-GCSS Intercomparison of Large-Eddy and Single-Column Models (http://atmgcm.msrc.sunysb.edu/cfmip_figs/Case_specification.html)
- CLUBB – Cloud Layers Unified by Binormals (parameterization) (http://club.larson-group.com/about.php/)
- CloudNet - Development of a European pilot network of stations for observing cloud profiles (http://www.cloud-net.org/index.html)
- CloudSat – NASA Earth observation satellite that uses radar to measure cloud properties (http://cloudsat.atmos.colostate.edu/)
- CMIP – Coupled Model Intercomparison Project (http://www-pcmdi.llnl.gov/projects/cmip/)
- CMOR= Climate Model Output Rewriter
- CNRM - Centre National de Recherches Météorologiques (http://www.cnrm.meteo.fr/)
- CNRM-GAME – CNRM Mesoscale Modelling Group
- CNRS - IPSL Centre National de la Recherche Scientifique - Institut Pierre Simon Laplace (http://www.ipsl.jussieu.fr/)
- COSP – CFMIP Observation Simulator Package (http://cfmip.metoffice.com/COSP.html)
- DALES – Dutch Atmospheric Large Eddy Simulation (http://www.knmi.nl/~siebesma/LES/)
- DKRZ – Deutsche Klimarechenzentrum (http://www.dkrz.de)
- EC - European Commission (http://ec.europa.eu/index_en.htm)
- EC-EARTH – Earth System Model based on the ECMWF integrated forecasting system (http://ecearth.knmi.nl)
- ECHAM – General Circulation Model of MPI Hamburg (http://www.mpimet.mpg.de/en/wissenschaft/modelle/echam.html)
- ECMWF – European Centre for Medium Range Weather Forecasts (http://ecmwf.int)
- ENSEMBLES - European project supported by the EC 6th Framework Programme as a 5 year Integrated Project from 2004-2009 (http://ensembles-eu.metoffice.com/index.html)
- ENSO – El Niño Southern Oscillation
- ERA40 – ECMWF reanalysis project 1957-2002 (http://www.ecmwf.int/products/data/archive/descriptions/e4/index.html)
- ESM – Earth System Model
- ETHZ - Eidgenössische Technische Hochschule Zürich (http://www.ethz.ch/)
- EU – European Union (http://europa.eu)
- EUCLIPSE – European Union CLoud Intercomparison, Process Study & Evaluation project
- EULAG – Eulerian LAGrangian (http://www.mmm.ucar.edu/eulag/)
- EUROCS – European Cloud Systems (http://www.cnrm.meteo.fr/gcss/EUROCS/EUROCS.html)
- FASTER - Fast-Physics System Testbed and Research Project (http://www.bnl.gov/esm/)
- FP – Framework Program
- GCM – General Circulation Model

- GCSS – GEWEX Cloud System Studies (http://www.gewex.org/gcss.html)
- GEWEX – Global Energy and Water cycle Experiment (http://www.gewex.org)
- GPCI - GCSS/WGNE Pacific Cross-section Intercomparison (http://www.igidl.ul.pt/cgul/projects/gpci.htm)
- GOCCP – GCM-Oriented Cloud CALIPSO Product (http://climserv.ipsl.polytechnique.fr/cfmip-atrain.html)
- GPCI : GEWEX Pacific Cross section Intercomparison
- HADGEM2-ES – Hadley Centre Global Environmental Model 2 (Earth System)
- IFS - Integrated Forecasting System
- IPCC - Intergovernmental Panel on Climate Change (http://www.ipcc.ch/)
- IPSL – Institut Pierre-Simon Laplace (http://www.ipsl.jussieu.fr/)
- ISCCP - International Satellite Cloud Climatology Project (http://isccp.giss.nasa.gov/)
- IS-ENES - INFRA-2008-1.1.2.21: establishing an European e-Infrastructure for earth system's understanding and modeling
- ITCZ – Inter Tropical Convergence Zone
- JMA – Japan Meteorological Agency (http://www.jma.go.jp/jma/indexe.html)
- JPL - Jet Propulsion Laboratory (http://www.jpl.nasa.gov/)
- KNMI - Royal Netherlands Meteorological Institute (http://www.knmi.nl)
- LES – Large Eddy Simulation
- LOCEAN – Laboratoire d'Océanographie et du Climat : Expérimentations et Approches Numériques (https://www.locean-ipsl.upmc.fr/index.php)
- LMD – Laboratoire de Météorologie Dynamique (http://www.lmd.jussieu.fr/)
- LMDz - Laboratoire de Météorologie Dynamique general circulation model
- LTS Lower Tropical Stability
- LWP – Liquid Water Path
- MB – Management Board
- METO - Met Office (http://www.metoffice.gov.uk/)
- MF-CNRM[4] - Météo-France - Centre National de Recherches Météorologiques (http://www.cnrm.meteo.fr/)
- MISR - Multi-angle Imaging SpectroRadiometer (http://www-misr.jpl.nasa.gov/)
- MISU – Department of Meteorology Stockholm University (http://www.misu.su.se/)
- MODIS - Moderate Resolution Imaging Spectroradiometer (http://modis.gsfc.nasa.gov/)
- MPG - Max Planck Gesellschaft (http://www.mpg.de)
- MOLEM – Met Office Large Eddy Model
- MPI-M – Max Planck Institute for Meteorology (http://www.mpimet.mpg.de/)
- NASA – National Aeronautics and Space Administration (http://www.nasa.gov/)
- NAO – North Atlantic Oscillation
- NWP – Numerical Weather Prediction
- OAGCM - Ocean-Atmosphere Global Climate Model
- PARASOL - Polarization & Anisotropy of Reflectances for Atmospheric Sciences coupled with Observations from a Lidar (http://smsc.cnes.fr/PARASOL/)
- PC – Project Coordinator
- PCMDI – Program for Climate Model Diagnosis and Intercomparison (http://www-pcmdi.llnl.gov/)
- RACMO - Regional Atmospheric Climate Model
- SAM – System for Atmospheric Modeling (http://rossby.msrc.sunysb.edu/~marat/SAM.html)
- SCM – Single Column Model
- SIRTA - Site Instrumental de Recherche par Télédétection Atmosphérique (http://sirta.ipsl.polytechnique.fr/)
- SPM – Summary for Policy Makers
- SST – Sea Surface Temperature
- SU - University of Stockholm (http://www.bbcc.su.se/)
- TKE – Turbulent Kinetic Energy

[4] CNRM is also affiliated to the Centre National de la recherché Scientifique (CNRS) under the name of Groupe d'Etude de l'Atmosphère Météorologique (GAME)

- TOA – Top Of Atmosphere
- TUD - Delft University of Technology (http://www.ws.tn.tudelft.nl)
- UCLA – University of California, Los Angeles (http://www.ucla.edu/)
- UKMO – United Kingdom Meteorological Office (http://www.metoffice.gov.uk/)
- UW - University of Warsaw (http://www.uw.edu.pl/en/)
- VOCALS – VAMOS Ocean-Cloud-Atmosphere-Land Study (http://www.eol.ucar.edu/projects/vocals/)
- WCRP – World Climate Research Program (http://wcrp.wmo.int)
- WGNE – Working Group on Numerical Experimentation
- WMO – World Meteorological Organisation (http://www.wmo.int)
- WP – Workpackage
- WU – Uniwersytet Warszawski (http://www.uw.edu.pl/)

3.3 Deliverables and milestones tables

Deliverables

The deliverables due in this reporting period, as indicated in Annex I to the Grant Agreement have to be uploaded by the responsible participants (as indicated in Annex I), and then approved and submitted by the Coordinator. Deliverables are of a nature other than periodic or final reports (ex: "prototypes", "demonstrators" or "others"). If the deliverables are not well explained in the periodic and/or final reports, then, a short descriptive report should be submitted, so that the Commission has a record of their existence.

If a deliverable has been cancelled or regrouped with another one, please indicate this in the column "Comments".
If a new deliverable is proposed, please indicate this in the column "Comments".

This table is cumulative, that is, it should always show all deliverables from the beginning of the project.

TABLE 1. DELIVERABLES											
Del. no.	**Deliverable name**	**Version**	**WP no.**	**Lead beneficiary**	**Nature**	**Dissemination level**	**Delivery date from Annex I (proj month)**	**Actual / Forecast delivery date Dd/mm/yyyy**	**Status No submitted /Submitted**	**Contractual Yes/No**	**Comments**
1	D1.2 Final versions of CALIPSO-PARASOL observational analysis product and of MODIS simulator	1.0	MAX PLANCK GESELLSCHAFT ZUR FOERDERUNG DER WISSENSCHAFTEN E.V.	6.0	Other	PU	30/04/2010 (3 months)	19-4-2011	Accepted		
1	D2.1 Evaluation of clouds, radiation and precipitation in ESMs using COSP, clustering an compositing techniques	1.0	MET OFFICE	38.0	Report	PU	31/07/2012 (30 months)	17-10-2012	Received		
2	D0.4 Public web site	1.0	KONINKLIJK NEDERLANDS METEOROLOGISCH INSTITUUT (KNMI)	2.0	Other	PU	31/07/2010 (6 months)	19-4-2011	Accepted		
3	D0.3 Kick-off Meeting	1.0	KONINKLIJK NEDERLANDS METEOROLOGISCH INSTITUUT (KNMI)	1.0	Other	PU	30/04/2010 (3 months)	19-4-2011	Accepted		
4	D1.3 ESM versions with COSP software	1.0	MET OFFICE	9.0	Other	PU	31/07/2010 (6 months)	19-4-2011	Accepted		
4	D2.4 ESM evaluation of the ITCZ, the intra-seasonal and inter-annual variabi9lity of the tropical atmosphere, and temperature extremes over Europe	1.0	METEO-FRANCE	12.0	Report	PU	31/01/2012 (24 months)	18-10-2012	Received		
5	D0.2 Internal web site	1.0	KONINKLIJK NEDERLANDS METEOROLOGISCH INSTITUUT (KNMI)	2.0	Other		30/04/2010 (3 months)	4-7-2011	Accepted		
6	D1.1 Final version of COSP software	1.0	MET OFFICE	2.0	Other	PU	30/04/2010 (3 months)	4-7-2011	Accepted		

7	D3.1 Description of the set-up for the ASTEX, the GPCI stratocumulus and shallow cumulus, and the SCM equilibrium state cases	1.0	TECHNISCHE UNIVERSITEIT DELFT	12.0	Other	PU	31/01/2011 (12 months)	14-7-2011	Accepted		
8	D0.1 Project Flyer	1.0	KONINKLIJK NEDERLANDS METEOROLOGISCH INSTITUUT (KNMI)	1.0	Other	PU	30/04/2010 (3 months)	16-9-2011	Accepted		
9	D1.5 Final versions of model evaluation packages	1.0	ACADEMY OF ATHENS	24.0		PU	31/07/2011 (18 months)	20-9-2011	Accepted		
11	D1.4 Final output of ESM simulations	1.0	MET OFFICE	16.0	Other	PU	31/01/2011 (12 months)	28-9-2011	Accepted		
12	D1.5 Final versions of model evaluation packages UPDATE	1.0	ACADEMY OF ATHENS	24.0	Other	PU	31/07/2011 (18 months)	5-10-2011	Accepted		
13	D3.2 Storage of instantaneous 3D LES fields and key statistical variables in a public archive	1.0	TECHNISCHE UNIVERSITEIT DELFT	6.0	Report	PU	31/01/2012 (24 months)	25-4-2012	Received		
15	D2.6 Diagnostic of the climate feedbacks, including global and regional spreads, produced ESMs and of cloud and precipitation responses to climate change for CMIP5 runs; comparisons with estimates from the CMIP3 models	1.0	CENTRE NATIONAL DE LA RECHERCHE SCIENTIFIQUE	18.0	Report	PU	31/01/2012 (24 months)	30-10-2012	Received		
16	D4.1 A developing database and protocol for parameter and structural (numerical) sensitivity studies.	1.0		16.0	Other	PU	31/01/2012 (24 months)	5-12-2012	Received		
17	D1.4 Final output of ESM simulations	1.0	MET OFFICE	16.0	Other	PU	31/07/2011 (18 months)	18-1-2013	Received		

18	D3.8 Development and application of methods to exploit high frequency for understanding cloud feedbacks	1.0	MET OFFICE	16.0	Report	PU	31/01/2013 (36 months)	28-1-2013	Received		
19	D2.7 Report on the identification of the processes or cloud types most responsible for the spread in climate change cloud feedbacks and precipitation responses.	1.0	MET OFFICE	12.0	Report	PU	31/01/2013 (36 months)	29-1-2013	Received		
20	D3.3 Detailed analyses of the LES and SCM results for ASTEX and the two GPCI columns	1.0	TECHNISCHE UNIVERSITEIT DELFT	3.0	Other	PU	31/07/2012 (30 months)	31-1-2013	Received		
21	D3.4 Identification and comparison of the key quantities used in ESM parameterization schemes with LES results and observations	1.0	TECHNISCHE UNIVERSITEIT DELFT	16.0	Report	PU	31/07/2012 (30 months)	31-1-2013	Received		
22	D3.5 SCM equilibrium states in the Hadley circulation	1.0	TECHNISCHE UNIVERSITEIT DELFT	8.0	Report	PU	31/07/2012 (30 months)	31-1-2013	Received		
23	D3.9 Quantification of the cloud-climate feedback and its uncertainty for prescribed large-scale conditions	1.0	MAX PLANCK GESELLSCHAFT ZUR FOERDERUNG DER WISSENSCHAFTEN E.V.	16.0	Report	PU	31/01/2013 (36 months)	31-1-2013	Received		
24	D2.2 Report on the evaluation of cloud-aerosols-radiation interactions in ESMs	1.0		1.0	Report	PU	31/07/2012 (30 months)	1-2-2013	Received		

Milestones

Please complete this table if milestones are specified in Annex I to the Grant Agreement. Milestones will be assessed against the specific criteria and performance indicators as defined in Annex I.

This table is cumulative, which means that it should always show all milestones from the beginning of the project.

TABLE 2. MILESTONES							
Mile stone no.	**Milestone name**	**WP no**	**Lead**	**Delivery date**	**Achieved Yes/No**	**Actual / Forecast achievement date dd/mm/yyyy**	**Comments**
M1.1	Completion of COSP and MODIS software and CALIPSO-PARASOL observational products	1	**METO**	3	Yes	**01/07/2011**	Prototype Models and Observational data sets
M1.2	Completion of the model evaluation packages	1	**AA**	18	Yes	**01/09/2011**	Prototype Model
M1.3	Delivery of the ESM simulation output	1	**DKRZ**	18	Yes	**30/11/2011**	Model data
M2.1	Evaluation of cloud-aerosol-radiation interaction achieved	2	**MPG**	30	Yes	**01/02/2013**	Report
M2.2	Metrics for clouds, precipitation and radiation developed and applied to ESMs and NWP	2	**METO**	36	No		Report
M3.1	Storage of 3D LES fields and LES diagnostics in a public archive	3	**TUD**	24	Yes	**25/04/2012**	Model data
M3.2	SCM equilibrium states in the Hadley circulation	3	**TUD**	30	Yes	**31/01/2013**	Report
M3.3	Detailed comparison of LES and SCM results of the stratocumulus to cumulus transition as observed during ASTEX	3	**TUD**	30	Yes	**31/01/2013**	Model data
M3.4	Identification and comparison of key quantities used in ESM parameterization schemes with LES results and observations	3	**KNMI**	30	Yes	**31/01/2013**	Report
M3.5	Comparison of the ESMs modelled hydrological and energy balances and cloud amount with observations at selected locations	3	**KNMI**	36	No		Report

M3.6	Quantification of the cloud-climate feedback for idealized large-scale forcing conditions in the Hadley circulation regime	3	**MPG**	36	Yes	**31/01/2013**	Report
M4.1	Summary of the relative advantages of the Initial Tendency versus Transpose-AMIP techniques for diagnosing systematic biases in climate runs	4	**ECM WF**	36	No		Report
M4.2	Description of experimental protocol for testing hypotheses relating to cloud-climate feedbacks	4	**MPG**	30	Yes	**05/12/2012**	Report
M4.3	Summary of the relative effects of one- versus two moment microphysical closures on a subset of the EUCLIPSE models on cloud-climate feedbacks for different aerosol concentrations	4	**ETHZ**	36	No		Report